

Low-dimensional approximations of the conditional law of Volterra processes: a non-positive curvature approach

Reza Arabpour*

Vector Institute and Department of Mathematics, McMaster University

ARABPOUR@MCMASTER.CA

John Armstrong*

Department of Mathematics, King's College London.

JOHN.ARMSTRONG@KCL.AC.UK

Luca Galimberti†

Department of Mathematics, King's College London

LUCA.GALIMBERTI@KCL.AC.UK

Anastasis Kratsios*†‡

Vector Institute and Department of Mathematics, McMaster University

KRATSIOA@MCMASTER.CA

Giulia Livieri†

Department of Statistics, London School of Economics and Political Science.

G.LIVIERI@LSE.AC.UK

Editor: TBD

Abstract

Predicting the conditional evolution of Volterra processes with stochastic volatility is a crucial challenge in mathematical finance. While deep neural network models offer promise in approximating the conditional law of such processes, their effectiveness is hindered by the curse of dimensionality caused by the infinite dimensionality and non-smooth nature of these problems. To address this, we propose a two-step solution. Firstly, we develop a stable dimension reduction technique, projecting the law of a reasonably broad class of Volterra process onto a low-dimensional statistical manifold of non-positive sectional curvature. Next, we introduce a sequentially deep learning model tailored to the manifold's geometry, which we show can approximate the projected conditional law of the Volterra process. Our model leverages an auxiliary hypernetwork to dynamically update its internal parameters, allowing it to encode non-stationary dynamics of the Volterra process, and it can be interpreted as a gating mechanism in a mixture of expert models where each expert is specialized at a specific point in time. Our hypernetwork further allows us to achieve approximation rates that would seemingly only be possible with very large networks.

Keywords: Geometric Deep Learning, Measure-Valued Stochastic Processes, Non-Positive Curvature, Barycenters, Universal Approximation, hypernetworks, Mixture of Experts.

1 Introduction

The dynamic prediction of the conditional distribution $\mathbb{P}[X_{t+1}|X_{[0:t]} = x_{[0:t]}]$ of a non-Markovian Volterra process $X_.$, conditioned on its realized path $x_{[0:t]}$ up to any given time t , is a fundamental problem spanning the sciences, ranging from Bayesian modelling (e.g., [Bernardo and Smith \(1994\)](#)) to mathematical finance (e.g., [Back et al. \(2004\)](#)). While there are several machine learning models for learning a process conditional distribution on its historical paths; e.g. [Bishop \(1994\)](#); [Gauthier \(2014\)](#); [Mirza and Osindero \(2014\)](#); [Borovykh et al. \(2017\)](#); [Chevyrev and Oberhauser \(2022\)](#) and deep learning models which can approximate signed measure-valued functions [Chen and Chen \(1995\)](#); [Korolev \(2022\)](#); [Benth et al. \(2023\)](#); [Cuchiero et al. \(2023\)](#), the available quantitative approximation bounds for measure-valued models; e.g. [Kratsios \(2023\)](#); [Acciaio et al. \(2023\)](#) suggest that the

*. Alphabetic ordering.

†. Primary authors, equal contribution, alphabetical ordering.

‡. Corresponding author.

measure-valued maps cannot be efficiently approximated. This is due to two factors; firstly, they are infinite-dimensional, meaning they suffer from extreme forms of the curse of dimensionality; see [Lanthaler and Stuart \(2023\)](#) for a lower-bound in the linear case. Secondly, most spaces of probability measures, e.g. Wasserstein spaces, do not have any smooth or linear structure, which a deep learning model can naturally leverage. To the best of the authors' knowledge, there are currently no available deep-learning models which can approximate the evolving conditional distribution of most stochastic processes while also depending on a computationally feasible number of parameters.

To address this issues, we present a two-step approach for dynamically approximating the conditional evolution of a class of discrete-time stochastic processes X . By allowing for an irreducible dimension-reduction-type error, our first step corrects the deficits of the geometries of most spaces of probability measures by projecting $\mathbb{P}[X_{t+1}|X_{[0:t]} = x_{[0:t]}]$ onto the (smooth) Riemannian manifold \mathcal{N}_d of non-singular d -dimensional Gaussian measures equipped with a new Riemannian metric which has a non-positively curved geometry when the $d \geq 2$. This can be contrasted with the standard Fisher(-Rao) metric ([Dowty, 2018](#)), from information geometry, which is only non-positively curved when $d = 1$ ([Skovgaard, 1984](#)). Critically, we show that (refer to [Theorem 9](#)), though our new projection shares an analogous characterization as “distance” minimizer to information-theoretic projections, e.g. the I -projection [Csiszár and Matus \(2003\)](#); [Csiszár \(1975\)](#), it preserves the dependence of $\mathbb{P}[X_{t+1}|X_{[0:t]} = x_{[0:t]}]$ on the realized path $x_{[0:t]}$ in a stable way as it is Lipschitz. Furthermore, the dependence of the projected dynamical system (see below) on the historical paths generated by X . is found to be proportional to the persistence of the memory of the stochastic process itself ([Theorem 11](#)).

The projection of the conditional distribution $\mathbb{P}[X_{t+1}|X_{[0:t]} = x_{[0:t]}]$ onto \mathcal{N}_d , defines a dynamical system on the Riemannian manifold \mathcal{N}_d . This long memory dynamical system is then approximated by a dynamic version of the geometric deep learning model of [Kratsios \(2023\)](#). We prove a quantitative universal approximation theorem which shows that this system can be approximated by our *sequential* deep learning model ([Theorem 13](#)). Our result has the following properties: 1) it shows that any infinite-memory dynamical systems between non-positively curved Riemannian manifolds, e.g. generalized hyperbolic spaces, can be approximated provided that its memory fades. This is similar to results in the reservoir computing literature [Grigoryeva and Ortega \(2018, 2019\)](#). 2) It shows that the geometric deep learning model does not suffer from the curse of dimensionality when the dynamical systems evolve according to smooth dynamics; in particular, this happens for the projected conditional law of X . when its generator is “smooth” and has no hidden random state. 3) In the static setting, i.e. when ignoring the flow of time, our bounds are polynomially tighter than the non-Euclidean universal approximation theorems of [Kratsios \(2023\)](#); [Acciaio et al. \(2023\)](#) and in the dynamic setting, our bounds are exponentially tighter than the static setting. 4) Our constructive proof yields a federated algorithm where a sequence of independent experts approximate the dynamical system at individual points in time, after which an overarching hypernetwork [Ha et al. \(2017\)](#) is used to synchronize them and create the recurrence without having to optimize (backpropagate) in time. While our approximation theorems hold for dynamical systems on any non-positively curved Riemannian manifold, we focus our exposition on the statistical manifold \mathcal{N}_d . We empirically verify the trainability of the proposed model and the role of each component via an ablation study evaluating the dependence of the model on its parameters.

All code can be found at <https://github.com/arabporr/HyperNetwork> .

Outline The paper is organized as follows.

1. Section 2 reviews notions from metric geometry required to formulate our main results.
2. Section 3 formalizes the setting and introduces our new perturbation of the Fisher metric on \mathcal{N}_d , which has a well-behaved geometry.
3. Section 4 contains our results on the Gaussian random projection of the conditional distribution of Volterra processes.

4. Section 5 contains universal approximation theorems for our model, first in the static and then in the dynamic settings.
5. Section 6 contains an ablation study of our model, which confirms our theoretical results.

All proofs are deferred to the appendix, which also describes results from differential geometry for which we have been unable to provide a proper reference in the literature. The appendix also contains an example outlining the problem with information projection for dimension reduction of the conditional law of Volterra processes.

We assume the reader to be familiar with the terminology of stochastic processes and optimal transport. Both notions are widely used in machine learning, for example in denoising diffusion models [Sohl-Dickstein et al. \(2015\)](#) and generative adversarial networks [Arjovsky et al. \(2017\)](#).

1.1 Related Work

Our results focus on the broad class of stochastic processes known as *Volterra processes*, which represent a rich yet well-structured class of *non-Markovian* stochastic differential equations (SDEs, henceforth) with latent stochastic factors. Both the discrete and the continuous versions of stochastic Volterra processes, and their generalizations [Jaber et al. \(2024\)](#), play a crucial role in mathematical finance (e.g., [Jacquier et al., 2018](#); [Abi Jaber et al., 2019](#); [Cuchiero and Teichmann, 2020](#); [Bondi et al., 2024](#)), reservoir computing (e.g., [Grigoryeva and Ortega \(2019\)](#); [Gonon et al. \(2022\)](#)), engineering (e.g., [Shiki et al. \(2017\)](#)), and computational biology (e.g., [Korenberg and Hunter \(1996\)](#)).

Our projection of the conditional law of stochastic Volterra processes exploits the existence and stability of barycenters of probability measures on Riemannian manifolds of non-positive curvature, in the sense of [Aleksandrov \(1951\)](#) and [Rešetnyak \(1960\)](#). Various notions of barycenters, e.g. Wasserstein barycenters ([Cuturi and Doucet, 2014](#); [Srivastava et al., 2018](#); [Puccetti et al., 2020](#); [Altschuler and Boix-Adserà, 2021](#); [Kolesov et al., 2024a,b](#)), have been used in generative modelling as they provide a natural tool for averaging distributions. The new element of our approach is to consider barycenters of distributions, also called the Karcher/Fréchet mean, whose definition is rooted in Riemannian ([Grove and Karcher, 1973](#); [Karcher, 1977b](#); [Kim and Pass, 2020](#)) and metric geometry ([Sturm, 2002, 2003](#); [Ohta, 2012](#); [Mendel and Naor, 2013](#); [Yokota, 2017](#)). These provide a non-linear generalization of the expectation of a random variable taking values in a non-linear space and are commonly used in computational geometry ([Bini and Iannazzo, 2013](#)), shape analysis ([Le, 2001](#); [Fletcher et al., 2004](#)), geometric statistics ([Lim and Pália, 2020](#); [Bhattacharya and Patrangenaru, 2003, 2005](#)), and recently in differential privacy ([Utpala et al., 2023](#)). We will use them to determine the single most representative d -dimensional non-singular Gaussian measure, amongst a family of random Gaussian measures in \mathcal{N}_d in which we encode the conditional law of the Volterra process.

This notion of barycenter, or intrinsic expectation, is only well-defined globally for manifolds with non-positive curvature ([Afsari, 2011](#)). Examples include the hyperbolic spaces used in hierarchical clustering ([Chami et al., 2020](#)) or latent graph inference for GNNs ([de Ocáriz Borde et al., 2022](#)). Such geometries appear for various statistical manifolds ([Pinele et al., 2020](#); [Le Brigant et al., 2021](#)) with the Fisher-Rao metric ([Ay et al., 2017](#)); notably the *one-dimensional* non-degenerate Gaussian distributions ([Atkinson and Mitchell, 1981](#); [Costa et al., 2015](#); [Pinele et al., 2020](#)). However, as shown in ([Skovgaard, 1984](#)), the space \mathcal{N}_d of multivariate non-degenerate Gaussian distributions fails to have non-positive curvature in dimension 2 or greater. Our perturbation of the standard information-theoretic geometry on the statistical manifold \mathcal{N}_d (see Proposition 7) identifies a non-positively curved complete Riemannian geometry on \mathcal{N}_d which coincides with the standard information geometry on any submanifolds of Gaussian distributions with fixed mean. This allows us to apply the intuition from information geometry, but with the analytic benefit of a non-positive metric geometry. Moreover our construction provides a closed-form expression for the Riemannian

distance: for typical statistical families, the Riemannian distance in the Fisher-Rao metric can only be computed numerically.

Projecting the conditional distribution of the stochastic Volterra process X_\cdot , conditioned on its realized path $x_{[0:t]}$ up to any time t , down to \mathcal{N}_d results in a (generalized) dynamical system between finite-dimensional spaces. Since all the resulting spaces are finite-dimensional and well-structured, one can reasonably hope that this system can be approximated without the curse of dimensionality if the involved maps are smooth enough, a feature not shared by infinite-dimensional approximation problems (Lanthaler and Stuart, 2023; Acciaio et al., 2023). There is a well-developed literature on the approximation of dynamical systems by recurrent deep learning models such as reservoir computers (Grigoryeva and Ortega, 2018; Gonon and Ortega, 2019; Grigoryeva and Ortega, 2019; Gonon and Ortega, 2021), recurrent neural networks (Li et al., 2022a; Hutter et al., 2022), or transformers Yun et al. (2020). However, the available universal approximation results in the literature only apply to dynamical systems between linear input spaces and systems whose dynamics do not change in time. We, therefore first extend the static *geometric deep learning* of Kratsios (2023) to a sequential/dynamic model capable of processing *sequences* of inputs and outputs in any given appropriate pair of non-positively curved Riemannian manifolds, e.g. on \mathcal{N}_d , and we then prove a universal approximation showing that it can approximate most time-inhomogeneous dynamical systems between these spaces, possibly having infinite but polynomially fading memory (Theorem 15).

Our estimates on the parameters and guarantees are novel even in the Euclidean setting: many of the aforementioned approximation theorems for recurrent neural networks (RNNs) are only qualitative and no rates are provided, especially for low-regularity dynamical systems with slowly-fading infinite memory. Even in the static setting, our results significantly improve the rates for the available universal approximation theorems for deep learning models between Riemannian manifolds Kratsios (2023); Acciaio et al. (2023). Furthermore, in the static setting (Theorem 17), our approximate rates are optimal since they match those of Yarotsky (2018); Yarotsky and Zhevnerchuk (2020); Lu et al. (2021); Shen et al. (2022) in the special case where the input space is Euclidean and the output space is the real line. In the static setting, there are other geometric deep learning models defined between Riemannian manifolds such as the geodesic convolutional model of (Masci et al., 2015), but no approximation theory for these models has yet been developed.

Mixture of experts (MoE) models such as DBRX MosaicAI (2024), Gemini (Google, 2024), Switch Transformers Fedus et al. (2022), Mixtral Jiang et al. (2024), and many others (e.g. Saad et al. (2023); Chowdhury et al. (2023); Li et al. (2024); Puigcerver et al. (2024); Saqr et al. (2024)) have taken a central role in modern deep learning, due to the need to scale-up the model complexity while maintaining a constant computational cost on the forward pass Kratsios et al. (2024); Furuya et al. (2024). This is achieved via a gating mechanism which routes any given input to one of a large number of “expert” neural network models, which is then used to produce a prediction from that input. Thus, only the gating network parameters and the selected “expert” neural network are ever activated for that input. One can interpret our (hyper-geometric network) as a mixture of infinitely many experts, and each of them specializes in predicting at exactly one specific moment in time. The hypernetwork in our HGN model acts as a gating mechanism which, given the current point in time, routes the input to the corresponding expert at that moment in time.

2 Geometric Background

We briefly overview some of the relevant notions from the geometry of non-positively curved metric spaces, also called (global) NPC spaces or Hadamard spaces. For further details we recommend the book by Bridson and Haefliger (1999) as well as the results of Sturm (2003).

Definition 1 (NPC space) A metric space (N, d) is called global NPC space if it is complete and for each $x_0, x_1 \in N$ there exists a point $y \in N$ with the property that for all points $z \in N$

$$d^2(z, y) \leq \frac{1}{2}d^2(z, x_0) + \frac{1}{2}d^2(z, x_1) - \frac{1}{4}d^2(x_0, x_1).$$

In particular, (N, d) is contractible and hence simply connected.

A primary example of global NPC spaces is provided by Cartan-Hadamard manifolds.

Proposition 2 (Manifolds (Proposition 3.1 in Sturm (2003))) Let (N, g) be a Riemannian manifold and let d be its induced Riemannian distance. Then (N, d) is a global NPC space if and only if it is complete, simply connected and of non-positive (sectional) curvature.

We will describe some results on barycenters of probability measures on metric spaces of NPC. First, we need to introduce the following notation; cfr. Sturm (2003), Section 4. Let (N, d) be a complete metric space. Denote by $\mathcal{P}(N)$ the set of all probability measures p on $(N, \mathcal{B}(N))$ with separable support $\text{supp}(p) \subset N$. For $1 \leq \theta < \infty$, $\mathcal{P}^\theta(N)$ denotes the set of $p \in \mathcal{P}(N)$ with $\int_N d^\theta(x, y)p(dy) < \infty$ for some (hence all) $x \in N$, and $\mathcal{P}^\infty(N)$ denotes the set of all $p \in \mathcal{P}(N)$ with bounded support. Denote by \mathcal{W}_1 the $(L^1 -)$ Wasserstein (or Kantorovich-Rubinstein) distance on $\mathcal{P}^1(N)$. Let $(\Omega, \mathcal{F}, \mathbb{P})$ be an arbitrary probability space and $X : \Omega \rightarrow N$ a *strongly*¹ measurable map. It defines a probability measure $X_*\mathbb{P} \in \mathcal{P}(N)$, called the *push forward measure* of \mathbb{P} under X , by

$$X_*\mathbb{P}[A] \stackrel{\text{def.}}{=} \mathbb{P}[X^{-1}(A)] = \mathbb{P}[\omega \in \Omega : X(\omega) \in A], \quad \forall A \in \mathcal{B}(N).$$

In probabilistic language, a strongly measurable map $X : \Omega \rightarrow N$ is called N -valued *random variable*, the push forward measure $X_*\mathbb{P}$ is called *distribution* of X and denoted by \mathbb{P}_X . In particular $\mathbb{P}_X \in \mathcal{P}^\theta(N) \Leftrightarrow X \in L^\theta(\Omega, N)$ where $L^\theta(\Omega, N)$ denotes the set of all (strongly) measurable maps $f : \Omega \rightarrow N$ such that $\int_\Omega d^\theta(x, f(\omega))\mathbb{P}(d\omega) < \infty$ for some (and hence all) $x \in N$. We have the following

Proposition 3 (Existence of barycenters (Proposition 4.3 in Sturm (2003))) Let (N, d) be a global NPC space and fix $y \in N$. For each $q \in \mathcal{P}^1(N)$ there exists a unique point $z \in N$ which minimizes the continuous function $z \mapsto \int_N [d^2(z, x) - d^2(y, x)] q(dx)$. This point is independent of y : it is called *barycenter* (or, more precisely, d^2 -barycenter) of q and denoted by

$$\beta(q) = \operatorname{argmin}_{z \in N} \int_N [d^2(z, x) - d^2(y, x)] q(dx).$$

If $q \in \mathcal{P}^2(N)$, then $\beta(q) = \operatorname{argmin}_{z \in N} \int_N d^2(z, x) q(dx)$.

As an example, if $q = \delta_{x_0}$, then trivially $\beta(q) = x_0$. For $X \in L^1(\Omega, N)$ we define its *expectation* by

$$\mathbb{E}[X] \stackrel{\text{def.}}{=} \operatorname{argmin}_{z \in N} \mathbb{E}[d^2(z, X) - d^2(y, X)] = \beta(\mathbb{P}_X).$$

That is, $\mathbb{E}[X]$ is the unique minimizer of the function $z \mapsto \int_N [d^2(z, x) - d^2(y, x)]\mathbb{P}_X(dx)$ on N (for each fixed $y \in N$). We recall the following:

Theorem 4 (Fundamental contraction property; (Sturm, 2003, Theorem 6.3))) For any given $p, q \in \mathcal{P}^1(N)$ it holds

$$d(b(p), b(q)) \leq \mathcal{W}_1(p, q). \tag{2.1}$$

1. Given a measurable space (M, \mathcal{M}) and (N, d) a metric space, a map $f : M \rightarrow N$ is called *strongly measurable* iff it is $\mathcal{M}/\mathcal{B}(N)$ measurable and has separable range $f(M)$.

3 Problem Setting

In this paper, for a fixed $T \in \mathbb{N}_+$ we consider a discrete-time stochastic process $X. = (X_t)_{t=0}^T \subset \mathbb{R}^d$, which evolves according to the following dynamics:

$$X_{t+1} = X_t + \text{Drift}(t, X_{[0:t]}) + \text{Diffusion}(t, X_{[0:t]}, \mathbf{S}_{[0:t]})W_t, \quad t = 0, \dots, T-1. \quad (\text{Volterra})$$

In the previous equation, $W. \stackrel{\text{def.}}{=} (W_t)_{t=0}^{T-1}$ is a Gaussian white-noise, i.e. an i.i.d. collection of \mathbb{R}^d -valued standard normal random variables defined on a probability space $(\Omega, \mathcal{F}, \mathbb{P})$, and $\mathbf{S}. \stackrel{\text{def.}}{=} (S_t)_{t=0}^{T-1}$ is a symmetric matrix-valued stochastic process independent of $W.$, and $X_0 = x_0 \in \mathbb{R}^d$. In this set-up, the direction and random fluctuations of the process $X.$, depend on its realized path and the path of a *latent (unobservable) stochastic factor* $\mathbf{S}.$

We focus on the case of discrete-time Volterra processes with non-singular diffusion. Let $\text{Sym}(d)$ (resp. $\text{Sym}_+(d)$) denote the set of $d \times d$ symmetric (resp. symmetric and positive definite) matrices with real entries. We will call a function whose best Lipschitz constant is at most L an L -Lipschitz function. A Volterra process with non-singular diffusion is a discrete-time stochastic process with $\text{Drift} : \mathbb{R} \times \mathbb{R}^{d(t+1)} \rightarrow \mathbb{R}^d$, and $\text{Diffusion} : \mathbb{R} \times \mathbb{R}^{d(t+1)} \times (\text{Sym}(d))^{t+1} \rightarrow \text{Sym}_+(d)$ satisfying:

$$\begin{aligned} \text{Drift}(t, x_{[0:t]}) &\stackrel{\text{def.}}{=} \sum_{r=0}^t \kappa(t, r) \mu(t, x_r), \\ \text{Diffusion}(t, x_{[0:t]}, s_{[0:t]}) &\stackrel{\text{def.}}{=} \exp\left(\frac{1}{2} \sum_{r=0}^t \kappa(t, r) [\sigma(t, x_r) + s_r]\right), \end{aligned} \quad (3.1)$$

for all $t \in \mathbb{N}_+$, $x_{[0,t]} \in \mathbb{R}^{d(t+1)}$, and $s_{[0,t]} \in (\text{Sym}(d))^{t+1}$. Here \exp denotes the matrix exponential, $\mu : \mathbb{R}^{1+d} \rightarrow \mathbb{R}^d$, $\sigma : \mathbb{R}^{1+d} \rightarrow \text{Sym}(d)$ are L_μ -Lipschitz and L_σ -Lipschitz functions respectively and the *Volterra kernel* κ is a real-valued function satisfying certain properties which we will describe below.

If the process $\mathbf{S}.$ is \mathbb{P} -a.s. equal to 0 then, we observe that for each time $t \in \mathbb{N}_+$ and each path $x_{[0:t]} \in \mathbb{R}^{(1+t)d}$ realized by the process $X.$ up to time t , the distribution of X_{t+1} conditioned on $X_{[0:t]} = x_{[0:t]}$ is *Gaussian* with mean $x_t + \text{Drift}(t, x_{[0:t]})$ and covariance equal to $\text{Diffusion}(t, x_{[0:t]}, \mathbf{0})^2 = \exp\left(\sum_{r=0}^t \kappa(t, r) \sigma(t, x_r)\right)$.

The *(discrete-time) Volterra kernel* in Equation (3.1) determines the persistence of $X.$'s memory on the distant past. A Volterra kernel is defined to be a map $\kappa : \{(t, r) : t, r \in \mathbb{N} \text{ and } r \leq t\} \rightarrow [0, 1]$ satisfying

$$0 < \sum_{r=0}^t \kappa(t, r) \leq 1 \text{ and } \kappa(t, 0) = 0$$

whenever $t > 0$. We typically require that the Volterra kernel satisfies either one of the following decay conditions

- i. **Exponential decay:** For some $0 < \alpha < 1$ and $C > 0$, $\kappa(T, r) \leq C \alpha^{T-r}$ for all integers $0 \leq r \leq T$;
- ii. **Polynomial decay:** For some $\alpha < -1$, $C > 0$, $\kappa(T, r) \leq C(T-r)^\alpha$ for all integers $0 \leq r < T$.

We define the “tangential version” of the Diffusion map via the matrix logarithm

$$\text{diffusion}(t, x_{[0:t]}, s_{[0:t]}) \stackrel{\text{def.}}{=} \log\left(\text{Diffusion}(t, x_{[0:t]}, s_{[0:t]})\right) = \frac{1}{2} \sum_{r=0}^t \kappa(t, r) [\sigma(t, x_r) + s_r],$$

where the uniqueness of the choice of branch, in this case the logarithm, is discussed in Appendix C.2. The intuition is that the inverse Riemannian exponential map at $\mathcal{N}(0, I_d)$ on the submanifold of \mathcal{N}_d of mean 0 normal distributions coincides with the matrix logarithm². The stochastic diffusion factor $s_{[0:t]}$ will be a realization of a $\text{Sym}(d)$ -valued stochastic process $\mathbf{S}_\cdot \stackrel{\text{def.}}{=} (\mathbf{S}_t)_{t=0}^{T-1}$ on $(\Omega, \mathcal{F}, \mathbb{P})$. We require that the stochastic $\text{Sym}(d)$ -valued process and the diffusive factor σ satisfy the following conditions.

Assumption 5 (Uniformly bounded stochastic factor) *We assume there is a constant $R > 0$ satisfying*

$$\sup_{t \leq T-1} \|\mathbf{S}_t\|_F \leq R, \quad \mathbb{P} - a.s. \quad (3.2)$$

where $\|\cdot\|_F$ denotes the Frobenius norm of a matrix, and that there is $M > 0$ such that

$$\sup_{t \leq T-1, x \in \mathbb{R}^d} \|\sigma(t, x)\|_F \leq M.$$

Remark 6 *Assumption 5 is required for the existence of a barycenter map. Though this boundedness assumption is a bit strong, it can potentially be relaxed to an exponentially decaying moment's assumption in technical future work.*

We now provide an example concerning discretization of stochastic delay differential equations that fit into our framework.

Example 1 (Stochastic delay differential equations) *Considered a filtered probability space $(\Omega, \mathcal{A}, (\mathcal{A}_u)_{u \in [0, \mathcal{T}]}, \mathbb{P})$ satisfying the usual assumptions and carrying a standard one-dimensional Wiener process $W(u)$ (u denotes the time-variable here). Let $f : \mathbb{R} \rightarrow \mathbb{R}$ and $g : \mathbb{R} \rightarrow \mathbb{R}_{>0}$ be bounded and Lipschitz continuous functions. Fix a time delay $\tau > 0$ and let $\psi(u)$ be an \mathcal{A}_0 -measurable $C([-\tau, 0], \mathbb{R})$ valued random variable satisfying $\mathbb{E}[\|\psi\|_\infty^2] < \infty$. Consider the following stochastic delay differential equation*

$$X(u) = X(0) + \int_0^u f(X(s - \tau))ds + \int_0^u g(X(s - \tau))dW(s)$$

for $0 \leq u \leq \mathcal{T}$ and with $X(u) = \psi(u)$ for $-\tau \leq u \leq 0$ (for further details see e.g. [Buckwar \(2000\)](#)). We consider a grid with a uniform step h on the interval $[0, \mathcal{T}]$ and $h = \mathcal{T}/N$, $u_t = th$, $t = 0, \dots, N$, and assume that there is an integer N_τ such that $\tau = hN_\tau$. The Euler-Maruyama scheme is

$$\tilde{X}_{t+1} = \tilde{X}_t + hf(\tilde{X}_{t-N_\tau}) + g(\tilde{X}_{t-N_\tau})\Delta W_{t+1}, \quad 0 \leq t \leq N-1 \quad (3.3)$$

where $\tilde{X}_{t-N_\tau} := \psi(u_t - \tau)$ for $t - N_\tau \leq 0$, and $\Delta W_{t+1} := W((t+1)h) - W(nh) \sim N(0, h)$ are independent.

Consider an identically zero stochastic factor \mathbf{S} , setting $\kappa(t, r) = 0$ for $r \neq t - N_\tau \geq 0$ and $\kappa(t, r) = 1$ for $r = t - N_\tau \geq 0$, $\mu(x) := hf(x)$ and $\sigma(x) = 2h \log g(x)$, from which we see that the discretization in (3.3) falls within our framework.

Nice applications involving stochastic differential are linked to, e.g., problems of optimal advertising under uncertainty for the introduction of a new product to the market ([Gozzi et al. \(2005\)](#)), some infinite-dimensional variants of the Black-Scholes equation for the fair price of an option ([Fuhrman et al. \(2010\)](#) and [Chang and Youree \(2007\)](#)), stochastic control problem with delay arising in a pension fund models ([Federico \(2011\)](#)).

2. See (3.10) in Proposition 7.

3.1 A Globally NPC perturbation of the Fisher geometry for Gaussian measures

Our target Riemannian (statistical) manifold of interest is the set \mathcal{N}_d of non-singular Gaussian measures of a given dimension d , and formally defined below, endowed with a perturbation of the Fisher Riemannian metric (Skovgaard (1984)), whose geometry we now review. Let \mathcal{N}_d be the collection of non-degenerate normal distributions of fixed dimension d , *i.e.*

$$\mathcal{N}_d \stackrel{\text{def.}}{=} \{\mathcal{N}_d(\mathbf{m}, \Sigma) : \mathbf{m} \in \mathbb{R}^d \text{ and } \Sigma \in \text{Sym}_+(d)\}, \quad (3.4)$$

where, we recall, $\text{Sym}_+(d)$ is the set of $d \times d$ positive definite symmetric matrices. Thus, $\mathcal{N}_d(\mathbf{m}, \Sigma)$ has Lebesgue density given by

$$p_{\mathbf{m}, \Sigma}(u) = \frac{e^{-\frac{1}{2}(u-\mathbf{m})^\top \Sigma^{-1}(u-\mathbf{m})}}{\sqrt{(2\pi)^d \det(\Sigma)}}, \quad u \in \mathbb{R}^d.$$

Through the identification

$$\varphi(\mathcal{N}_d(\mathbf{m}, \Sigma)) = ((\mathbf{m}_i)_{i=1}^d, (\Sigma_{ij})_{i \leq j}), \quad (3.5)$$

where $\mathbf{m} = (\mathbf{m}_1, \dots, \mathbf{m}_d)^\top$, $\Sigma = (\Sigma_{ij})_{i,j=1}^d$, we see that \mathcal{N}_d is isomorphic to an open subset $\Theta \subset \mathbb{R}^m$, $m = (d^2 + 3d)/2$. Hence, \mathcal{N}_d can be considered as a differentiable manifold of dimension m , with (\mathcal{N}_d, φ) as a global chart. We define a basis, in this coordinate system, of the set of vector fields on \mathcal{N}_d

$$\frac{\partial}{\partial \mathbf{m}_i}, \quad i = 1, \dots, d, \quad \frac{\partial}{\partial \Sigma_{ij}}, \quad i, j = 1, \dots, d, \quad i \leq j.$$

We identify these vector fields with the vectors and matrices

$$\begin{aligned} \frac{\partial}{\partial \mathbf{m}_i} &\leftrightarrow e_i \in \mathbb{R}^d, \quad i = 1, \dots, d, \\ \frac{\partial}{\partial \Sigma_{ij}} &\leftrightarrow E_{ij} \in \text{Sym}_+(d), \quad i, j = 1, \dots, d, \quad i \leq j, \end{aligned}$$

where $(e_i)_i$ is the canonical basis of \mathbb{R}^d and

$$E_{ij} \stackrel{\text{def.}}{=} \begin{cases} I_{(i,j)}, & i = j \\ I_{(i,j)} + I_{(j,i)}, & i \neq j, \end{cases}$$

where $I_{(i,j)}$ denotes the $d \times d$ matrix whose (i, j) -th entry is equal to 1, while all the remaining entries are zero. Therefore, each smooth vector field A on \mathcal{N}_d can be decomposed as

$$A = \sum_{i=1}^d F_i e_i + \sum_{\substack{i, j=1 \\ i \leq j}}^d G_{ij} E_{ij}$$

where $F_i, G_{ij} : \mathcal{N}_d \rightarrow \mathbb{R}$ are smooth functions. We shall call the two terms in this last equation the components of A in the \mathbf{m} - and Σ -direction, respectively. The space \mathcal{N}_d can be turned into a Riemannian manifold by using the Fisher information as its Riemannian metric. More precisely, we define at an arbitrary point (\mathbf{m}, Σ) the following Riemannian metric \mathcal{I}^F

$$\begin{aligned} \mathcal{I}^F \left(\frac{\partial}{\partial \mathbf{m}_i}, \frac{\partial}{\partial \mathbf{m}_j} \right) &\equiv \mathcal{I}^F(e_i, e_j) \stackrel{\text{def.}}{=} \Sigma^{ij}, \\ \mathcal{I}^F \left(\frac{\partial}{\partial \mathbf{m}_i}, \frac{\partial}{\partial \Sigma_{kl}} \right) &\equiv \mathcal{I}^F(e_i, E_{kl}) \stackrel{\text{def.}}{=} 0, \\ \mathcal{I}^F \left(\frac{\partial}{\partial \Sigma_{ij}}, \frac{\partial}{\partial \Sigma_{kl}} \right) &\equiv \mathcal{I}^F(E_{ij}, E_{kl}) \stackrel{\text{def.}}{=} \frac{1}{2} \text{tr}(\Sigma^{-1} E_{ij} \Sigma^{-1} E_{kl}) = \Sigma^{il} \Sigma^{jk} + \Sigma^{ik} \Sigma^{jl}, \end{aligned} \quad (3.6)$$

for $i, j, k, l = 1, \dots, d$, $i \leq j$ and $k \leq l$; where $\Sigma^{-1} = (\Sigma^{ij})_{i,j=1}^d$ denotes the inverse of Σ , and tr is the trace operator. From the last equation, by the bilinearity of the metric \mathcal{I}^F , we see that

$$\mathcal{I}^F(X, Y) = \frac{1}{2} \text{tr}(\Sigma^{-1} X \Sigma^{-1} Y), \quad X, Y \in \text{Sym}(d). \quad (3.7)$$

Though the Fisher metric is the canonical Riemannian metric on the smooth manifold \mathcal{N}_d , in the sense of Chentsov's Theorem (Csiszár, 1984; Dowty, 2018) from information geometry, its geometry is not amenable to intrinsically averaging in dimension above 1. When $d > 1$ the Fisher geometry on \mathcal{N}_d exhibits positive sectional curvature along tangent planes in the directions spanned by $\frac{\partial}{\partial \mathbf{m}_i}$ and $\frac{\partial}{\partial \mathbf{m}_j}$ for distinct $i, j = 1, \dots, d$ (see (Skovgaard, 1984, Theorem 2.2)). These directions of positive sectional curvature do not exist in univariate setting, since no such tangent plane exist when $d = 1$, and the only tangent plane at any point is generated by $\frac{\partial}{\partial \mathbf{m}_1}$ and $\frac{\partial}{\partial \Sigma_{1,1}}$ whose sectional curvature equals $-1/2$; this leads to the well-known identification of the Fisher geometry on \mathcal{N}_1 with that of the hyperbolic plane.

As we have learnt above from the results of Sturm (2003), lack of globally NPC on the Fisher geometry of \mathcal{N}_d for $d > 1$ makes it unsuitable to intrinsic averaging. Furthermore, there are no known closed-form expressions for the geodesic distance and for the Riemannian exponential map about any point for Fisher geometry on \mathcal{N}_d , in dimension larger than 1. Both these limitations make the Fisher geometry on \mathcal{N}_d incompatible with the available tools for probability theory on NPC spaces and approximation theory between Riemannian manifold (Kratsios and Papon (2022)). In light of this, we perturb the Fisher metric (3.6) as follows

$$\begin{aligned} \mathfrak{I}\left(\frac{\partial}{\partial \mathbf{m}_i}, \frac{\partial}{\partial \mathbf{m}_j}\right) &= \delta_{ij}, \\ \mathfrak{I}\left(\frac{\partial}{\partial \mathbf{m}_i}, \frac{\partial}{\partial \Sigma_{kl}}\right) &= 0, \\ \mathfrak{I}\left(\frac{\partial}{\partial \Sigma_{ij}}, \frac{\partial}{\partial \Sigma_{kl}}\right) &= \frac{1}{2} \text{tr}(\Sigma^{-1} E_{ij} \Sigma^{-1} E_{kl}) = \Sigma^{il} \Sigma^{jk} + \Sigma^{ik} \Sigma^{jl}, \end{aligned} \quad (3.8)$$

for $i, j, k, l = 1, \dots, d$, $i \leq j$ and $k \leq l$, where δ denotes the standard Riemannian metric of \mathbb{R}^d . Besides being a non-positively curved perturbation of the geometry induced by Fisher metric, which also has a closed-form distance function, the Riemannian metric \mathfrak{I} has a second simple geometric interpretation. Namely, $(\mathcal{N}_d, \mathfrak{I})$ is isometric as a Riemannian manifold to $\mathbb{R}^d \times \text{Sym}_+(d)$ equipped with the product between the Euclidean metric δ on \mathbb{R}^d and the well-studied affine-invariant metric on $\text{Sym}_+(d)$, see Smith (2005); Pennec et al. (2006); Schiratti et al. (2017); Brooks et al. (2019); Criscitiello and Boumal (2022). Some of the key geometric properties of $(\mathcal{N}_d, \mathfrak{I})$ can now be recorded. Below, $d_{\mathfrak{I}}$ will denote the distance function induced by \mathfrak{I} .

Proposition 7 (The geometry of $(\mathcal{N}_d, \mathfrak{I})$) *For any $d \geq 1$, $(\mathcal{N}_d, d_{\mathfrak{I}})$ is a complete, path-connected and simply connected, Riemannian manifold with sectional curvatures in $[-1/2, 0]$. Therefore, $(\mathcal{N}_d, d_{\mathfrak{I}})$ is a global NPC space, and for any $\mathcal{N}_d(\mathbf{m}_0, \Sigma_0), \mathcal{N}_d(\mathbf{m}_1, \Sigma_1) \in \mathcal{N}_d$, $d_{\mathfrak{I}}$ admits the closed-form expression*

$$d_{\mathfrak{I}}(\mathcal{N}_d(\mathbf{m}_0, \Sigma_0), \mathcal{N}_d(\mathbf{m}_1, \Sigma_1)) = \left[\|\mathbf{m}_0 - \mathbf{m}_1\|_2^2 + \frac{1}{2} \sum_{i=1}^d \ln(\lambda_i)^2 \right]^{1/2}, \quad (3.9)$$

where $0 < \lambda_1 \leq \dots \leq \lambda_d$ are the eigenvalues of $\Sigma_0^{-1} \Sigma_1$.

For any $\mathbf{m} \in \mathbb{R}^d$, $\Sigma \in \text{Sym}_+(d)$, and any $(\tilde{\mathbf{m}}, X) \in T_{\mathcal{N}_d(\mathbf{m}, \Sigma)} \mathcal{N}_d \cong \mathbb{R}^d \times \text{Sym}(d)$ the Riemannian exponential map is given by

$$\text{Exp}_{\mathcal{N}_d(\mathbf{m}, \Sigma)}(\tilde{\mathbf{m}}, X) = \mathcal{N}\left(\mathbf{m} + \tilde{\mathbf{m}}, \Sigma^{1/2} \exp(\Sigma^{-1/2} X \Sigma^{-1/2}) \Sigma^{1/2}\right), \quad (3.10)$$

where $T_{\mathcal{N}_d(\mathbf{m}, \Sigma)} \mathcal{N}_d$ denotes the tangent space of \mathcal{N}_d at the point $\mathcal{N}_d(\mathbf{m}, \Sigma)$.

■

Proof See Appendix D.1.1.

3.1.1 COMPARISON WITH OTHER GEOMETRIES ON \mathcal{N}_d

We may further motivate the proposed Riemannian geometry on \mathcal{N}_d by contrasting it with other standard geometries on the set \mathcal{N}_d , occurring in optimal transport and information geometry. Our discussion is summarized concisely in Table 1.

Table 1: Comparison of topological, metric, and computational properties between different geometries of non-singular Gaussian measures from information geometry and optimal transport.

Geometry	Complete	NPC (Barycenters)	Closed-Form Dist.	Isometric Copies ($\mathcal{N}_d^m, \mathcal{I}$)	Reference
$(\mathcal{N}_d, d_{\mathfrak{J}})$	✓	✓	✓	✓	Equation (3.8)
$(\mathcal{N}_d, d_{\mathcal{I}})$	✓	✗ (✓ $d = 1$)	✗	✓	Skovgaard (1984)
$(\mathcal{N}_d, \mathcal{W}_2)$	✗	?	✓	✗	Takatsu (2011)
(\mathcal{N}_d, g_{SL})	✓	✓	✓	✗	Lovrić et al. (2000)

In what follows, we linearly identify the spaces via the symmetrization map sym defined by

$$\text{sym} : \mathbb{R}^{d(d+1)/2} \rightarrow \text{Sym}(d), \quad v \mapsto \begin{pmatrix} v_1 & v_2 & \dots & v_d \\ v_2 & v_{d+1} & & \cdot \\ \vdots & & \ddots & \vdots \\ v_d & \dots & & v_{d(d+1)/2} \end{pmatrix} \quad (3.11)$$

whose inverse is often denoted by vec (see (Petersen et al., 2008, Section 10.2.2)). We observe that the linear identification is not an isometry, but it is a bi-Lipschitz map, when $\text{Sym}(d)$ is equipped with Fröbenius inner-product $\langle \Sigma_1, \Sigma_2 \rangle \stackrel{\text{def.}}{=} \text{tr}(\Sigma_1 \Sigma_2)$ and $\mathbb{R}^{d(d+1)/2}$.

Table 1 compares the Riemannian geometry $(\mathcal{N}_d, \mathfrak{J})$ with alternative geometries found in the literature. Specifically, it contrasts $(\mathcal{N}_d, \mathfrak{J})$ with the standard Fisher information geometry as studied in Skovgaard (1984), the Riemannian geometry inducing the 2-Wasserstein metric (\mathcal{W}_2) on \mathcal{N}_d as presented in Takatsu (2011), and a non-positive curvature geometry on \mathcal{N}_d , denoted g_{SL} , constructed in Lovrić et al. (2000) by identifying \mathcal{N}_d with a subset of a special linear group, modulo the action of a special orthogonal group. The columns of Table 1 should be self-explanatory apart from the penultimate column. Here we say that the geometry admits isometric copies of $(\mathcal{N}_d, \mathcal{I})$ if for each $\mathfrak{m} \in \mathbb{R}^d$, the submanifold $\mathcal{N}_d^m \subset \mathcal{N}_d$ whose points have mean \mathfrak{m} is isometric to $(\mathcal{N}_d^m, \mathcal{I})$.

Finally, we remark that the the manifolds $(\mathcal{N}_d, \mathcal{W}_2)$, $(\mathcal{N}_d, \mathfrak{J})$, and $(\mathcal{N}_d, \mathcal{I})$ are diffeomorphic; in particular, their topologies coincide. Nevertheless, we emphasize that all three structures are different as Riemannian manifolds and as metric spaces.

4 Gaussian random projections

The law of the process X in (Volterra), conditioned on any realized path up to a given time $t \in \mathbb{N}$, is an arbitrary probability distribution on \mathbb{R}^d with a priori no favourable structure. For instance, the space of probability distribution on \mathbb{R}^d , e.g. with the Lévy-Prokhorov metric, see e.g. (Bogachev, 2007, Theorem 8.3.2), is neither a finite-dimensional as a topological space nor is it a vector space (even though it is convex). This lack of structure implies that its elements cannot be approximated by simpler probability measures, such as finitely supported measures, without facing the curse of dimensionality (see, e.g. (Graf and Luschgy, 2000, Theorem 6.2)).

Intuitive idea However, if we had access to the unobserved realized path of the “stochastic factor process” $\mathbf{S}_{[0:t]}$, we could leverage the fact that X_{t+1} is Gaussian when conditioned on the realized path $X_{[0:t]}$ and belongs to \mathcal{N}_d , the smooth manifold of non-singular d -dimensional Gaussian measures. This motivates the family of probability measures $\{\Lambda_{x_{[0:t]}, s_{[0:t]}}; x_{[0:t]} \in \mathbb{R}^{(1+t)d}, s_{[0:t]} \in \text{Sym}(d)^{1+t}\} \subset \mathcal{N}_d$, defined by

$$\Lambda_{x_{[0:t]}, s_{[0:t]}}[\cdot] \stackrel{\text{def.}}{=} \mathbb{P}[X_{t+1} \in \cdot | X_{[0:t]} = x_{[0:t]}, \mathbf{S}_{[0:t]} = s_{[0:t]}], \quad x_{[0:t]} \in \mathbb{R}^{(1+t)d}, s_{[0:t]} \in \text{Sym}(d)^{1+t} \quad (4.1)$$

but since the process \mathbf{S}_{\cdot} is latent, we need to reintroduce its “random effects” into the family of probability measures $\Lambda_{x_{[0:t]}, s_{[0:t]}}$. Traditionally, this is achieved by integrating against the law of $\mathbf{S}_{[0:t]}$. Informally, we instead reinsert the observed path $\mathbf{S}_{[0:t]}$ as the conditional state $s_{[0:t]}$, *i.e.*:

$$\mathbb{Q}_{x_{[0:t]}}(\omega) \stackrel{\text{informal}}{=} \Lambda_{x_{[0:t]}, \mathbf{S}_{[0:t]}(\omega)}, \quad \omega \in \Omega. \quad (4.2)$$

A rigorous construction of (4.2), formalized below in Definition 8, hinges on our Riemannian geometry on \mathcal{N}_d and it enjoys Lipschitz stability, meaning that it is a Lipschitz function of path realized by the process X_{\cdot} . In some cases, the dependence of $\mathbb{Q}_{x_{[0:t]}}$ on the realized path of X_{\cdot} is even smooth, meaning that deep learning model can approximate it with a feasible number of parameters. This is generally not true with geometric deep learning models on non-smooth metric spaces, see [Acciaio et al. \(2023\)](#). The results of [Sturm \(2003\)](#) guarantee that there is a unique point $\Pi_{x_{[0:t]}}$ in \mathcal{N}_d which best represents the intrinsic average behaviour of $\mathbb{Q}_{x_{[0:t]}}$

$$\Pi_{x_{[0:t]}} \stackrel{\text{def.}}{=} \operatorname{argmin}_{u \in \mathcal{N}_d} \int_{v \in \mathcal{N}_d} d_{\mathfrak{J}}^2(u, v) \text{Law}(\mathbb{Q}_{x_{[0:t]}} \in dv), \quad (4.3)$$

where $d_{\mathfrak{J}}$ is the *geodesic distance* induced by our perturbation of the Fisher Riemannian metric on \mathcal{N}_d . Unlike information projections, the map defined by (4.3) enjoys the following stability properties and can even be smooth in certain cases.

Informal Results 1 (Gaussian projections Theorem) *Under mild conditions, if the Drift and Diffusion maps in (Volterra) are L -Lipschitz, then the map $x_{[0:t]} \mapsto \Pi_{x_{[0:t]}}$ is well-defined, $\mathcal{O}(L)$ -Lipschitz, and it solves the following minimization problem*

$$\Pi_{x_{[0:t]}} = \operatorname{argmin}_{\mu \in \mathcal{N}_d} \mathbb{E}[d_{\mathfrak{J}}^2(\mu, \mathbb{Q}_{x_{[0:t]}})]$$

Furthermore, if the latent factor process $\mathbf{S}_{\cdot} = 0$ then

$$\Pi_{x_{[0:t]}} = \mathbb{P}[X_{t+1} \in \cdot | X_{[0:t]} = x_{[0:t]}]$$

for each time $t \in \mathbb{N}_+$ and every realized path $x_{[0:t]} \in \mathbb{R}^{(1+t)d}$.

We now formalize our notion of projection of the conditional law of the stochastic process (Volterra), called a *Gaussian random projection*. The terminology should not be understood in the sense of the Johnson-Lindenstrauss lemma, see ([Matoušek, 2002](#), Theorem 12.2.1), but rather in the sense of [Ohta \(2009\)](#). That is, as a Lipschitz measure-valued function with the property that a certain class of inputs are fixed in certain sense (see Corollary 10).

4.1 Encoding the conditional distribution of a Volterra process in \mathcal{N}_d

Our argument centers around the geometry of the regular conditional distribution (RCD) function sending any $(x_{[0:t]}, s_{[0:t]})$ to

$$\mathbb{P}[X_{t+1} \in \cdot | X_{[0:t]} = x_{[0:t]}, \mathbf{S}_{[0:t]} = s_{[0:t]}].$$

Our first observation is to note that the RCD's image lies in \mathcal{N}_d .

The map $\tilde{\varphi} : \mathcal{N}_d \rightarrow \mathbb{R}^d \times \mathbb{R}^{d(d+1)/2}$, defined by $\mathcal{N}_d(\mathbf{m}, \Sigma) \xrightarrow{\tilde{\varphi}} (\mathbf{m}, \text{vec}(\log(\Sigma)))$, is a smooth chart. This is because it is the composition of the maps $1_{\mathbb{R}^d} \times \text{vec}$, $\mathbb{R}^d \times \text{Sym}(d)$, \log^3 , $1_{\mathbb{R}^d} \times \log$ and φ , defined in (3.5), each of which are diffeomorphisms. Thus,

$$\begin{aligned} \psi : \mathbb{R}^{d(d+3)/2} &\rightarrow \mathcal{N}_d \\ (u, v) &\mapsto \tilde{\varphi}^{-1}(u, v) = \mathcal{N}_d(u, \exp(\text{sym}(v))) \end{aligned} \tag{4.4}$$

defines a smooth global chart on \mathcal{N}_d . For every $t \in \mathbb{N}_+$, the maps

$$\begin{aligned} \mathbb{R}^{(1+t)d} &\ni x_{[0:t]} \mapsto \text{Drift}(t, x_{[0:t]}) \in \mathbb{R}^d \\ \mathbb{R}^{(1+t)d} \times \text{Sym}(d)^{(1+t)} &\ni (x_{[0:t]}, s_{[0:t]}) \mapsto \text{Diffusion}(t, x_{[0:t]}, s_{[0:t]}) \in \text{Sym}_+(d) \end{aligned}$$

are locally Lipschitz continuous. Thus, for every $t \in \mathbb{N}_+$, the map

$$\mathbb{R}^{(1+t)d} \times \mathbb{R}^{(1+t)d(d+1)/2} \ni (x_{[0:t]}, y_{[0:t]}) \mapsto \text{Diffusion}(t, x_{[0:t]}, \text{sym}(y_{[0:t]})) \in \text{Sym}_+(d),$$

where sym is applied componentwise, is locally Lipschitz continuous. Thus, for every $t \in \mathbb{N}_+$ the map $\Psi_t : \mathbb{R}^{(1+t)d} \times \mathbb{R}^{(1+t)d(d+1)/2} \rightarrow \mathcal{N}_d$ defined for any $x_{[0:t]} \in \mathbb{R}^{(1+t)d}$ and $y_{[0:t]} \in \mathbb{R}^{(1+t)d(d+1)/2}$ by

$$\begin{aligned} \Psi_t(x_{[0:t]}, y_{[0:t]}) &\stackrel{\text{def.}}{=} \psi(x_t + \text{Drift}(t, x_{[0:t]}), \text{vec} \circ \log \circ \text{Diffusion}(t, x_{[0:t]}, \text{sym}(y_{[0:t]}))) \\ &= \mathcal{N}_d \left(x_t + \text{Drift}(t, x_{[0:t]}), \exp \left(\sum_{r=0}^t \kappa(t, r) [\sigma(t, x_r) + \text{sym}(y_r)] \right) \right) \end{aligned} \tag{4.5}$$

must also be locally-Lipschitz when \mathcal{N}_d is equipped with the Riemannian distance function $d_{\mathfrak{J}}$. Note that $\text{Diffusion}(t, x_{[0:t]}, \text{sym}(s_{[0:t]}))$ is positive definite. Therefore we can assume that its eigenvalues are such that $0 < \lambda_1 \leq \dots \leq \lambda_d$. Furthermore, if μ and σ are smooth, then each Ψ_t is also smooth by composition. Consequently, we may rigorously define the \mathcal{N}_d -valued stochastic process as the composition of $x_{[0:t]}$ and $\mathbf{S}_{[0:t]}$ and the locally Lipschitz continuous map Ψ_t , namely $\Psi_t(x_{[0:t]}, \text{vec} \circ \mathbf{S}_{[0:t]})$.

We note that $\|e^A\|_{op} \leq e^{\|A\|_{op}}$ for any $d \times d$ matrix A ; hence, for some universal constants $c_1, c_2 > 0$ depending only d , $\|e^A\|_F \leq c_1 e^{c_2 \|A\|_F}$; therefore the boundedness of S and the image of σ in Assumption 5 imply that the law of $\Psi_t(x_{[0:t]}, \text{vec} \circ \mathbf{S}_{[0:t]})$ is compactly supported on \mathcal{N}_d . Therefore, $\Psi_t(x_{[0:t]}, \text{vec} \circ \mathbf{S}_{[0:t]})$ is integrable over the global NPC space $(\mathcal{N}_d, d_{\mathfrak{J}})$, in the sense that it belongs to $L^1(\Omega, \mathcal{N}_d)$, and the barycenter of its law is well-defined.

Definition 8 (Gaussian random projection of X .) Given a Volterra process X in (3.1), we define the Gaussian Random projection of X as the map, sending any $x_{[0:t]} \in \mathbb{R}^{(1+t)d}$ to the measure $\Pi_{x_{[0:t]}} \in \mathcal{N}_d$ defined by

$$\Pi_{x_{[0:t]}} \stackrel{\text{def.}}{=} \beta(\text{Law}(\Psi_t(x_{[0:t]}, \text{vec}(\mathbf{S}_{[0:t]})))) \in \mathcal{N}_d \tag{4.6}$$

where β is given in Proposition 3. For the sake of brevity, we will henceforth write $\Pi_{x_{[0:t]}} = \beta(\mathbb{Q}_{x_{[0:t]}})$, where $\mathbb{Q}_{x_{[0:t]}} \stackrel{\text{def.}}{=} \text{Law}(\Psi_t(x_{[0:t]}, \text{vec}(\mathbf{S}_{[0:t]})))$.

In particular, notice that if we have $\mathbf{S}_{[0:t]} = s_{[0:t]}$, then

$$\Pi_{x_{[0:t]}} = \mathcal{N}_d(x_t + \text{Drift}(t, x_{[0:t]}), \text{Diffusion}(t, x_{[0:t]}, s_{[0:t]})^2)$$

where $\text{Diffusion}(t, x_{[0:t]}, s_{[0:t]})^2 = \exp \left(\sum_{r=0}^t \kappa(t, r) [\sigma(t, x_r) + s_r] \right)$. We now have the following.

3. See (Hilgert and Neeb, 2012, Proposition 3.3.5).

Theorem 9 (Optimality and Lipschitz Stability of the Gaussian Random Projection) *Fix $t \in \mathbb{N}$ and a compact $\mathcal{K}_{[0:t]} \subseteq \mathbb{R}^{(1+t)d}$. If (3.1) and Assumption 5 hold then, $\Pi : x_{[0:t]} \mapsto \beta(\mathbb{Q}_{x_{[0:t]}})$ is well-defined and Lipschitz and*

$$\Pi_{x_{[0:t]}} = \operatorname{argmin}_{u \in \mathcal{N}_d} \int_{v \in \mathcal{N}_d} d_{\mathfrak{J}}^2(u, v) \mathbb{Q}_{x_{[0:t]}}(dv).$$

Furthermore, the Lipschitz constant of Π depends only on t and R , as defined in Assumption 5.

Proof As regards the Lipschitz part, we refer to Proposition E.5. The remainder of the proof follows from the discussion near (4.6). \blacksquare

The smooth structure on \mathcal{N}_d has the advantage of granting meaning to the smoothness of the map Π when μ and σ are smooth and $\mathbf{S}_{[0:t]}$ is almost surely constant. Smoothness is beneficial from an approximation perspective since neural networks can effectively approximate smooth Lipschitz functions between Riemannian manifolds. This is demonstrated in Theorem 13 below. In contrast, even in the Euclidean setting, non-smooth Lipschitz functions between Euclidean spaces on simple, compact subsets cannot be accurately approximated by feasible neural networks, as shown in (Yarotsky, 2017, Theorem 5).

The following Corollary provides a natural sufficient condition for the smoothness of Π . Namely, if the maps μ and σ , which define the drift and diffusion maps of the Volterra process, are smooth, and that \mathbf{S} is constantly 0 then Π is also smooth.

Proposition 10 (Smoothness) *Suppose that $\mathbf{S}_t = 0$ for every $t \in \mathbb{N}$, Assumption 5 holds and that μ and σ are of class C^∞ . Then for every $t \in \mathbb{N}$, the following map is C^∞*

$$\begin{aligned} \Pi_{\cdot} : (\mathbb{R}^{(1+t)d}, \|\cdot\|) &\rightarrow (\mathcal{N}_d, d_{\mathfrak{J}}) \\ x_{[0:t]} &\mapsto \Pi_{x_{[0:t]}}. \end{aligned}$$

Proof See Appendix E. \blacksquare

Next, we study how the Volterra kernel dictates the rate at which the Gaussian random projection forgets the distant history of any realized path of a Volterra process.

4.2 Memory decay of Π given a decaying Volterra kernel

In order for the map $x_{[0:t]} \mapsto \Pi_{x_{[0:t]}}$ to be approximable by any model which only processes the path realized by X up to the current time, we need that the stochastic Volterra process does not exhibit a persistent memory of its distant past. As one may expect, a stochastic Volterra process exhibits no persistent long-term memory if its Volterra kernel does not place large weights on long-past states realized by the process X . Similar phenomena have been observed in the RNN literature when approximating linear state-space systems with exponentially decaying impulse response in (Hutter et al., 2022) or in (Li et al., 2022b, Theorem 11) when quantifying the approximability of linear functionals by linear continuous-time RNNs. Our next result shows that if the Volterra kernels decay at least polynomially, then one has a quantitative analogue of the fading memory property in reservoir computing (Grigoryeva and Ortega, 2018, Definition 3), and of the approximable complexity property of (Acciaio et al., 2023, Definition 4.9).

Theorem 11 (Memory Decay Rate of Gaussian Projection of Volterra Process)

Suppose Assumption 5 holds and the Volterra-kernel κ either satisfies (i) or (ii). For every $T \in \mathbb{N}_+$, each compact $\mathcal{K}_{[0:T]} \subseteq \mathbb{R}^{(1+T)d}$, there is a constant $C_{M,R,\mu} > 0$ such that for every pair of integers H

and t , with $0 \leq H < t \leq T$, there is a Lipschitz function $\tilde{f}^{(t,H)} : (\mathbb{R}^{(1+H)d}, \|\cdot\|) \rightarrow (\mathcal{N}_d, d_{\mathfrak{J}})$ satisfying

$$d_{\mathfrak{J}}(\Pi_{x_{[0:t]}}, \tilde{f}^{(t,H)}(x_{[t-H:t]})) \leq C_{M,R,\mu} \operatorname{diam}(\mathcal{K}_{[0:T]}) \begin{cases} \frac{C\alpha}{\alpha-1} (\alpha^t - \alpha^H) & \text{if (i) holds} \\ C(H+1)^\alpha (t-H) & \text{if (ii) holds} \end{cases}$$

for every $x_{[0:T]} \in \mathcal{K}_{[0:T]}$. ■

Proof See Appendix E

Our next objective is to approximate the map $x_{[0:T]} \mapsto (\Pi_{x_{[0:t]}})_{t=0}^T$ while respecting the forward flow of information in time. We will accomplish this by developing a more general approximation theory for causal maps between Riemannian manifolds which are global NPC spaces.

5 Universal approximation of manifold-valued processes

In this section, we introduce our *sequential* geometric deep learning model, called the HGN and defined below in (Static). We then use it to prove a universal approximation theorem guaranteeing that the map $x_{[0:t]} \rightarrow \Pi_{x_{[0:t]}}$ can be causally (in time) approximated to arbitrary precision if the memory of the Volterra process decays at-least polynomially.

Informal Results 2 (HGNs can approximate projected RCDs) *For every time-horizon T , and every suitable process X , defined by (Volterra), for each $\varepsilon > 0$ and every compact set of inputs $\mathcal{K}_{[0:T]} \subseteq \mathbb{R}^{(1+T)d}$, there exists a HGN $F : (\mathbb{R}^d)^T \rightarrow \mathcal{M}^T$, as in Figure 2, satisfying*

$$\max_{x_{[0:T]} \in \mathcal{K}_{[0:T]}} \max_{t=T-H, \dots, T} d_g(\Pi_{x_{[0:t]}}, F(x.)_t) < \varepsilon.$$

The number of parameters and structure of the HGN depends quantitatively on $\varepsilon, H, \mathcal{K}_{[0:T]}$, and on the Drift and Diffusion, and on the Volterra kernel κ , where $H \in \mathbb{N}$ is the history of the HGN.

The main result of this section (Theorem 17) is a significant generalization of Informal Result 2, as it applies to infinite-memory dynamical systems between any pair of well-behaved non-positively curved complete Riemannian manifolds. We now present our main approximation theoretic results.

5.1 Standing Assumptions for Universal Approximation Results

In this section, we present our model and build on the theory of causal maps, as formulated in Acciaio et al. (2023), between a source and target connected Riemannian manifolds (\mathcal{N}, h) and (\mathcal{M}, g) .

Assumption 12 (Regularity of input and output manifolds) *Consider two C^∞ Riemannian manifolds (\mathcal{N}, h) and (\mathcal{M}, g) of dimensions $D \in \mathbb{N}$ and $d \in \mathbb{N}$ respectively. We assume that:*

- (i) (\mathcal{N}, h) and (\mathcal{M}, g) are geodesically complete and simply connected.
- (ii) Their sectional curvatures are bounded in $[-\kappa, 0]$ for some $\kappa > 0$.

We denote the geodesic distance on these spaces respectively by d_h and d_g . Under Assumption 12, (\mathcal{N}, d_h) and (\mathcal{M}, d_g) are complete separable metrics spaces of NPC in the sense of Sturm (2003); see Proposition 2.

Example 2 *The Euclidean space (\mathbb{R}^d, δ) satisfies Assumption 12 with $\kappa = 0$.*

Example 3 *By Proposition 7, (\mathcal{N}_d, h) satisfies Assumption 12 with $\kappa = -1/2$.*

5.2 Static Case

We begin by defining the static version of our main (dynamical) model, in which time is not yet considered. This geometric deep-learning model extends the geometric deep network of [Kratsios and Papon \(2022\)](#), thus we use the same name. From the technical standpoint, our main approximation theorem for the static case (Theorem 13) is a significant technical improvement of the main result of [Kratsios \(2023\)](#) as it has optimal rates, matching the optimal bounds of [Shen et al. \(2022\)](#) in the classical Euclidean setting when the target function is Lipschitz and/or smooth; this is an exponential improvement of the guarantees in [Kratsios \(2023\)](#) for the ReLU case. Moreover, we obtain probabilistic approximation guarantees for Borel measurable and for general functions being approximated on finite subsets of the input space. The static case will serve as the first main technical tool for our main approximation theorem for the dynamic case, (Theorem 17),

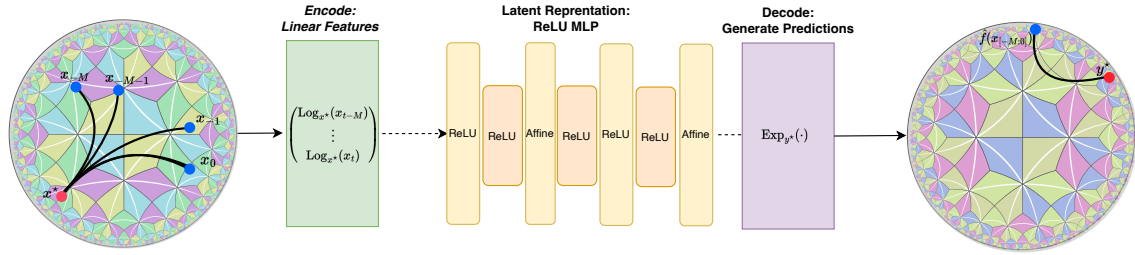


Figure 1: The GDN Model: GDN model process an input in $x_{[-M:0]} \in \mathcal{N}^{1+H}$, interpreted as sequential points x_{-M}, \dots, x_0 inputs in \mathcal{M} , in three steps: an encoding, transformation, and decoding phase. First, it linearized (purple) the inputs in \mathcal{N}^{1+H} along products of geodesics emanating from a set of reference points x_0^*, \dots, x_M^* in \mathcal{N}^{1+H} . It then transforms the linearized features and maps them to a vector v in the tangent space of \mathcal{M} using a standard ReLU-MLP (yellow). In the decoding phase (green), the model maps v to a point $\hat{f}(x_{[-M:0]})$ on \mathcal{M} by travelling geodesics in \mathcal{M} emanating from a reference point y^* therein with initial velocity v .

We now formalize the static version of our model, illustrated in Figure 1, and extend the geometric deep network (GDN) of [Kratsios and Papon \(2022\)](#). Fix $J, H \in \mathbb{N}$, with $J > 0$, and a multi-index $[\mathbf{d}] \stackrel{\text{def.}}{=} (d_0, \dots, d_J)$ with $d_0 = (1+H)D$ and $d_J = d$, and let $P([\mathbf{d}]) \stackrel{\text{def.}}{=} (1+H)D + d + \sum_{j=0}^J d_{j+1}(1+d_j)$. Weights, biases, and base-point parameters are encoded as a unique parameter $\theta \in \mathbb{R}^{P([\mathbf{d}])}$ with

$$\theta \leftrightarrow \left((A^{(j)}, b^{(j)})_{j=0}^J, (\tilde{x}_m)_{m=0}^H, \tilde{y} \right) \quad (5.1)$$

where for $j = 0, \dots, J$, $A^{(j)} \in \mathbb{R}^{d_{j+1} \times d_j}$, $b^{(j)} \in \mathbb{R}^{d_{j+1}}$, $\tilde{y} \in \mathbb{R}^d$, and $\tilde{x}_m \in \mathbb{R}^D$ for $m = 0, \dots, H$. We henceforth denote componentwise composition of the ReLU $\stackrel{\text{def.}}{=} \max\{0, \cdot\}$ activation function with any vector $u \in \mathbb{R}^n$ for any $n \in \mathbb{N}_+$, by $\text{ReLU} \bullet x \stackrel{\text{def.}}{=} (\text{ReLU}(x_i))_{i=1}^n$. Given $H \in \mathbb{N}$, a GDN model is a (parameterized) map $f_\theta : \mathbb{R}^{P([\mathbf{d}])} \times \mathcal{N}^{1+H} \rightarrow \mathcal{M}$ sending any $(\theta, x_{[0:H]}) \in \mathbb{R}^{P([\mathbf{d}])} \times \mathcal{N}^{1+H}$ to

$$\begin{aligned} f(\theta, x_{[0:H]}) &\stackrel{\text{def.}}{=} f_\theta(x_{[0:H]}) = \text{Exp}_{\bar{y}}^g \circ \iota_{\mathcal{M}, \bar{y}}^{-1}(A^{(J)}x^{(J)} + b^{(J)}) \\ &x^{(j+1)} \stackrel{\text{def.}}{=} \text{ReLU} \bullet (A^{(j)}x^{(j)} + b^{(j)}) \quad \text{for } j = 0, \dots, J-1, \\ &x^{(0)} \stackrel{\text{def.}}{=} \left(\text{Log}_{\tilde{x}_m}^h \circ \iota_{\mathcal{N}, \tilde{x}_m}(x_m) \right)_{m=0}^H, \end{aligned} \quad (\text{Static})$$

where the *encoding/feature* and *decoding/readout* maps are defined by the product of Riemannian exponential map at pre-specified points and its inverse up to identification with the relevant Euclidean spaces via choices of linear isomorphisms $\iota_{\mathcal{N}, \tilde{x}_m} : T_{\tilde{x}_m} \mathcal{M} \rightarrow \mathbb{R}^d$ and $\iota_{\mathcal{M}, y} : T_y \mathcal{M} \rightarrow \mathbb{R}^d$.

We encode the trainable parameters $\bar{x}_{[0:H]} = (\tilde{x}_m)_{m=0}^H \in \mathcal{N}^{1+H}$ and $\bar{y} \in \mathcal{M}$ vectorially via

$$\bar{x}_{[0:H]} \stackrel{\text{def.}}{=} (\text{Exp}_{x^*}^h(\tilde{x}_m))_{m=0}^H \quad \text{and} \quad \bar{y} \stackrel{\text{def.}}{=} \text{Exp}_{y^*}^g(\tilde{y}), \quad (5.2)$$

where $\tilde{x}_{[0:H]} \in \mathbb{R}^{(1+H)D} \cong (T_{x^*}\mathcal{N})^{1+H}$, $\tilde{y} \in \mathbb{R}^d \cong T_{y^*}\mathcal{M}$ for arbitrary, but a-priori fixed, points $x^* \in \mathcal{N}$ and $y^* \in \mathcal{M}$. The set of all GDNs with representation (Static)-(5.2) is denoted by $\mathcal{GDN}_{[d],H}$.

The following universal approximation theorem significantly improves on (Kratsios and Papon, 2022, Theorem 9) in three ways. First, when the target function is smooth, we obtain dimension-free approximation rates, unlike (Kratsios and Papon, 2022, Theorem 9), which only gives cursed approximation rates regardless of the regularity of the target function (on infinite sets). Second, it exponentially improves on the loose rate given therein when approximating α -Hölder functions; indeed, when (\mathcal{N}, h) is a Euclidean space and (\mathcal{M}, g) is the real line with Euclidean metric, our result matches the optimal approximation rates of (Shen et al., 2022, Theorem 2.4). Third, when the compact set on which the function is being approximated is finite, we obtain approximation guarantees without assuming any continuity of the target function using the fact that such functions have smooth extensions.

Theorem 13 (Approximation capacity of GDNs for smooth and Hölder concept classes)
Fix a depth parameter $J \in \mathbb{N}_+$. Suppose that (\mathcal{N}, h) and (\mathcal{M}, g) satisfy Assumptions 12, $H \in \mathbb{N}_+$, and $0 < \varepsilon \leq 1$. Fix reference points $\bar{x} \in \mathcal{N}^{1+H}$ and $\bar{y} \in \mathcal{M}$ as in (Static). For every locally α -Hölder map (resp. k -times continuously differentiable, resp. arbitrary if \mathcal{K} is finite) $f : \mathcal{N}^{H+1} \rightarrow \mathcal{M}$, for some $0 < \alpha \leq 1$ (resp. $k \in \mathbb{N}_+$), and each non-empty compact $\mathcal{K}_{[0:H]} \subseteq \mathcal{N}^{H+1}$ there is a GDN $\hat{f} : \mathcal{N}^{H+1} \rightarrow \mathcal{M}$ satisfying

$$\sup_{x_{[0:H]} \in \mathcal{K}_{[0:H]}} d_g(f(x_{[0:H]}), \hat{f}(x_{[0:H]})) < \varepsilon.$$

and depth and width as recorded in Table 10. ■

Proof See Appendix F.

By randomizing, we obtain a global probabilistic universal approximation theorem for general Borel functions. This result can be interpreted as a non-Euclidean generalization of (Hornik et al., 1989, Theorem 2.3) where the authors quantify the accuracy with which MLPs can approximate Borel functions between Euclidean spaces, which are not necessarily in some L^p -space, using a weaker notion than uniform convergence on compact sets.

Table 2: Complexity estimates for the GDN in Theorem 13

C^k -Times Cnt. Diff. ($k \in \mathbb{N}_+$)	
Depth	$\tilde{\mathcal{O}}(D(J + k^2 + H d))$
Width Parameter	$\tilde{\mathcal{O}}(J(\sqrt{D}/\varepsilon)^{(1+H)/(2k)})$
Locally α -Hölder ($0 < \alpha \leq 1$)	
Depth	$\mathcal{O}(JD)$
Width Parameter	$\mathcal{O}(H d V(J^{-2} \varepsilon)^{\frac{1}{\alpha(1+H)d}})$
No. Reg. - Finite $N \stackrel{\text{def.}}{=} \mathcal{K}_{[0:H]}$	
Depth	$\mathcal{O}(N^2 J)$
Width Parameter	$\mathcal{O}(\varepsilon^{-\frac{1}{2N^2 J}} + N)$

Explicit expressions for all constants are given in Table 10.

Corollary 14 (GDN are universal approximators of Borel functions) *Let (\mathcal{N}, h) and (\mathcal{M}, g) be Riemannian manifolds satisfying Assumptions 12. Let $H \in \mathbb{N}_+$ and X_0, \dots, X_H are i.i.d. \mathcal{N} -valued random variables defined on a common probability space $(\mathcal{S}, \mathcal{A}, \mu)$. For any Borel function $f : \mathcal{N}^{1+H} \rightarrow \mathcal{M}$ and every approximation error $0 < \varepsilon \leq 1$, there is a GDN $\hat{f} : \mathcal{N}^{1+H} \rightarrow \mathcal{M}$ satisfying the probabilistic bound*

$$\mu(d_h(f(X_{[0:H]}), \hat{f}(X_{[0:H]})) < \varepsilon) > 1 - \varepsilon.$$

Proof See Appendix F. ■

Next, we consider the dynamic version of our results, and our main approximation theorem.

5.3 Dynamic/Sequential universality

Before presenting the dynamic universal approximation theorems for GDNs, we formalize their architecture summarized graphically in Figure 2. Briefly, the blue loop is an auxiliary feed-forward neural network defined on the GDN model's parameter space. This auxiliary feedforward neural network, called *hypernetwork* (e.g., Von Oswald et al. (2019)), synchronizes the parameters of several GDNs each of which independently/in parallel approximates the map $x_{[0:T]} \mapsto (\Pi_{x_{[0:t]}})_{t=0}^T$ for a unique t . The hypernetwork synchronizes these GDNs, memorizing the parameters of an optimal GDN at time $t+1$ from those defining an optimal one at time t , for each $t = 0, \dots, T$. Since memorization requires exponentially fewer parameters than approximation, then the HGN can approximate the causal map $x_{[0:T]} \mapsto (\Pi_{x_{[0:t]}})_{t=0}^T$ using roughly the same number of parameters as one GDN needed to approximate the map at any one step in time. This allows us to obtain our main “dynamic” approximation theorem.

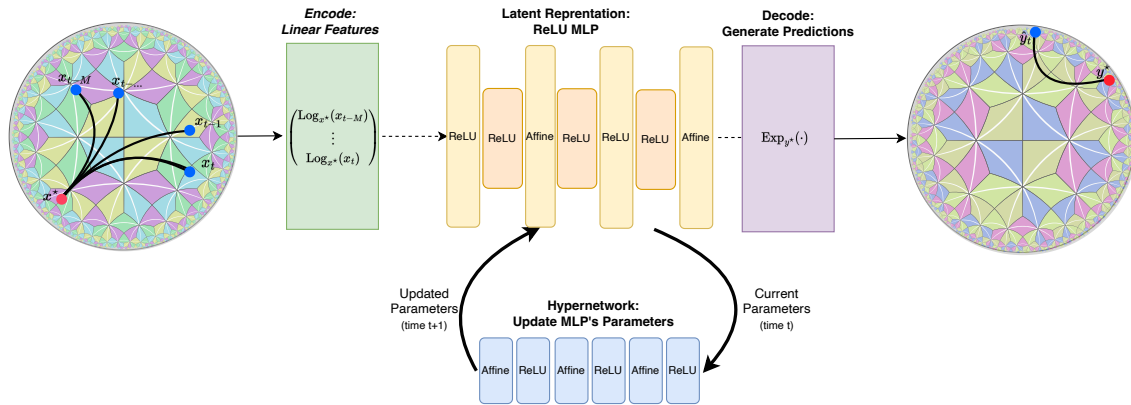


Figure 2: The HGN Model: The green layer encodes sequence segments in the input manifold into distances relative to a reference/landmark point x^* therein. These linearized features are then processed through a ReLU MLP, illustrated by the yellow repeated applying fully-connected affine (also called linear) layers interspersed with ReLU activation functions orange. Finally, the purple decodes the vector v generated by the downsampled CNN into a manifold-valued prediction, by travelling along a geodesic emanating from a reference/landmark point y^* therein with initial velocity v .

The HGN Model: Applies the GDN model while iteratively updating its internal parameters, at each time step, using an (blue) auxiliary ReLU network, called a *hypernetwork*.

Definition 15 ((HGN) Hypergeometric Network) *A map $F : \mathcal{N}^{\mathbb{Z}} \rightarrow \mathcal{M}^{\mathbb{Z}}$ is called a hypergeometric network (HGN) if there are $H, d^*, d, D \in \mathbb{N}_+$, a multi-index $[\mathbf{d}] \stackrel{\text{def.}}{=} (d_0 = (1+H)D, \dots, d_J = d)$, a hypernetwork given by a ReLU MLP $h : \mathbb{R}^{d^*} \rightarrow \mathbb{R}^{d^*}$, an initial parameter $z \in \mathbb{R}^{d^*}$, and a linear*

readout map $\tilde{L} : \mathbb{R}^{d^*} \rightarrow \mathbb{R}^{P([\mathbf{d}])}$ representing F as

$$F(x.)_t = f_{\tilde{L}(z_t)}(x_{[t-H:t]})$$

$$z_t = \begin{cases} h(z_{t-1}) & \text{if } t > 0 \\ z & \text{if } t \leq 0 \end{cases},$$

for every $t \in \mathbb{Z}$ and each sequence $x \in \mathcal{N}^{\mathbb{Z}}$, where $f_\theta \in \mathcal{GDN}_{[\mathbf{d}], H}$. The quadruple $(z, \tilde{L}, h, [\mathbf{d}])$ is called a HGN with history H and latent dimension d^* . The causal map F is called the representation of the HGN $(z, \tilde{L}, h, [\mathbf{d}])$.

When clear from the context, we refer to the representation of a HGN simply as a HGN.

We now formalize what it means for a map $f : \mathcal{N}^{\mathbb{N}} \rightarrow \mathcal{M}^{\mathbb{N}}$ to flow information forward in time while not overemphasizing the arbitrarily distant past. When \mathcal{N} and \mathcal{M} are the Euclidean space, this definition is a quantitative version of the fading memory property for reservoir systems (e.g., Lukoševičius and Jaeger (2009); Gonon and Ortega (2021)) and it is a variant of the approximable complexity property of Acciaio et al. (2023) and the related notion introduced in (Galimberti et al., 2022, Definition 9). We use $C_\alpha^\lambda(\mathcal{N}^H, \mathcal{M})$ to denote the space of α -Hölder functions from \mathcal{N}^H to \mathcal{M} whose α -Hölder coefficients is at most λ -Lipschitz. We use $C^{k,\lambda}(\mathcal{N}^H, \mathcal{M})$ to denote the space of all C^k -functions $f : \mathcal{N}^H \rightarrow \mathcal{M}$ for which there exists $x_1, \dots, x_H \in \mathcal{N}^H$ and some $y \in \mathcal{M}$ such that

$$\text{Log}_y^g \circ f \circ \left(\prod_{m=1}^H \text{Exp}_{x_m}^h \right)$$

has at most λ -Lipschitz k^{th} partial derivatives.

Definition 16 (Causal maps of finite virtual memory between Hadamard manifolds)

A map $f : \mathcal{K} \rightarrow \mathcal{M}^{\mathbb{Z}}$ from a compact subset $\mathcal{K} \subseteq \mathcal{N}^{\mathbb{Z}}$ is called a causal map with virtual memory $r \geq 0$, if for every “compression level” $\varepsilon > 0$ and each “time-horizon” $T \in \mathbb{N}_+$ there is a positive integer $H \stackrel{\text{def.}}{=} H(\varepsilon, T, \mathcal{K}) \in O(\varepsilon^{-r})$ with $H \leq T$ and functions $f_1, \dots, f_T \in C(\mathcal{N}^H, \mathcal{M})$ satisfying

$$\max_{t \in [[T]]} \sup_{x \in \mathcal{K}} d_g(f(x)_t, f_t(x_{(t-H:t)})) < \varepsilon. \quad (5.3)$$

We say that f is (r, k, λ) -smooth if there are $k \in \mathbb{N}_+$ and $\lambda > 0$ such that each $t \in \mathbb{N}_+$ the map f_t belongs to $C^{k,\lambda}(\mathcal{N}^H, \mathcal{M})$.

We say that f is (r, α, λ) -Hölder $k \in \mathbb{N}_+$ and $0 < \alpha \leq 1$ such that for each $t \in \mathbb{N}_+$ the map f_t belongs to $C_\alpha^\lambda(\mathcal{N}^H, \mathcal{M})$.

In order for causal maps to be uniformly approximable on compact sets, they need to possess a basic level of continuity. Therefore, we focus on the following two classes of “high regularity” and “low regularity” causal maps of finite virtual memory as approximable target functions, respectively. These definitions were adapted from the infinite-dimensional linear analogues in Galimberti et al. (2022) to the finite-dimensional non-vectorial setting considered herein.

We may now state our main *universal approximation theorem*, which shows that HGN can approximate causal maps of finite virtual memory. Quantitative rates are obtained when the target function is either smooth or Hölder in the above sense. Our result is quantitative and depends only on the regularity and memory of the target causal map being approximated, as well on the structure of the compact path space over which the uniform spatio-temporal approximation is guaranteed.

Theorem 17 (Universal approximation of causal maps between Hadamard manifolds)

Under Assumption 12, let \mathcal{K} be a non-empty compact subset of $\mathcal{N}^{\mathbb{Z}}$, and let $f : \mathcal{K} \rightarrow \mathcal{M}^{\mathbb{Z}}$ be a causal map of finite virtual memory. Fix depth and memory hyperparameters $J, Q \in \mathbb{N}_+$ and $0 < \delta < 1$.

Table 3: Complexity estimates for the HGN in Theorem 17

Hyperparam.	Estimate
Depth	$\tilde{\mathcal{O}}(T^{3/2})$
Width	$\mathcal{O}(P([\bar{J}]) + Q)T$
N. Parameters	$\tilde{\mathcal{O}}(T^4(P([J]) + Q)^3)$,
Latent Dimension	$\Theta(P([\mathbf{d}]))$

The depth, width, and value of $P([\mathbf{d}])$ is as in Table 10 and as determined by the regularity of f (and the cardinality of $\mathcal{K}_{[0:T]}$) in Theorem 13, with the value of ε instead set to be $\varepsilon/2$.

Suppose either that 1) f is (r, k, λ) -smooth ($r, \lambda \geq 0$ and $k \in \mathbb{N}_+$), or 2) f is (r, α, λ) -Hölder ($r, \lambda \geq 0$ and $\alpha \in (0, 1]$) or 3) that each \mathcal{K}_t is finite for $t \in \mathbb{Z}$ and f has a finite virtual memory $r \geq 0$.

For every “approximation error” $\varepsilon > 0$ and each “time-horizon” $T_{\delta, Q} \stackrel{\text{def.}}{=} \lfloor \delta^{-Q} \rfloor$, there is an integer $0 \leq H \lesssim \min\{T_{\delta, Q}, \varepsilon^{-r}\}$, and an HGN $F : \mathcal{N}^{\mathbb{Z}} \rightarrow \mathcal{M}^{\mathbb{Z}}$ with history H and latent dimension $d^* = Q + D$ satisfying the uniform approximation guaranteee

$$\max_{t=0, \dots, T_{\delta, Q}} \sup_{x \in \mathcal{K}} d_g(f(x)_t, F(x)_t) < \varepsilon.$$

Moreover, the structure and number of parameters determining \hat{h} are recorded in Tables 2 and 3. ■

Proof See Appendix G. ■

6 Ablation Study

We now complement our theoretic analysis of the *Gaussian random projection* and the *HGN* with a numerical analysis of these new tools. The primary purpose of this section is to show how such a pipeline can be implemented and to explain the role of each component of our model and how each of these interacts with the Volterra process X . Since there are no available benchmarks for approximating dynamical systems on Riemannian manifolds, which are guaranteed to be universal, we instead perform an ablation study to better understand the dependence of each of these various factors determining the process X . Additional details are provided in Appendix I.

Experiment Setup Consider a family of i.i.d. random Bernoulli variables $(B_t)_{t=0}^{\infty}$ taking values in $\{0, 1\}$ with equal probabilities of each state. Fix a “randomness” parameter $\lambda \geq 0$ and define the random matrices

$$\mathbf{S}_t \stackrel{\text{def.}}{=} \lambda B_t \cdot I_d$$

where $t \in \mathbb{N}$. Fix a weight $w \in (0, 1]$, Lipschitz functions $\mu : \mathbb{R}^d \rightarrow \mathbb{R}^d$, $\varsigma : \mathbb{R}^d \rightarrow (0, 2]$, and a $d \times d$ symmetric positive-definite matrix σ . Consider the d -dimensional stochastic process

$$\begin{aligned} X_{t+1} &= X_t + \text{Drift}(X_{[t-1:t]}) + \text{Diffusion}(X_t, \mathbf{S}_t) W_t \\ \text{Drift}(z, x) &\stackrel{\text{def.}}{=} w\mu(x) + (1-w)\mu(z) \\ \text{Diffusion}(x, s) &\stackrel{\text{def.}}{=} \varsigma(x) \cdot \sigma + s, \end{aligned} \tag{6.1}$$

for $t \in \mathbb{N}$, where $(W_t)_{t=0}^T$ are i.i.d. d -dimensional standard normal random variables independent of $(B_t)_{t=0}^T$, and both X_{-1}, X_0 are d -dimensional standard normal random variables. The diffusion

component of the process X_t , conditionally on X_t , randomly moves between $\varsigma(X_t) \cdot \sigma$ and $\varsigma(X_t) \cdot \sigma + \lambda I_d$ with equal probabilities, independently of the driving Brownian motion. For any $T \in \mathbb{N}_+$, path $x_{[-1:T]} \in \mathbb{R}^{(2+T)d}$, and integer $0 \leq t \leq T$, the \mathcal{N}_d -valued random variable $\mathbb{Q}_{x_{[-1:t]}}$ is distributed according to

$$\begin{aligned}\mathbb{P}[\mathbb{Q}_{x_{[-1:t]}} = \mathcal{N}_d(x_t + \text{Drift}(x_{[t-1:t]}), \varsigma(x_t)^2 \cdot \sigma^2)] &= \frac{1}{2} \\ \mathbb{P}[\mathbb{Q}_{x_{[-1:t]}} = \mathcal{N}_d(x_t + \text{Drift}(x_{[t-1:t]}), (\varsigma(x_t) \cdot \sigma + \lambda I_d)^2)] &= \frac{1}{2}.\end{aligned}\quad (6.2)$$

By (Sturm, 2003, Proposition 5.5) and the product Riemannian structure on $(\mathcal{N}_d, \mathfrak{J})$ we have that the barycenter of Law($\mathbb{Q}_{x_{[0:t]}}$) is the Cartesian product of the barycenters of its components, up to identification of $(\mathcal{N}_d, \mathfrak{J})$ with $(\mathbb{R}^d \times \text{Sym}_+(d), \delta \oplus g)$. Using, see (Bini and Iannazzo, 2013, page 1701), for the expression of the barycenter between two-points in $(\text{Sym}_+(d), g)$ we find that

$$\beta(\mathbb{Q}_{x_{[-1:t]}}) = \mathcal{N}_d(x_t + \text{Drift}(x_{[t-1:t]}), \varsigma(x_t) \cdot \sigma^2 (\sigma^{-2}(\lambda I_d + \varsigma(x_t) \cdot \sigma)^2)^{1/2}). \quad (6.3)$$

Next, we confirm that the HGN model can indeed approximate the map $x_{[-1:t]} \rightarrow \beta(\mathbb{Q}_{x_{[-1:t]}})$ in practice. Furthermore, we inspect the dependence of each of the components of our framework on the parameters defining the Volterra process (6.1); namely, the drift μ , the diffusion σ , ς , the “randomness of the stochastic factor process” $\lambda > 0$, and the effect of non-Markovianity w .

HGN Training Pipeline The HGN model is trained as follows. First, we sample several $N \in \mathbb{N}_+$ paths segments $\{x_{[-1:T]}^{(n)}\}_{n=1}^N$ up to time $T \in \mathbb{N}_+$ and we train a GDN to predict $y_1^{(n)} \stackrel{\text{def.}}{=} \beta(\mathbb{Q}_{x_{[-1:1]}^{(n)}})$ given each sampled path, by minimizing the intrinsic mean squared error (IMSE)

$$\ell_1(\theta) \stackrel{\text{def.}}{=} \sum_{n=1}^N d_g(f_\theta(x_{[-1:1]}^{(n)}), y_1^{(n)})^2$$

where θ parameterized a set of GDNs of pre-specified depth and width. The IMSE is optimized using the native ADAM optimizer built into Pytorch until a suitable GDN parameter θ_1 is obtained.

Then, for every subsequent time t , each we train a GDN by rolling the training window forward and minimizing the corresponding GDN

$$\ell_t(\theta) \stackrel{\text{def.}}{=} \sum_{n=1}^N d_g(f_\theta(x_{[-t-2:t]}^{(n)}), y_t^{(n)})^2 \quad (6.4)$$

where $y_t^{(n)} \stackrel{\text{def.}}{=} \beta(\mathbb{Q}_{x_{[-t-2:t]}^{(n)}})$. To avoid instability due to the several symmetries present in the parameter space of most MLPs, see e.g. Ainsworth et al. (2023); Sharma et al. (2024), and thus of our GDNs, we initialize the optimization of each GDN at time $t+1$ using the optimized parameters θ_t obtained by minimizing ℓ_t at time t . Additionally, this implicitly encodes a transfer-learning effect, whereby the GDN responsible for predicting at time t encodes the pre-trained structure in previous times. We note that when training the first GDN, 20 ADAM epochs are used while subsequent GDNs are sequentially fine-tuned using 10 ADAM epochs.

Once we have trained each “expert” GDN $\{f_{\theta_t}\}_{t=0}^T$, specialized only on approximating $\beta(\mathbb{Q}_\cdot)$ at each time t , the HGN can be trained by simply minimizing the “hyper-MSE” ℓ_{hyper} in the common parameter space \mathbb{R}^p of the GDNs. Namely,

$$\ell_{\text{hyper}}(\vartheta) \stackrel{\text{def.}}{=} \sum_{t=0}^{T-1} \|h_\vartheta(\theta_t) - \theta_{t+1}\|^2,$$

where ϑ encodes the parameters of a hypernetwork of fixed depth and width. The HGN is then fully encoded into the pair (θ_0, h) . Additional details, and pseudo-code is contained in Appendix I and our code can be found at our Github page <https://github.com/arabporr/HyperNetwork>.

6.1 Ablation Results

We study the sensitivity of the HGN and GDN models to the principle characteristics dictating the stochastic evolution of X . We subsequently study the effect of encoding a large number GDN “experts” into a single HGN.

We fixed one base problem (a process with a specific set of parameters) and 30 additional variations used during our ablation study, each with a similar set of parameters but with exactly one hyperparameter different (e.g. drift, volatility, etc...) perturbed during each ablation. The training set consists of the first $t = 0, \dots, 159$ time steps and the test set consists of the final $160, \dots, 200$ time steps of the process X . In each result we report 95% empirical confidence intervals. All experiment details on the computational resources used are in Appendix I.1.

Sensitivities to aspects of X . We begin by ablating the sensitivity of the HGN and GDN models to: the simplicity/complexity of the drift (μ), the level of randomness (λ) in the stochastic factor \mathbf{S} , the effect of large/small fluctuations (ς) in the diffusion, the dimension (d) of the process X , and the level of non-Markovianity/persistence of memory (w) of the process X . In each case, we report the intrinsic mean squared error for the GDN and HGN models and the confidence intervals formed from one standard deviation of the loss distribution about the (mean) intrinsic mean squared error across all time steps in the test set.

Table 4: **Drift Ablation:** Sensitivity to the structure of the drift (μ) of X .

μ	GDN Loss Mean	GDN Loss 95% C.I.	HGN Loss Mean	HGN Loss 95% C.I.
$\frac{1}{100}$	1.27×10^{-6}	$[1.18, 1.36] \times 10^{-6}$	4.78×10^{-4}	$[3.89, 5.67] \times 10^{-4}$
$\frac{1}{10}$	2.21×10^{-6}	$[2.03, 2.39] \times 10^{-6}$	4.39×10^{-2}	$[3.65, 5.13] \times 10^{-2}$
$\frac{1}{2}(\frac{1}{100} - x)$	1.58×10^{-3}	$[1.55, 1.60] \times 10^{-3}$	1.58×10^{-3}	$[1.55, 1.60] \times 10^{-3}$
$e^{-x} + \cos(\frac{x}{100})$	1.04×10^{-5}	$[0.88, 1.19] \times 10^{-5}$	$1.41 \times 10^{+1}$	$[1.29, 1.53] \times 10^{+1}$

Table 4 shows that the HGN and GDN models can predict Volterra processes whose drift is both simple, e.g. constant, or complicated, e.g. exhibiting osculations $\cos(x/100)$ and decay such as e^{-x} . Nevertheless, as one would expect, the more complicated drifts are more difficult to learn for both models; as reflected by larger test set errors. Moreover, as the drift becomes more complicated the gap between the test set performance of the HGN and GDN models grows as the parameters of the GDN become increasingly difficult to predict for the hypernetwork in the HGN model.

Table 5: **Random Factor Ablation:** Sensitivity to the randomness (λ) in the stochastic factor process \mathbf{S} .

λ	GDN Loss Mean	GDN Loss 95% C.I.	HGN Loss Mean	HGN Loss 95% C.I.
0	3.47×10^{-7}	$[3.36, 3.58] \times 10^{-7}$	3.49×10^{-7}	$[3.41, 3.58] \times 10^{-7}$
0.1	1.58×10^{-3}	$[1.55, 1.60] \times 10^{-3}$	1.58×10^{-3}	$[1.55, 1.60] \times 10^{-3}$
0.25	2.32×10^{-5}	$[2.19, 2.46] \times 10^{-5}$	7.67×10^{-4}	$[6.87, 8.46] \times 10^{-4}$
0.5	8.94×10^{-5}	$[8.25, 9.63] \times 10^{-5}$	4.22×10^{-3}	$[3.75, 4.69] \times 10^{-3}$
0.75	2.25×10^{-4}	$[2.07, 2.44] \times 10^{-4}$	1.34×10^{-2}	$[1.21, 1.47] \times 10^{-2}$
0.9	3.30×10^{-4}	$[3.00, 3.60] \times 10^{-4}$	1.69×10^{-2}	$[1.55, 1.83] \times 10^{-2}$
1	4.30×10^{-4}	$[3.91, 4.69] \times 10^{-4}$	2.12×10^{-2}	$[1.94, 2.30] \times 10^{-2}$

Table 5 shows that all models have increasingly larger challenges when predicting from processes with large levels of randomness (λ) in the stochastic factor \mathbf{S} , influencing their diffusion component. This is because the larger λ is, the more spread out both states (6.2) of the random variable $\mathbb{Q}_{x_{[1:t]}}$ becomes and, consequentially, the more information is lost when computing the intrinsic averaging using β . As anticipated, highly random stochastic factors produce a larger gap in the test set

performance of the GDN and the HGN models. In contrast, less randomness in the stochastic factor yields a smaller test set performance gap between the GDN and HGN models.

Table 6: **Dimension Ablation:** Sensitivity to Dimension (d) of the Volterra Process X .

d	GDN Loss Mean	GDN Loss 95% C.I.	HGN Loss Mean	HGN Loss 95% C.I.
2	3.84×10^{-6}	$[3.32, 4.36] \times 10^{-6}$	4.27×10^{-5}	$[3.83, 4.71] \times 10^{-5}$
5	4.44×10^{-6}	$[4.14, 4.75] \times 10^{-6}$	9.56×10^{-5}	$[0.88, 1.04] \times 10^{-4}$
10	1.58×10^{-3}	$[1.55, 1.60] \times 10^{-3}$	1.58×10^{-3}	$[1.55, 1.60] \times 10^{-3}$
20	1.77×10^{-3}	$[1.73, 1.81] \times 10^{-3}$	1.76×10^{-3}	$[1.72, 1.80] \times 10^{-3}$

Table 6 confirms the effect of dimensionality on the expressive power of the HGN and GDN models, described in Theorems 13 and 17 and detailed in Table 2. Importantly, the performance of the HGN consistently mirrors that of the GDN model in dimensions 2 to 20. Since roughly the same number of parameters are used in each case, then, naturally, the performance of both models is higher in low dimensions than in higher dimensions.

Table 7: **Non-Markovianity Ablation:** Sensitivity to the persistence of memory (w) in X .

Memory	GDN Loss Mean	GDN Loss 95% C.I.	HGN Loss Mean	HGN Loss 95% C.I.
0	3.34×10^{-8}	$[2.82, 3.85] \times 10^{-8}$	7.97×10^{-6}	$[6.63, 9.31] \times 10^{-6}$
0.1	9.31×10^{-5}	$[8.64, 9.98] \times 10^{-5}$	9.32×10^{-5}	$[0.86, 1.00] \times 10^{-4}$
0.25	1.02×10^{-4}	$[0.94, 1.10] \times 10^{-4}$	1.02×10^{-4}	$[0.94, 1.10] \times 10^{-4}$
0.5	1.58×10^{-3}	$[1.55, 1.60] \times 10^{-3}$	1.58×10^{-3}	$[1.55, 1.60] \times 10^{-3}$

Both the HGN and GDN models perform nearly identically for all degrees of memory persistence, from Markovianity to higher levels of non-Markovian memory. This confirms that the hypernetwork can reliably predict GDN parameters regardless of the degree of memory, as in Theorem 17.

Table 8: **Diffusion Ablation:** Sensitivity to the size of the fluctuations (ς) in the diffusion of X .

ς	GDN Loss Mean	GDN Loss 95% C.I.	HGN Loss Mean	HGN Loss 95% C.I.
0.005	4.53×10^{-6}	$[4.19, 4.88] \times 10^{-6}$	1.39×10^{-4}	$[1.25, 1.54] \times 10^{-4}$
0.01	5.02×10^{-6}	$[4.67, 5.37] \times 10^{-6}$	1.46×10^{-4}	$[1.27, 1.66] \times 10^{-4}$
0.05	1.01×10^{-5}	$[0.94, 1.08] \times 10^{-5}$	4.04×10^{-4}	$[3.55, 4.54] \times 10^{-4}$
0.1	1.90×10^{-5}	$[1.79, 2.02] \times 10^{-5}$	7.30×10^{-4}	$[6.43, 8.17] \times 10^{-4}$
1	1.17×10^{-3}	$[1.09, 1.24] \times 10^{-3}$	3.33×10^{-2}	$[2.97, 3.70] \times 10^{-2}$
10	4.13×10^{-1}	$[3.69, 4.57] \times 10^{-1}$	$4.56 \times 10^{+0}$	$[4.14, 4.99] \times 10^{+0}$
100	$2.80 \times 10^{+3}$	$[2.74, 2.86] \times 10^{+3}$	$3.27 \times 10^{+3}$	$[3.18, 3.35] \times 10^{+3}$
1000	$3.10 \times 10^{+5}$	$[3.01, 3.18] \times 10^{+5}$	$3.15 \times 10^{+5}$	$[3.07, 3.23] \times 10^{+5}$

Table 8 shows that both models can reliably predict regardless of the diffusion component of the process X . has large or small fluctuations. As expected, the reliability of the HGN predictions deteriorates when ς increases, as can be seen by an increase in the standard deviation of the loss.

Table 9: **Curvature Ablation:** Sensitivity to the size of the fluctuations (ς) in the diffusion of X .

ς	GDN Loss Mean	GDN Loss 95% C.I.	HGN Loss Mean	HGN Loss 95% C.I.
0.000001	2.34×10^{-3}	$[2.30, 2.38] \times 10^{-3}$	2.32×10^{-3}	$[2.28, 2.36] \times 10^{-3}$
0.0001	1.52×10^{-3}	$[1.48, 1.57] \times 10^{-3}$	1.54×10^{-3}	$[1.50, 1.58] \times 10^{-3}$
0.001	1.58×10^{-3}	$[1.55, 1.60] \times 10^{-3}$	1.58×10^{-3}	$[1.55, 1.60] \times 10^{-3}$

One may a priori expect that a very small variance hyperparameter ς (near 0) would further improve the performance of the GDN and HGN models. As illustrated by Table 9, this is not the case since Gaussian measures with nearly singular covariance matrices (which happens when $\varsigma \approx 0$) are near the (*Gromov*) boundary⁴ “at infinity” of our non-positively curved Riemannian manifold $(\mathcal{N}_d, \mathfrak{J})$. The trouble here is that the Lipschitz constant of the exponential map/layer based at a Gaussian measure far from the boundary is very large (see Lemma C.1) which translates to constants in our approximation guarantees in Theorem 13 (see Table 10). Consequentially, significantly more parameters are required for the HGN to achieve a comparable approximation accuracy when the target Gaussian measure is near the Gaussian measure used as the base point of the exponential layer of the GDN (as in Table 8). This shows that the constants in our main result concretely impact practical implementations of the GDN and the HGN models.

The next set of ablation studies will continue to examine the efficacy of the hypernetwork in encoding and predicting GDN parameters in the test set.

6.1.1 ABLATION OF THE HYPERNETWORK ENCODING

Theorem 17 guarantees that the hypernetwork can effectively encode a large number of GDNs. In particular, doing so suggests that the HGN model can be recursively rolled, allowing us to predict well into the future. Two questions naturally arise: 1) In practice, is a hypernetwork encoding of a sequence of GDN models legitimately trainable? 2) Does the hypernetwork continue to generate well-performing GDN models out-of-sample in future times? This section yields an affirmative *yes* to both of these questions; thus showing the feasibility and reliability of the hypernetwork in the HGN model.

In this next experiment, we test this by comparing three different degrees of hypernetwork encoding. These experiments are run with a subset of the same configurations from the last section; which we annotate in each figure caption. Each of the figures 3 and 4 plot the test set performance of each model, which begins at time $t = 160$ and ends at time $t = 200$.

1) (GDN) no hypernetwork is used and only a different GDN “expert” is used to generate predictions at any time, trained at time $t - 1$. 2) (HGN 1 step) at every time t , the hypernetwork loads the predictions of the GDN at time $t - 1$ and uses them to predict a GDN, which is then used to predict at time t . In this case, the hypernetwork component of the HGN is only ever used to make one-step-ahead predictions. 3) (HGN) loads the GDN parameters at time 160 and then sequentially predicts the parameters at every subsequent time t using its predicted parameters at time $t - 1$; up until the terminal time $t = 200$. All three models perform nearly identically, as illustrated by the log-scale losses. This shows that the hypernetwork encoding of the GDN models is as practically effective as in Theorem 17.

4. This concept generalizes the circle/boundary of the hyperbolic disc model used in the visualization in Figure 2. Importantly, all points in this so-called Gromov boundary are infinitely far from points genuinely inside the non-positively curved Riemannian manifold. See (Bridson and Haefliger, 1999, Chapter II.8) for details.



Figure 3: Situation I - Nearly Logarithmic Degradation of HGN Accuracy: The HGN performance slowly (logarithmically) departs from that of the GDN as time rolls forward. This is typically what is observed in most of our experiments.

Our experiments uncover two types of behaviours which the HGN can exhibit. In the former case, seen in Figure 3, there is a small but growing gap between the test set performance of the HGN and the GDN model which increases as time flows forward. Furthermore, this gap is roughly the same for both the 1-step and recurrent HGN models.

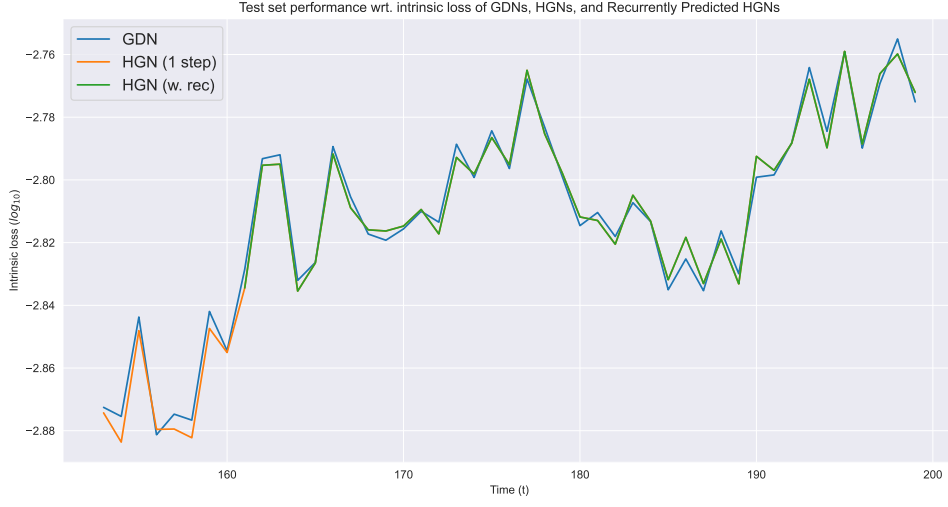


Figure 4: Situation II - Nearly Perfect GDN Prediction by HGN: The HGN continues to nearly perfectly predict the performance of the GDN as time rolls forward. This occurs in a subset of experiments where the GDN parameters do not change significantly between time steps.

Occasionally, the GDN training suffers from exploding gradients during training and one can re-run the stochastic gradient descent algorithm when this happens. We note that there is nothing apriori particular about instances when this happens (see Appendix I.4).

7 Conclusion

We presented a framework for obtaining low-dimensional approximations of the conditional distribution (non-Markovian) stochastic Volterra processes in discrete time. First, we develop a tool, the Gaussian projection, for projecting the condition of such processes down onto the smooth manifold \mathcal{N}_d of non-singular Gaussian measure with a perturbation \mathfrak{J} of its standard information geometry with favourable geometric and computational properties (see Table 1). Like classical tools for dimension reduction of probability measures (e.g. information projections) the Gaussian projection is a projection-type optimization problem; however, unlike those tools the Gaussian projection is a Lipschitz operation (Theorem 9 and Proposition 10) and can even be a *smooth* map under additional conditions (Proposition 10).

Using these insights, we then constructed a sequential geometric deep learning model which is compatible with the non-positive curvature of $(\mathcal{N}_d, \mathfrak{J})$. We showed that this model is a universal approximator of generalized dynamical systems (Theorem 17), possibly with long memory, and we obtained quantitative approximation rates therefor (Theorem 13). In the static case our model reduces the GDN model of Kratsios and Papon (2022); in this case, our main universal approximation theorem yields improved rates (compared to (Kratsios and Papon, 2022, Theorem 9)) when approximating both Hölder, as well as better rates when approximating functions on finite set (compare Table 2 against (Kratsios and Papon, 2022, Theorem 20)). We additionally obtain new probabilistic approximation guarantees for any Borel measurable function in that setting (Corollary 14).

We numerically illustrated the HGN model showing its practical viability. We conducted an ablation study, confirming our main theoretical results. Further, our ablation study shows that certain geometric constants appearing in our parametric complexity estimates (Table 2), depending on the sectional curvature of the underlying space, are legitimately non-negligible in practice.

Future Research

In future work, we would like to extend our analysis to general stochastic processes, going beyond the stochastic Volterra setting. We would also like to explore the impact of projecting onto different information-like geometries when approximation the conditional law of various processes and how to choose such geometries if one has information on the structure of these processes.

8 Acknowledgment and Funding

AK acknowledges financial support from an NSERC Discovery Grant No. RGPIN-2023-04482. AK also acknowledges that resources used in preparing this research were provided, in part, by the Province of Ontario, the Government of Canada through CIFAR, and companies sponsoring the Vector Institute <https://vectorinstitute.ai/partnerships/current-partners/>.

The authors would like to extend a very special thanks to Deane Yang from Courant Institute for his helpful references on Riemannian Centers of Mass. They would also like to thank McKenzie Yuen-Kong Wang from McMaster University for his references on the regularity of the exponential map. Both sets of references significantly helped our derivations.

Appendix A. Explicit Tables

This section records the versions of Tables 10, 11, and 12 with explicit constants.

A.1 Static Case

Table 10: Detailed Complexity estimates for the GDN in Theorem 13.

k -Times Continuously Differentiable f	$k \in \mathbb{N}_+$
Depth (J)	$D\left(1 + 18k^2(J+2)\log_2(4J) + 2(1+H)d\right)$
Width Parameter (w)	$C_0 + C_1\left(2 + \left\lceil J\left(\varepsilon^{-1}C_{\bar{f}}D^{1/2}\right)^{(1+H)/(2k)}\right\rceil\right)\log_2\left(8\left\lceil J\left(\varepsilon^{-1}C_{\bar{f}}D^{1/2}\right)^{(1+H)d/(2k)}\right\rceil\right)$
Locally α -Hölder	$0 < \alpha \leq 1$
Depth (J)	$D\left(11J + C_2\right)$
Width Parameter (w)	$C_0 + C_1 \max\left\{(1+H)d\left(\lceil V(J^{-2}(C_2\varepsilon/C_f)^{d/\alpha})\rceil\right)^{1/(1+H)d}, 2 + \lceil V(J^{-2}(C_2\varepsilon/C_f)^{1/(\alpha(1+H)d)})\rceil\right\}$
No. Reg. - Finite $\mathcal{K}_{[0:H]}$	$N \stackrel{\text{def.}}{=} \#\mathcal{K}_{[0:H]}$
Depth (J)	$D(28N^2J)$
Width Parameter (w)	$\lceil(\varepsilon^{-1}C)^{1/(2N^2J)}\rceil - 1 + 2N - 8$

Details about Constants in Table 10: (1) When f is of class C^k , the constants are $C_0 \stackrel{\text{def.}}{=} d(1+H)(D-1)$, $C_1 \stackrel{\text{def.}}{=} 17k^{d(1+H)+1}3^{d(1+H)}$ and

$$C_{\bar{f}} \stackrel{\text{def.}}{=} \max_{i=1,\dots,D} \|(\rho^{-1} \circ f \circ \varphi^{-1} \circ W)_i\|_{C^k([0,1]^{(1+H)d})} / \max\{1, \text{Lip}(\rho|f \circ \varphi(\overline{\text{Ball}(\mathcal{K}_{[0:H]}, 1)})\}$$

where W is any bijective affine self-map on $\mathbb{R}^{(1+H)d}$ mapping $W(\overline{\text{Ball}(\varphi(\mathcal{K}_{[0:H]}), 1)})$ into $[0, 1]^{(1+H)d}$.

(2) When f is α -Hölder, the constants are $C_0 \stackrel{\text{def.}}{=} (1+H)d(D-1)$, $C_1 \stackrel{\text{def.}}{=} 3^{(1+H)d+3}$, $C_2 \stackrel{\text{def.}}{=} 19 + 2(1+H)d$, $C_3 \stackrel{\text{def.}}{=} (131((1+H)dD)^{1/2})$,

$$C_f \stackrel{\text{def.}}{=} \text{Lip}_\alpha(\rho^{-1} \circ f \circ \varphi^{-1}|\varphi(\overline{\text{Ball}(\mathcal{K}_{[0:H]}, 1)}),$$

and $V : [0, \infty) \rightarrow [0, \infty)$ is the “special function” defined as the inverse of $t \mapsto t^2 \log_3(t+2)$.

(3) When \mathcal{K} is finite, $C = (1+H)d(D-1) + 9(\text{diam}(f(\mathcal{K}_{[0:H]}))\left(\frac{(1+H)d}{2(1+H)d+2}\right)^{1/2}DN$.

A.2 Dynamic Case

Next, we provide detailed expressions for the constants in the dynamic case.

Table 11: Complexity estimates for the HGN in Theorem 17

k -Times Continuously Differentiable f	$k \in \mathbb{N}_+$
Depth (J)	$D\left(1 + 18k^2(J+2)\log_2(4J) + 2(1+H)d\right)$
Width Parameter (w)	$C_0 + C_1\left(2 + \left\lceil J\left(\varepsilon^{-1}C_{\bar{f}}D^{1/2}\right)^{(1+H)/(2k)}\right\rceil\right)\log_2\left(8\left\lceil J\left(\varepsilon^{-1}C_{\bar{f}}D^{1/2}\right)^{(1+H)d/(2k)}\right\rceil\right)$
Locally α -Hölder	$0 < \alpha \leq 1$
Depth (J)	$D\left(11J + C_2\right)$
Width Parameter (w)	$C_0 + C_1 \max\left\{(1+H)d\left(\lceil V(J^{-2}(C_2\varepsilon/C_f)^{d/\alpha})\rceil\right)^{1/(1+H)d}, 2 + \lceil V(J^{-2}(C_2\varepsilon/C_f)^{1/(\alpha(1+H)d)})\rceil\right\}$
No. Reg. - Finite $\mathcal{K}_{[0:H]}$	$N \stackrel{\text{def.}}{=} \#\mathcal{K}_{[0:H]}$
Depth (J)	$D(28N^2J)$
Width Parameter (w)	$\lceil(\varepsilon^{-1}C)^{1/(2N^2J)}\rceil - 1 + 2N - 8$

Details about Constants in Table 17

(1) When f is (r, k, λ) -smooth: the constants are $C_0 \stackrel{\text{def.}}{=} d(1+H)(D-1)$, $C_1 \stackrel{\text{def.}}{=} 17k^{d(1+H)+1}3^{d(1+H)}$ and $C_{\bar{f}} \stackrel{\text{def.}}{=} \max_{t=T-H, \dots, T} \frac{\|(\rho^{-1} \circ f_t \circ \varphi^{-1} \circ W_t)_i\|_{C^k([0,1]^d)}}{\max\{1, \text{Lip}(\rho|f_t \circ \varphi(\mathcal{K}^{*T}))\}}$; where for each $t = H, \dots, T$, $W_t : \mathbb{R}^{(1+H)d} \ni$

$\frac{1}{C_{\tilde{x}}\sqrt{M}2r}\sqrt{\frac{2d(1+H)+2}{d(1+H)}}(x - \tilde{x}_t) \in \mathbb{R}^{(1+H)d}$ is affine.

(2) When f is (r, α, λ) -Hölder: the constants are $C_0 \stackrel{\text{def.}}{=} (1+H)d(D-1)$, $C_1 \stackrel{\text{def.}}{=} 3^{(1+H)d+3}$, $C_2 \stackrel{\text{def.}}{=} 19 + 2(1+H)d$, $C_3 \stackrel{\text{def.}}{=} (131((1+H)dD)^{1/2})$, $C_f \stackrel{\text{def.}}{=} \text{Lip}_\alpha(\rho^{-1} \circ f \circ \varphi^{-1}|\varphi(\text{Ball}(\mathcal{K}_{[0:H]}, 1))$, and $V : [0, \infty) \rightarrow [0, \infty)$ is the “special function” defined as the inverse of $t \mapsto t^2 \log_3(t+2)$.

(3) When $\mathcal{K}_{[0:T]}$ is finite: $C \stackrel{\text{def.}}{=} (1+H)d(D-1) + 9(\text{diam}(f(\mathcal{K}_{[0:H]})) \left(\frac{(1+H)d}{2(1+H)d+2}\right)^{1/2} DN$ and $N \stackrel{\text{def.}}{=} \left(\frac{\max_{t=0, \dots, T} \mathcal{K}_t + M - 1}{M}\right)$.

We complete this section by providing more resolution on the rates in Table 3, with exact expressions wherever possible.

Table 12: Complexity estimates for the HGN in Theorem 17

Hyperparam.	Estimate
Depth	$\mathcal{O}\left(T\left(1 + \sqrt{T \log(T)}\left(1 + \frac{\log(2)}{\log(T)}\left[C + \frac{\left(\log(T^2 2^{1/2}) - \log(\delta)\right)}{\log(2)}\right]_+\right)\right)\right)$
Width	$(P([\bar{J}]) + Q)T + 12$
N. Parameters	$\mathcal{O}\left(T^3(P([\bar{J}]) + Q)^2 \left(1 + (P([\bar{J}]) + Q)\sqrt{T \log(T)}\left(1 + \frac{\log(2)}{\log(T)}\left[C_d + \frac{\left(\log(T^2 2^{1/2}) - \log(\delta)\right)}{\log(2)}\right]_+\right)\right)\right)$,
Latent Dimension	$d^* \geq \max\{12, P([\mathbf{d}]) + 1\}$ (free parameter)

The values of (J) and (w) are as in Table 10 and $P([\bar{J}])$ is determined accordingly by Theorem 13, with the value of ε set to be $\varepsilon/2$. These depend only on the regularity of the map f and the cardinality of $\mathcal{K}_{[0:T]}$.

Appendix B. A problem with information projections for regime-switching processes

Consider the special case of (Volterra) where X_\cdot evolves according to the regime-switching type hidden Markov model, with dynamics given by

$$X_t = \sum_{s=0}^t S_s W_s,$$

where $\{\mathbf{S}_s, W_s\}_{s=0}^T$ are independent random variables where the “regimes” are encoded by the identically distributed Bernoulli $\{0, 1\}$ random variables S_s with equal probabilities and the $(W_s)_{s=0}^T$ are standard Gaussian random variables. Let $x \in \mathbb{R}$ be a realized state of the process at time 0; the process X_\cdot is defined on the measurable space $(\mathbb{R}^N, \mathcal{B}(\mathbb{R}^N))$ where $\mathcal{B}(\mathbb{R}^N)$ is the Borel σ -algebra on countable product \mathbb{R}^N . These processes are such that the corresponding RCD being projected does not admit a Lebesgue density. More precisely, $\mathbb{P}[X_1 \in \cdot | X_0 = x]$ does not admit a well-defined I -projection on the set of d -dimensional Gaussian probability measures \mathcal{N}_d with non-singular covariance, since for an I -projection to exist and be unique, the measure $\mathbb{P}[X_1 \in \cdot | X_0 = x]$ must admit a (Lebesgue) density.

Appendix C. Auxiliary differential geometric results

This appendix contains the required differential geometric results on which many of our proofs are built.

C.1 Results from Riemannian geometry

The following result is due to (Rauch, 1951), but we make use of the formulation which is essentially found in (Karcher, 1977a, C.1 and the remark following (A4.2)). We record the additional minor details.

In what follows, for any d -dimensional Riemannian manifold (\mathcal{M}, g) and any point $p \in \mathcal{M}$, we fix a linear isomorphism $\iota_p : \mathbb{R}^d \rightarrow T_p \mathcal{M}$ which formalizes the identification of the tangent space of \mathcal{M} at p with the d -dimensional Euclidean space.

Lemma C.1 ((Rauch, 1951; Karcher, 1977a)) *Let (\mathcal{M}, g) be a d -dimensional Cartan-Hadamard manifold with sectional curvatures bounded between $[-\kappa, 0]$ for some constant $\kappa > 0$. For every $\bar{r} > 0$ and every $p \in \mathcal{M}$, we have that*

$$\text{Lip} \left(\text{Exp}_p \circ \iota_p | \overline{\text{Ball}_{(\mathbb{R}^d, \|\cdot\|)}(0, \bar{r}/c_p)} \right) \leq 2c_p \frac{\sinh(\sqrt{\kappa}\bar{r})}{\sqrt{\kappa}\bar{r}},$$

where $\text{Lip} \left(\text{Exp}_p \circ \iota_p | \overline{\text{Ball}_{(\mathbb{R}^d, \|\cdot\|)}(0, \bar{r}/c_p)} \right)$ denotes the best local Lipschitz constant of $\text{Exp}_p \circ \iota_p$ on the the closed ball about the origin of radius \bar{r}/c_p and $c_p \stackrel{\text{def.}}{=} |\iota_p|_{op}$ denotes the operator norm of ι_p .

Proof of Lemma C.1 First of all, let us recall the following general fact: given (\mathfrak{X}, g) and (\mathfrak{Y}, h) Riemannian manifolds, with \mathfrak{X} connected, and $F : \mathfrak{X} \rightarrow \mathfrak{Y}$ a C^1 map, we have that the following are equivalent:

1. $d_{\mathfrak{Y}}(F(x_1), F(x_2)) \leq C d_{\mathfrak{X}}(x_1, x_2)$ with $x_1, x_2 \in \mathfrak{X}$;
2. $|dF_x|_{op} \leq C$ with $x \in \mathfrak{X}$;

where $|dF_x|_{op} \stackrel{\text{def.}}{=} \sup_{|V|_x=1} |dF_x(V)|_{F(x)}$ and where $|\cdot|_x$ simply denotes $\sqrt{g(\cdot, \cdot)_x}$, and similarly $|\cdot|_{F(x)} = \sqrt{h(\cdot, \cdot)_{F(x)}}$.

Fix $p \in \mathcal{M}$, and for any $w \in T_p \mathcal{M}$, identify $T_w(T_p \mathcal{M})$ with $T_p \mathcal{M}$ itself.

Under our hypothesis, we can apply (Karcher, 1977a, C.1): therefore, for any $A, v \in T_p \mathcal{M}$ with $|A|_p = |v|_p = 1$ and $A \perp v$ (i.e. orthogonal), and $r > 0$ it holds

$$|d(\text{Exp}_p)_{rv}(A)|_{\text{Exp}_p(rv)} \leq \frac{\sinh(\sqrt{\kappa}r)}{\sqrt{\kappa}r} \tag{C.1}$$

where again $|\cdot|_p$ simply denotes $\sqrt{g(\cdot, \cdot)_p}$, and similarly for $|\cdot|_{\text{Exp}_p(rv)}$.

Let us now show an analogous bound for the general case in which not necessarily it holds $A \perp v$. In an obvious notation, write $A = A^{\parallel} + A^{\perp}$, where A^{\perp} is orthogonal to v and A^{\parallel} is parallel to v . Then, by linearity of the differential, we have, for arbitrary $|A|_p = |v|_p = 1$:

$$\begin{aligned} |d(\text{Exp}_p)_{rv}(A)|_{\text{Exp}_p(rv)} &\leq |d(\text{Exp}_p)_{rv}(A^{\parallel})|_{\text{Exp}_p(rv)} + |d(\text{Exp}_p)_{rv}(A^{\perp})|_{\text{Exp}_p(rv)} \\ &\leq |A^{\parallel}|_p |d(\text{Exp}_p)_{rv}(v)|_{\text{Exp}_p(rv)} + |A^{\perp}|_p \frac{\sinh(\sqrt{\kappa}r)}{\sqrt{\kappa}r}, \end{aligned}$$

where in the second line we have used (C.1). By (Karcher, 1977a, C.1) again, we have that $|d(\text{Exp}_p)_{rv}(v)|_{\text{Exp}_p(rv)} = |v|_p = 1$. Besides, $1 \leq \frac{\sinh(\xi)}{\xi}$ for any $\xi > 0$. Hence, we may write,

$$|d(\text{Exp}_p)_{rv}(A)|_{\text{Exp}_p(rv)} \leq \left[|A^{\parallel}|_p + |A^{\perp}|_p \right] \frac{\sinh(\sqrt{\kappa}r)}{\sqrt{\kappa}r} \leq 2 \frac{\sinh(\sqrt{\kappa}r)}{\sqrt{\kappa}r}.$$

In conclusion, we have proved that for any $p \in \mathcal{M}$, $r > 0$ and $|A|_p = |v|_p = 1$, it holds

$$|d(\text{Exp}_p)_{rv}(A)|_{\text{Exp}_p(rv)} \leq 2 \frac{\sinh(\sqrt{\kappa}r)}{\sqrt{\kappa}r},$$

i.e.

$$|d(\text{Exp}_p)_{rv}|_{op} \leq 2 \frac{\sinh(\sqrt{\kappa}r)}{\sqrt{\kappa}r}.$$

Since $(0, \infty) \ni \xi \mapsto \frac{\sinh(\xi)}{\xi}$ is (strictly) increasing, given $\bar{r} > 0$, we have $|d(\text{Exp}_p)_{rv}|_{op} \leq 2 \frac{\sinh(\sqrt{\kappa}\bar{r})}{\sqrt{\kappa}\bar{r}}$ for $r \leq \bar{r}$, i.e.

$$|d(\text{Exp}_p)_w|_{op} \leq 2 \frac{\sinh(\sqrt{\kappa}\bar{r})}{\sqrt{\kappa}\bar{r}}, \quad p \in \mathcal{M}, w \in T_p\mathcal{M}, |w|_p \leq \bar{r}.$$

Therefore, we conclude that

$$d_M(\text{Exp}_p(w_1), \text{Exp}_p(w_2)) \leq 2 \frac{\sinh(\sqrt{\kappa}\bar{r})}{\sqrt{\kappa}\bar{r}} |w_1 - w_2|_p, \quad p \in \mathcal{M}, w_1, w_2 \in T_p\mathcal{M}, |w_1|_p, |w_2|_p \leq \bar{r}. \quad (\text{C.2})$$

Let $c_p \stackrel{\text{def.}}{=} |\iota_p|_{op}$ and suppose now that $v_1, v_2 \in \overline{\text{Ball}_{\mathbb{R}^d, \|\cdot\|}(0, \bar{r}/c_p)}$. Then, $\iota_p(v_1), \iota_p(v_2) \in \overline{\text{Ball}_{T_p\mathcal{M}, g}(0, \bar{r})}$. Whence, (C.2) implies that

$$d_M(\text{Exp}_p(\iota_p(v_1)), \text{Exp}_p(\iota_p(v_2))) \leq 2 \frac{\sinh(\sqrt{\kappa}\bar{r})}{\sqrt{\kappa}\bar{r}} |\iota_p(v_1) - \iota_p(v_2)|_p \leq 2 \frac{\sinh(\sqrt{\kappa}\bar{r})}{\sqrt{\kappa}\bar{r}} c_p \|v_1 - v_2\|.$$

This yields the conclusion. ■

Lemma C.1 and the Cartan-Hadamard Theorem (([Jost, 2017](#), Corollary 6.9.1)), which states that the Riemannian exponential map is a global diffeomorphism with 1-Lipschitz inverse on a simply connected complete Riemannian manifold of non-positive sectional curvature, imply local-regularity estimates for the feature map φ , the readout map ρ , and their inverses; where φ and ρ are defined as follows

$$\begin{aligned} \rho(y) &\stackrel{\text{def.}}{=} \text{Exp}_{\bar{y}}^g \circ \iota_{\mathcal{M}, \bar{y}}^{-1}(y) \\ \varphi(x_1, \dots, x_m) &\stackrel{\text{def.}}{=} (\text{Log}_{\bar{x}_m}^h \circ \iota_{\mathcal{N}, \bar{x}_m}(x_m))_{m=0}^M, \end{aligned} \quad (\text{C.3})$$

where $x_1, \dots, x_m \in \mathbb{N}^M$ and $y \in \mathcal{M}$.

Lemma C.2 (Regularity of feature map (φ)) *Suppose that (\mathcal{N}, h) satisfies Assumption 12, $M \in \mathbb{N}$, $\bar{x}_{[0:H]} \in \mathcal{N}^H$, and φ is as in (C.3). Then $\varphi : \mathcal{N}^{1+H} \rightarrow \mathbb{R}^{(1+H)d}$ is*

- (i) *smooth and $C_{\bar{x}}$ -Lipschitz (globally) for some $C_{\bar{x}} > 0$ depending only on \bar{x} (see below),*
- (ii) *φ^{-1} exists, it is smooth, and for any $\mathcal{K}_{[0:H]} \stackrel{\text{def.}}{=} \prod_{i=0}^H \mathcal{K}_i \subseteq \mathbb{R}^{(1+H)d}$ where $\mathcal{K}_0, \dots, \mathcal{K}_H$ are non-empty compact sets, we have*

$$\text{Lip}(\varphi^{-1} | \mathcal{K}_{[0:H]}) \leq \max_{\tilde{m}=0, \dots, H} c_{\bar{x}_m} \frac{\sinh(\kappa^{1/2} c_{\bar{x}_m} \|K_m\|)}{\kappa^{1/2} c_{\bar{x}_m} \|K_m\|},$$

where $c_{\bar{x}_m} \stackrel{\text{def.}}{=} \|\iota_{\bar{x}_m}\|_{op}$ for $m = 0, \dots, H$.

Where for any non-empty subset $A \subseteq \mathbb{R}^d$ we define $\|A\| \stackrel{\text{def.}}{=} \sup_{u \in A} \|u\|$ where $C_{\bar{x}} \stackrel{\text{def.}}{=} \max_{m=0, \dots, H} |\iota_{\bar{x}_m}^{-1}|_{op}$.

Proof of Lemma C.2 Since \mathcal{N} is simply connected, complete, and has non-positive sectional curvatures then the first statement in the Cartan-Hadamard theorem, as formulated in (Jost, 2017, Corollary 6.9.1), guarantees that each $\text{Log}_{\bar{x}_m}^h \stackrel{\text{def.}}{=} (\text{Exp}_{\bar{x}_m}^h)^{-1} : \mathcal{N} \rightarrow T_{\bar{x}_m} \mathcal{N}$, for $m = 0, \dots, H$ is well-defined and smooth. Moreover, the second statement of (Jost, 2017, Corollary 6.9.1) implies that each $\text{Log}_{\bar{x}_m}^h$ is a 1-Lipschitz map (globally on (\mathcal{N}, d_h)). Consequentially, for every $x_{[0:H]}, \tilde{x}_{[0:H]} \in \mathcal{N}^H$ it follows that

$$\begin{aligned} \|\varphi(x_{[1:H]}) - \varphi(\tilde{x}_{[1:M]})\| &= \left(\sum_{m=0}^H \left\| \text{Log}_{\bar{x}_m} \circ \iota_{\bar{x}_m}^{-1}(x_r) - \text{Log}_{\bar{x}_m} \circ \iota_{\bar{x}_m}^{-1}(\tilde{x}_r) \right\|_2^2 \right)^{1/2} \\ &\leq \left(\sum_{m=0}^H [|\iota_{\bar{x}_m}^{-1}| d_h(x_r, \tilde{x}_r)]^2 \right)^{1/2} \\ &\leq C_{\bar{x}} \left(\sum_{m=0}^H d_h(x_r, \tilde{x}_r)^2 \right)^{1/2} \\ &= C_{\bar{x}} d_{h:2}(x_{[1:H]}, \tilde{x}_{[1:M]}). \end{aligned}$$

This yields claim (i), where $d_{h:2}$ is the $(1+H)$ -fold 2-product metric on \mathcal{N}^{1+H} of the geodesic distance d_h on (\mathcal{N}, h) .

Let $u_{[0:H]}, \tilde{u}_{[0:H]} \in (\mathbb{R}^d)^{1+H} \cong \mathbb{R}^{(1+H)d}$. Under the sectional curvature lower-bound in Assumption 12 (iii), we may apply Lemma C.1 to deduce that, for any $r_0, \dots, r_H > 0$ and each $m = 0, \dots, H$, the restriction of the map $\text{Exp}_{\bar{x}_m}$ to the closed Euclidean ball $\overline{\text{Ball}_{(\mathbb{R}^d, \ell_2^2)}(0, c_{\bar{x}_m} r_m / c_{\bar{x}_m})}$ is Lipschitz with Lipschitz constant at-most $c_{\bar{x}_m} \frac{\sinh(\kappa^{1/2} c_{\bar{x}_m} r_m)}{\kappa^{1/2} c_{\bar{x}_m} r_m}$. Therefore, we have that

$$\begin{aligned} d_{h:2}(\varphi^{-1}(u_{[0:H]}), \varphi^{-1}(\tilde{u}_{[0:H]})) &= \left(\sum_{m=0}^H d_h(\text{Exp}_{\bar{x}_m}(u_m), \text{Exp}_{\bar{x}_m}(\tilde{u}_m))^2 \right)^{1/2} \\ &\leq \left(\sum_{m=0}^H \left(c_{\bar{x}_m} \frac{\sinh(\kappa^{1/2} c_{\bar{x}_m} r_m)}{\kappa^{1/2} c_{\bar{x}_m} r_m} \|u_m - \tilde{u}_m\| \right)^2 \right)^{1/2} \\ &\leq \left(\sum_{m=0}^H \left[\max_{\tilde{m}=0, \dots, H} c_{\bar{x}_m} \left(\frac{\sinh(\kappa^{1/2} r_{\tilde{m}})}{\kappa^{1/2} r_{\tilde{m}}} \right) \right]^2 \|u_m - \tilde{u}_m\|^2 \right)^{1/2} \\ &\leq \left[\max_{\tilde{m}=0, \dots, H} c_{\bar{x}_m} \frac{\sinh(\kappa^{1/2} r_{\tilde{m}})}{\kappa^{1/2} r_{\tilde{m}}} \right] \left(\sum_{m=0}^H \|u_m - \tilde{u}_m\|^2 \right)^{1/2} \\ &= \left[\max_{\tilde{m}=0, \dots, H} c_{\bar{x}_m} \frac{\sinh(\kappa^{1/2} r_{\tilde{m}})}{\kappa^{1/2} r_{\tilde{m}}} \right] \|u_{[0:H]} - \tilde{u}_{[0:H]}\|. \end{aligned}$$

Note that each $K_m \subseteq \overline{\text{Ball}_{(\mathbb{R}^d, \ell_2^2)}(0, \|K_m\|)}$, for $m = 0, \dots, H$. Upon setting $r_m \stackrel{\text{def.}}{=} \|K_m\|$, for each $m = 0, \dots, H$, we obtain the conclusion. \blacksquare

Remark C.3 Lemma C.2 shows that a poor choice of base-points \bar{x}_m when defining the feature map φ will require a larger network to compensate for the unnecessarily large Lipschitz constant of φ^{-1} .

Since ρ is φ^{-1} when interchanging the roles of \mathcal{M} and \mathcal{N} in Lemma (C.2), in the special case where $M = 1$, then Lemma C.2 directly implies the following.

Lemma C.4 (Regularity of readout map (ρ)) Suppose that (\mathcal{M}, g) satisfies Assumption 12 (i) and (iii). Fix a $\bar{y} \in \mathcal{M}$ and define ρ as in (C.3). Then, $\rho : \mathbb{R}^D \rightarrow \mathcal{M}$ satisfies

(i) ρ is smooth and on any non-empty compact $K \subseteq \mathbb{R}^D$ its local-Lipschitz constant is

$$\text{Lip}(\rho|K) \leq c_{\bar{y}} \frac{c_{\bar{y}} \sinh(\kappa^{1/2} \text{diam}(K))}{c_{\bar{y}} \kappa^{1/2} \text{diam}(K)},$$

where $c_{\bar{y}} \stackrel{\text{def.}}{=} 2 \|\iota_{\bar{y}}\|_{op}$.

(ii) ρ^{-1} exists, it is smooth, and it is C_p -Lipschitz (globally) where where $C_{\bar{p}} \stackrel{\text{def.}}{=} |\iota_p^{-1}|_{op}$.

Proof Point (i) follows from Lemma C.1, by setting $\bar{r} = c_{\bar{y}} \text{diam}(K)$ and noting that $x \mapsto \sinh(\kappa^{1/2}x)/(\kappa^{1/2}x)$ is monotonically increasing on $[0, \infty)$. Point (ii) follows from the second statement of the Cartan-Hadamard Theorem (Jost, 2017, Corollary 6.9.1) and upon recalling that we have linearly isomorphically identified the Hilbert spaces $\iota_p : (T_p(\mathcal{M}), \|\cdot\|_{g_p}) \rightarrow (\mathbb{R}^D, \|\cdot\|)$ (which needn't be an isometry); whence $\text{Lip}(\iota_p^{-1}) = C_{\bar{p}} \stackrel{\text{def.}}{=} |\iota_p^{-1}|_{op} > 0$ (and need not equal to 1). \blacksquare

C.2 Results from matrix theory

This appendix contains a short proof of some folklore results in matrix theory.

Recall that, for a negative integer t and an invertible matrix Σ , the matrix Σ^t is defined to be $(\Sigma^{-1})^{|t|}$. That is, Σ^t is the t -fold product of Σ^{-1} with itself.

The next lemma justifies the definition of the real exponent of a symmetric positive definite matrix.

Lemma C.5 (Powers of symmetric positive-definite matrices) *For each $\Sigma \in \text{Sym}_+(d)$ and each $t \in \mathbb{R}$, $\exp(t \log(\Sigma))$ is a well-defined element of $\text{Sym}_+(d)$. Furthermore, if $t \in \mathbb{Z}$ then*

$$\exp(t \log(\Sigma)) = \Sigma^t.$$

Proof of Lemma C.5 By (Hilgert and Neeb, 2012, Proposition 3.3.5) the restriction of the matrix exponential map to $\text{Sym}(d)$ is a diffeomorphism onto the open subset $\text{Sym}_+(d)$ of $\text{Sym}(d)$, and by definition, the matrix logarithm \log is the inverse of \exp on $\text{Sym}_+(d)$. Therefore, $X \stackrel{\text{def.}}{=} \log(\Sigma)$ is a well-defined element of $\text{Sym}(d)$. Consequentially, tX belongs to $\text{Sym}(d)$ for every $t \in \mathbb{R}$. Thus, $\exp(tX) \in \text{Sym}_+(d)$ and the first claim follows.

Let now be $t \in \mathbb{Z}$ with $t \neq 0$ (otherwise the statement is trivial). If $t > 0$, then, since X trivially commutes with itself, it easily follows that

$$\exp(tX) = \underbrace{\exp(X) \dots \exp(X)}_{t\text{-times}} = (\exp(X))^t.$$

If on the other hand $t < 0$, then, from we have just proved, $\exp(tX) = \exp(-t(-X)) = (\exp(-X))^{|t|}$. But since $\exp(X)$ is invertible with $\exp(-X) = \exp(X)^{-1}$, from the observation at the beginning of this section we infer $\exp(tX) = (\exp(X))^t$.

So, we have that $\exp(tX) = (\exp(X))^t$ for every $t \in \mathbb{Z}$. Plugging in the definition of X and using the fact that \log is the inverse of \exp on $\text{Sym}_+(d)$ yields the conclusion, namely that

$$\exp(t \log(\Sigma)) = (\exp(\log(\Sigma)))^t = \Sigma^t,$$

concluding our proof. \blacksquare

Appendix D. Proofs

This section contains the proofs of our main results.

D.1 Proof of Proposition 7

In order to prove Proposition 7, we need some preliminary results.

D.1.1 THE GLOBAL NPC GEOMETRY ON THE SPACE OF NON-SINGULAR GAUSSIAN MEASURES

The following result is well-known in the metric geometry literature; however, parts of its proof were difficult to track down outside that literature, so we record it here.

Lemma D.1 (The Geometry of Sym_+) *For every $d \in \mathbb{N}$, $\text{Sym}_+(d)$ is a $d(d+1)/2$ -dimensional Cartan-Hadamard manifold whose tangent spaces are identifiable with $\text{Sym}(d)$. The Riemannian metric is given by*

$$\hat{g}_\Sigma(X, Y) \stackrel{\text{def.}}{=} \text{tr}(\Sigma^{-1}X\Sigma^{-1}Y), \quad \Sigma \in \text{Sym}_+(d), X, Y \in \text{Sym}(d).$$

Moreover, the sectional curvatures are bounded in $[-1/2, 0]$.

Proof of Lemma D.1 As discussed on (Bridson and Haefliger, 1999, page 314, section 10.31), $\text{Sym}_+(d)$ is a smooth manifold of dimension $d(d+1)/2$ with tangent spaces identifiable with $\text{Sym}(d)$ (see (Petersen et al., 2008, Section 10.2.2)): a smooth global chart is provided by $\text{vec} : \text{Sym}_+(d) \rightarrow \text{vec}(\text{Sym}_+(d)) \subset \mathbb{R}^{d(d+1)/2}$ (recall that $\text{vec} : \mathbb{R}^{d(d+1)/2} \rightarrow \text{Sym}(d)$ is the inverse of the vector space isomorphism sym defined in (3.11)); moreover $\text{Sym}_+(d)$ can be endowed with the Riemannian metric $\hat{g}_\Sigma(X, Y) \stackrel{\text{def.}}{=} \text{tr}(\Sigma^{-1}X\Sigma^{-1}Y)$, where $\Sigma \in \text{Sym}_+(d)$ and $X, Y \in \text{Sym}(d)$.

By Theorem (Bridson and Haefliger, 1999, 10.39), $(\text{Sym}_+, d_{\hat{g}})$ is a CAT(0) space⁵ and since (Sym_+, \hat{g}) is a Riemannian manifold then (Bridson and Haefliger, 1999, Theorem II.1A.6)⁶ implies that the sectional curvatures of (Sym_+, \hat{g}) are all bounded-above by 0. On the other hand, (Criscitiello and Boumal, 2022, Proposition I.1)⁷ we see that the sectional curvatures in (Sym_+, \hat{g}) are bounded-below by $-1/2$. ■

In what follows, for any $\mathbf{m} \in \mathbb{R}^d$, we let $\mathcal{N}_d^{\mathbf{m}} \stackrel{\text{def.}}{=} \{\mathcal{N}_d(\mathbf{m}, \Sigma) : \Sigma \in \text{Sym}_+(d)\}$. Since $\mathcal{N}_d^{\mathbf{m}}$ is a Riemannian submanifold of dimension $d(d+1)/2$ of $(\mathcal{N}_d, \mathcal{I}^F)$ (with metric pullback via the inclusion map ι), by defining

$$\Phi : \text{Sym}_+(d) \rightarrow \mathcal{N}_d^{\mathbf{m}}, \quad \Sigma \mapsto \mathcal{N}(\mathbf{m}, \Sigma) \tag{D.1}$$

it is easy to see that Φ is an isometry between $(\text{Sym}_+(d), \hat{g})$ and $(\mathcal{N}_d^{\mathbf{m}}, \iota^* \mathcal{I}^F)$: see also (3.7). Lemma D.1 this implies the following.

Corollary D.2 (The geometry of $\mathcal{N}_d^{\mathbf{m}}$) *For every $d \in \mathbb{N}$ and each $\mathbf{m} \in \mathbb{R}^d$, $\mathcal{N}_d^{\mathbf{m}}$ is a $d(d+1)/2$ -dimensional Cartan-Hadamard manifold. Moreover, their sectional curvatures are bounded in $[-1/2, 0]$. In particular, $(\mathcal{N}_d^{\mathbf{m}}, d_{\mathcal{I}^F})$ is a global NPC space.*

We are now in place to prove Proposition 7.

Proof of Proposition 7 We begin by determining a suitable Riemannian structure for \mathcal{N}_d before studying its metric and topological characteristics, as well as obtaining estimates on its curvature.

5. See (Bridson and Haefliger, 1999, Definition II.1.1).

6. Due to Cartan (1988).

7. In their extended appendix in the ArXiV version.

Manifold structure We have just seen that $(\mathcal{N}_d^m, \iota^* \mathcal{I}^F)$ is a Riemannian submanifold (of dimension $d(d+1)/2$). Consider \mathbb{R}^d endowed with its standard Euclidean metric δ , namely the identity matrix. Define (\mathcal{U}, g) to be the product of these two Riemannian manifolds

$$\mathcal{U} \stackrel{\text{def.}}{=} \mathbb{R}^d \times \mathcal{N}_d^0, \quad g \stackrel{\text{def.}}{=} \delta \oplus \iota^* \mathcal{I}^F,$$

where a global chart for \mathcal{U} is clearly given by $\kappa(\mathbf{m}, \mathcal{N}_d(0, \Sigma)) = (\mathbf{m}, \text{vec}(\Sigma))$. Consider the following bijective map $\chi : \mathcal{N}_d \rightarrow \mathcal{U}$ so defined

$$\chi : \mathcal{N}_d(\mathbf{m}, \Sigma) \mapsto (\mathbf{m}, \mathcal{N}_d(0, \Sigma)).$$

It is immediate to see that (refer to Section 3.1 for unexplained notation) $\varphi^{-1} \circ \chi \circ \kappa : \mathcal{U} \rightarrow \Theta$ is the identity map, and thus smooth. The same holds for the inverse χ^{-1} : we deduce that χ is a diffeomorphism and that the matrix representation of χ_* is the identity matrix of \mathbb{R}^m , $m = (d^2 + 3d)/2$.

We finally pullback g via χ on \mathcal{N}_d , and we set $\mathfrak{J} \stackrel{\text{def.}}{=} \chi^* g$. It is straightforward to see that at an arbitrary point $\mathcal{N}_d(\mathbf{m}, \Sigma)$ (3.8) is fulfilled. By construction, $(\mathcal{N}_d, \mathfrak{J})$ is isometric to (\mathcal{U}, g) . From now on, we will work on (\mathcal{U}, g) : whence, geometric statements valid for (\mathcal{U}, g) will also be valid for $(\mathcal{N}_d, \mathfrak{J})$.

Topological properties Observe that $\text{Sym}_+(d)$ is a convex cone, thus it is contractible⁸. Therefore, it is connected and simply connected⁹. Consequentially, \mathcal{N}_d^0 is connected since it is homeomorphic to $\text{Sym}_+(d)$. Therefore, \mathcal{U} is connected since it is the product of two connected spaces. Moreover, \mathcal{N}_d^0 is also connected and simply connected, because $\text{Sym}_+(d)$ is.

Since \mathbb{R}^d is also path connected, \mathcal{U} is the Cartesian product of path connected spaces, then¹⁰ the fundamental group $\pi(\mathcal{U})$ of \mathcal{U} is isomorphic¹¹ to the direct product $\pi(\mathbb{R}^d) \oplus \pi(\mathcal{N}_d^0) \cong \{0\}$ of the fundamental groups of \mathbb{R}^d and \mathcal{N}_d^0 , which are both trivial¹². Since \mathcal{U} is homeomorphic to \mathcal{N}_d then (Spanier, 1989, Theorem 1.8.8) implies that $\pi(\mathcal{N}_d) \cong \{0\}$; thus, \mathcal{N}_d is simply connected.

Metric structure By Lemma E.1, the distance function on the \mathcal{U} equals to the 2-product metric given, for any $u_0 = (\mathbf{m}_0, \mathcal{N}_d(0, \Sigma_0)) \in \mathcal{U}$ and $u_1 = (\mathbf{m}_1, \mathcal{N}_d(0, \Sigma_1)) \in \mathcal{U}$, by

$$d_g((\mathbf{m}_0, \mathcal{N}_d(0, \Sigma_0)), (\mathbf{m}_1, \mathcal{N}_d(0, \Sigma_1))) = \left[\|\mathbf{m}_0 - \mathbf{m}_1\|_2^2 + d_{\iota^* \mathcal{I}^F}(\mathcal{N}_d(0, \Sigma_0), \mathcal{N}_d(0, \Sigma_1))^2 \right]^{1/2}. \quad (\text{D.2})$$

Since $(\mathcal{N}_d^0, \iota^* \mathcal{I}^F)$ is *totally geodesic* see (Skovgaard, 1984, page 214), then¹³

$$d_{\iota^* \mathcal{I}^F}(\mathcal{N}_d(0, \Sigma_0), \mathcal{N}_d(0, \Sigma_1)) = d_{\mathcal{I}^F}(\mathcal{N}_d(0, \Sigma_0), \mathcal{N}_d(0, \Sigma_1)) \quad (\text{D.3})$$

for every $\Sigma_0, \Sigma_1 \in \text{Sym}_+(d)$. (D.3) and (D.2) imply that for any $(\mathbf{m}_0, \mathcal{N}_d(0, \Sigma_0)), (\mathbf{m}_1, \mathcal{N}_d(0, \Sigma_1)) \in \mathcal{U}$

$$d_g((\mathbf{m}_0, \mathcal{N}_d(0, \Sigma_0)), (\mathbf{m}_1, \mathcal{N}_d(0, \Sigma_1))) = \left[\|\mathbf{m}_0 - \mathbf{m}_1\|_2^2 + \frac{1}{2} \sum_{i=1}^d \ln(\lambda_i)^2 \right]^{1/2}$$

where $\lambda_1, \dots, \lambda_d$ are the eigenvalues of $\Sigma_0^{-1} \Sigma_1$. Since $(\mathcal{N}_d, \mathfrak{J})$ is isometric to (\mathcal{U}, g) we find that

$$d_{\mathfrak{J}}(\mathcal{N}_d(\mathbf{m}_0, \Sigma_0), \mathcal{N}_d(\mathbf{m}_1, \Sigma_1)) = \left[\|\mathbf{m}_0 - \mathbf{m}_1\|_2^2 + \frac{1}{2} \sum_{i=1}^d \ln(\lambda_i)^2 \right]^{1/2}, \quad \mathcal{N}_d(\mathbf{m}_0, \Sigma_0), \mathcal{N}_d(\mathbf{m}_1, \Sigma_1) \in \mathcal{N}_d.$$

8. E.g. via the homotopy $(t, \Sigma) \mapsto t\Sigma + (1-t)I_d$

9. See (Spanier, 1989, Theorem 1.10).

10. See (Spanier, 1989, Exercise 1.G).

11. Here, \cong denotes an isomorphism in the category of groups and group homomorphisms.

12. I.e. homeomorphic, as groups, to the trivial group $\{0\}$.

13. This can be shown similarly to the Lemma on (Kobayashi and Nomizu, 1996, 181), by instead considering a distance-minimizing geodesic between two given points which exists since \mathcal{N}_d is complete as a metric space (and this geodesically complete by the Hopf-Rinow theorem).

Curvature and NPC space By (Atçeken and Keleş, 2003, Equation (2.1)), the product of Riemannian manifolds we have that

$$Rm^{\mathcal{U}}(X_1 + X_2, Y_1 + Y_2, Z_1 + Z_2, W_1 + W_2) = Rm^{\mathbb{R}^d}(X_1, Y_1, Z_1, W_1) + Rm^{\mathcal{N}_d^0}(X_2, Y_2, Z_2, W_2)$$

for all X_1, Y_1, Z_1, W_1 tangent vectors of \mathbb{R}^d , for all X_2, Y_2, Z_2, W_2 tangent vectors of \mathcal{N}_d^0 , and where $Rm^{\mathcal{U}}, Rm^{\mathbb{R}^d}, Rm^{\mathcal{N}_d^0}$ denotes the Riemann curvature tensors of $\mathcal{U}, \mathbb{R}^d$ and \mathcal{N}_d^0 respectively. Since trivially $Rm^{\mathbb{R}^d}$ is identically zero, the previous identity simplifies to

$$Rm^{\mathcal{U}}(X_1 + X_2, Y_1 + Y_2, Z_1 + Z_2, W_1 + W_2) = Rm^{\mathcal{N}_d^0}(X_2, Y_2, Z_2, W_2). \quad (\text{D.4})$$

This fact has striking consequences: in the following $K^{\mathcal{U}}(X_1 + X_2, Y_1 + Y_2)$ will denote the sectional curve of \mathcal{U} spanned by the linearly independent vectors $X_1 + X_2$ and $Y_1 + Y_2$; similarly, $K^{\mathcal{N}_d^0}(A, B)$ will denote the sectional curve of \mathcal{N}_d^0 spanned by the linearly independent vectors A and B .

Given $X_1 + X_2$ and $Y_1 + Y_2$ orthonormal with respect to g , we have from (D.4)

$$K^{\mathcal{U}}(X_1 + X_2, Y_1 + Y_2) = Rm^{\mathcal{N}_d^0}(X_2, Y_2, X_2, Y_2)$$

and

$$\begin{cases} 1 = \delta(X_1, X_1) + \iota^* \mathcal{I}^F(X_2, X_2) \\ 1 = \delta(Y_1, Y_1) + \iota^* \mathcal{I}^F(Y_2, Y_2) \\ 0 = \delta(X_1, Y_1) + \iota^* \mathcal{I}^F(X_2, Y_2), \end{cases}$$

which implies $\mathcal{I}^F(X_2, X_2), \mathcal{I}^F(Y_2, Y_2) \leq 1$. To obtain the claimed sectional curvature bounds for (\mathcal{U}, g) , and thus for $(\mathcal{N}_d, \mathfrak{J})$ we must consider three distinct cases:

- (i) If $X_2 = 0$ or $Y_2 = 0$ then, $K^{\mathcal{U}}(X_1 + X_2, Y_1 + Y_2) = 0$.
- (ii) If $X_2 \neq 0$, $Y_2 \neq 0$ and linearly dependent then, $Y_2 = \gamma X_2$ for some $\gamma \neq 0$. We then get $K^{\mathcal{U}}(X_1 + X_2, Y_1 + Y_2) = \gamma^2 Rm^{\mathcal{N}_d^0}(X_2, X_2, X_2, X_2) = 0$.
- (iii) If X_2 and Y_2 are linearly independent (and hence $\neq 0$), then set for brevity

$$t(X_2, Y_2) := \iota^* \mathcal{I}^F(X_2, X_2) \iota^* \mathcal{I}^F(Y_2, Y_2) - \iota^* \mathcal{I}^F(X_2, Y_2)^2$$

which is > 0 by Cauchy-Schwartz inequality. Besides, from above we also have

$$t(X_2, Y_2) \leq \iota^* \mathcal{I}^F(X_2, X_2) \iota^* \mathcal{I}^F(Y_2, Y_2) \leq 1,$$

and thus $0 < t(X_2, Y_2) \leq 1$. We then obtain

$$K^{\mathcal{U}}(X_1 + X_2, Y_1 + Y_2) = K^{\mathcal{N}_d^0}(X_2, Y_2) t(X_2, Y_2).$$

Since (Criscitiello and Boumal, 2022, Proposition I.1)¹⁴ shows that the sectional curvatures in $\text{Sym}_+(d)$ are bounded in $[-1/2, 0]$ and since \mathcal{N}_d^0 , endowed with $\iota^* \mathcal{I}^F$, is isometric¹⁵ by construction to $\text{Sym}_+(d)$, then $K^{\mathcal{N}_d^0}(\cdot, \cdot) \in [-1/2, 0]$. Therefore, $K^{\mathcal{U}}(X_1 + X_2, Y_1 + Y_2) \in [-1/2, 0]$.

By exhaustion, (i)-(iii) imply that all for possible planes in $T_{(\mathfrak{m}, \mathcal{N}_d(0, \Sigma))} \mathcal{U}$ one has $K^{\mathcal{U}}(X_1 + X_2, Y_1 + Y_2) \in [-1/2, 0]$. Since the point $(\mathfrak{m}, \mathcal{N}_d(0, \Sigma)) \in \mathcal{U}$ was arbitrary and since (\mathcal{U}, g) and $(\mathcal{N}_d, \mathfrak{J})$ are isometric, then, $K^{\mathcal{N}_d} \in [-1/2, 0]$. In particular, $(\mathcal{N}_d, \mathfrak{J})$ is a Cartan-Hadamard manifold and thus (Sturm, 2003, Proposition 3.1) implies that it is a global NPC space.

14. In their extended appendix in the ArXiV version.

15. In the Riemannian sense.

Exponential map at $\mathcal{N}_d(0, I_d)$ Lastly, since (\mathcal{U}, g) is a product Riemannian manifold, then (O’Neill, 1987, Corollary 57) implies that a curve $\gamma : [0, 1] \rightarrow \mathbb{R}^d \times \mathcal{N}_d^0$ is a geodesic in (\mathcal{U}, g) if and only if $\gamma(t) = (\gamma_1(t), \gamma_2(t))$, where γ_1 is a geodesic in \mathbb{R}^d and γ_2 is a geodesic in \mathcal{N}_d^0 .

Moreover, as shown on (Pennec et al., 2006, page 47), the (unique) geodesic emanating from $\Sigma \in \text{Sym}_+(d)$ with initial velocity $X \in \text{Sym}(d)$ is given by

$$t \mapsto \Sigma^{1/2} \exp(t \Sigma^{-1/2} X \Sigma^{-1/2}) \Sigma^{1/2}.$$

Since $\text{Sym}_+(d)$ is diffeomorphic to \mathcal{N}_d^0 (compare (D.1)), we conclude that

$$\gamma(t) = \left(\mathbf{m} + t \tilde{\mathbf{m}}, \mathcal{N} \left(0, \Sigma^{1/2} \exp \left(t \Sigma^{-1/2} X \Sigma^{-1/2} \right) \Sigma^{1/2} \right) \right) \in \mathcal{U}.$$

Thus, the geodesics emanating from $\mathcal{N}(\mathbf{m}, \Sigma)$ with velocity $(\tilde{\mathbf{m}}, X) \in \mathbb{R}^d \times \text{Sym}(d)$ reads as

$$t \mapsto \mathcal{N} \left(\mathbf{m} + t \tilde{\mathbf{m}}, \Sigma^{1/2} \exp \left(t \Sigma^{-1/2} X \Sigma^{-1/2} \right) \Sigma^{1/2} \right) \in \mathcal{N}_d. \quad (\text{D.5})$$

The expression of the Riemann exponential map of \mathcal{N}_d follows upon taking $t = 1$ in (D.5). ■

Appendix E. Proof of Theorem 11

The proof of Theorem 11 hinges on some preparatory material, we are now going to state and prove.

E.1 Riemann distance function on a product manifold

We are now going to prove the following Lemma from Riemannian geometry, for which we have been unable to provide a suitable reference in the literature.

Lemma E.1 *Let (M_1, h_1) and (M_2, h_2) be two smooth connected Riemannian manifolds, and let d_1 and d_2 be the respective induced Riemannian distance functions. Let $M \stackrel{\text{def.}}{=} M_1 \times M_2$ be the product manifold, endowed with the canonical Riemannian metric $h \stackrel{\text{def.}}{=} h_1 \oplus h_2$, and let d be the induced Riemannian distance function. Then, it holds*

$$d((x_1, x_2), (y_1, y_2)) = \sqrt{d_1(x_1, y_1)^2 + d_2(x_2, y_2)^2}, \quad (x_1, x_2), (y_1, y_2) \in M.$$

Proof Consider $p = (p_1, p_2) : [0, 1] \rightarrow M$ an arbitrary piecewise regular smooth path connecting (x_1, x_2) to (y_1, y_2) , with $(x_1, x_2) \neq (y_1, y_2)$. Evidently, also p_1 and p_2 are piecewise regular smooth path, connecting x_i to y_i , $i = 1, 2$. Let ℓ_i denote the length of p_i , $i = 1, 2$. We have by Cauchy-Schwartz inequality

$$\begin{aligned} \text{length}(p) \cdot \sqrt{\ell_1^2 + \ell_2^2} &= \int_0^1 \sqrt{|\dot{p}_1(t)|_{h_1}^2 + |\dot{p}_2(t)|_{h_2}^2} dt \cdot \sqrt{\ell_1^2 + \ell_2^2} \\ &\geq \ell_1 \int_0^1 |\dot{p}_1(t)|_{h_1} dt + \ell_2 \int_0^1 |\dot{p}_2(t)|_{h_2} dt \\ &= \ell_1^2 + \ell_2^2, \end{aligned}$$

leading to $\text{length}(p) \geq \sqrt{\ell_1^2 + \ell_2^2} \geq \sqrt{d_1(x_1, y_1)^2 + d_2(x_2, y_2)^2}$ and hence

$$d((x_1, x_2), (y_1, y_2)) \geq \sqrt{d_1(x_1, y_1)^2 + d_2(x_2, y_2)^2}.$$

To prove the reverse inequality, consider now $\gamma_i : [0, \lambda_i] \rightarrow M_i$ arbitrary piecewise regular smooth curve, parametrized by arc-length, joining x_i to y_i , $i = 1, 2$: here $\lambda_i \stackrel{\text{def.}}{=} \text{length}(\gamma_i)$.

Then, $\gamma : [0, 1] \rightarrow M$, $\gamma(t) = (\gamma_1(\lambda_1 t), \gamma_2(\lambda_2 t))$ is a piecewise regular smooth curve connecting (x_1, x_2) to (y_1, y_2) , whose length equals $\sqrt{\lambda_1^2 + \lambda_2^2}$. We infer

$$\sqrt{\lambda_1^2 + \lambda_2^2} \geq d((x_1, x_2), (y_1, y_2)),$$

and hence

$$\sqrt{d_1(x_1, y_1)^2 + d_2(x_2, y_2)^2} \geq d((x_1, x_2), (y_1, y_2)).$$

■

E.1.1 ADDITIONAL LEMMATA

Lemma E.2 (Control of the perturbed Fisher distance $d_{\mathfrak{J}}$ with constant mean) *Let $d \in \mathbb{N}_+$ and $M > 0$. For any $V, \tilde{V} \in \mathbb{R}^{d(d+1)/2}$ satisfying $\|V\|, \|\tilde{V}\| \leq M$ and any $\mathfrak{m} \in \mathbb{R}^d$ we have*

$$d_{\mathfrak{J}}(\mathcal{N}_d(\mathfrak{m}, \exp(\text{sym}(V))), \mathcal{N}_d(\mathfrak{m}, \exp(\text{sym}(\tilde{V})))) \leq \frac{2^{3/2}}{M} \sinh\left(\frac{M c_p}{\sqrt{2}}\right) \|V - \tilde{V}\|.$$

Proof of Lemma E.2 First remark that by Proposition 7, specifically (3.10),

$$\text{Exp}_p(0, X) = \mathcal{N}_d(\mathfrak{m}, \exp(X))$$

where we have set $p \stackrel{\text{def.}}{=} \mathcal{N}_d(\mathfrak{m}, I_d)$ for brevity.

By the sectional curvature estimates on $(\mathcal{N}_d, \mathfrak{J})$ in Proposition 7, we may apply Lemma C.1 to deduce that $\text{Exp}_p \circ \iota_p$ is not only locally-Lipschitz but its Lipschitz constant on the compact set $\overline{\text{Ball}_{(\mathbb{R}^{d(d+1)/2}, \|\cdot\|)}(0, M)}$ is bounded-above by

$$\text{Lip}(\text{Exp}_p \circ \iota_p | \overline{\text{Ball}_{(\mathbb{R}^d, \|\cdot\|)}(0, M)}) \leq 2c_p \frac{\sqrt{2}}{M c_p} \sinh\left(\frac{M c_p}{\sqrt{2}}\right) = \frac{2^{3/2}}{M} \sinh\left(\frac{M c_p}{\sqrt{2}}\right), \quad (\text{E.1})$$

where $\iota_p \stackrel{\text{def.}}{=} 1_{\mathbb{R}^d} \times \text{sym}$. For any $v \in \mathbb{R}^d$ and $z \in \mathbb{R}^{d(d+1)/2}$, by definition of \mathfrak{J} it holds

$$|\iota_p(v, z)|_p^2 = \|v\|_2^2 + \|\text{sym}(z)\|_F^2 \leq \|v\|_2^2 + \sqrt{2}\|z\|_2^2 \leq \|(v, z)\|^2$$

and thus, $|\iota_p|_{op} \leq 1$. Therefore, (E.1) yields

$$\text{Lip}(\text{Exp}_p \circ \iota_p | \overline{\text{Ball}_{(\mathbb{R}^d, \|\cdot\|)}(0, M)}) \leq \frac{2^{3/2}}{M} \sinh\left(\frac{M c_p}{\sqrt{2}}\right)$$

and hence the claim follows. ■

Lemma E.3 (Main path-wise stability estimate) *Fix $t \in \mathbb{N}_+$ and $R > 0$. Under Assumption 5, there exists $c > 0$ such that for $x_{[0:t]}, \tilde{x}_{[0:t]} \in \mathbb{R}^{(1+t)d}$ and $s_{[0:t]}, \tilde{s}_{[0:t]} \in \overline{\text{Ball}_{(\text{Sym}(d), \|\cdot\|_F)}(\mathbf{0}_d, R)}^{1+t}$*

$$d_{\mathfrak{J}}(\Psi_t(x_{[0:t]}, \text{vec} \circ s_{[0:t]}), \Psi_t(\tilde{x}_{[0:t]}, \text{vec} \circ \tilde{s}_{[0:t]})) \leq c \left(\|x_t - \tilde{x}_t\| + \sum_{r=0}^t \kappa(t, r) (\|x_r - \tilde{x}_r\| + \|s_r - \tilde{s}_r\|_F) \right). \quad (\text{E.2})$$

In particular, we have the Lipschitz condition

$$d_{\mathfrak{J}}(\Psi_t(x_{[0:t]}, \text{vec} \circ s_{[0:t]}), \Psi_t(\tilde{x}_{[0:t]}, \text{vec} \circ \tilde{s}_{[0:t]})) \leq c (\|x_{[0:t]} - \tilde{x}_{[0:t]}\| + \|s_{[0:t]} - \tilde{s}_{[0:t]}\|_F).$$

Moreover, the Lipschitz constant c is

$$c \stackrel{\text{def.}}{=} 2 \max\{1, L_{\mu}\} + \frac{2^{3/2} \max\{1, L_{\sigma}\}}{M + R} \sinh\left(\frac{M + R}{\sqrt{2}}\right).$$

Proof of Lemma E.3 By the triangle inequality, we can write

$$\begin{aligned}
 & d_{\mathfrak{J}}(\Psi_t(x_{[0:t]}, \text{vec} \circ s_{[0:t]}), \Psi_t(\tilde{x}_{[0:t]}, \text{vec} \circ \tilde{s}_{[0:t]})) \\
 &= d_{\mathfrak{J}}(\mathcal{N}_d(x_t + \text{Drift}(t, x_{[0:t]}), \Sigma_{t,x_{[0:t]},s_{[0:t]}}), \mathcal{N}_d(\tilde{x}_t + \text{Drift}(t, \tilde{x}_{[0:t]}), \Sigma_{t,\tilde{x}_{[0:t]},\tilde{s}_{[0:t]}})) \\
 &\leq d_{\mathfrak{J}}(\mathcal{N}_d(x_t + \text{Drift}(t, x_{[0:t]}), \Sigma_{t,x_{[0:t]},s_{[0:t]}}), \mathcal{N}_d(\tilde{x}_t + \text{Drift}(t, \tilde{x}_{[0:t]}), \Sigma_{t,x_{[0:t]},s_{[0:t]}})) \quad (\text{Mean-Term}) \\
 &\quad + d_{\mathfrak{J}}(\mathcal{N}_d(\tilde{x}_t + \text{Drift}(t, \tilde{x}_{[0:t]}), \Sigma_{t,x_{[0:t]},s_{[0:t]}}), \mathcal{N}_d(\tilde{x}_t + \text{Drift}(t, \tilde{x}_{[0:t]}), \Sigma_{t,\tilde{x}_{[0:t]},\tilde{s}_{[0:t]}})), \quad (\text{Cov-Term})
 \end{aligned}$$

where the function Σ . is defined to be

$$\Sigma_{t,x_{[0:t]},s_{[0:t]}} \stackrel{\text{def.}}{=} \exp\left(\sum_{r=0}^t \kappa(t,r) [\sigma(t,x_r) + s_r]\right). \quad (\text{E.3})$$

We first bound (Cov-Term) term. Under assumption 5, we have that $\sup_{t \in \mathbb{N}_+, x \in \mathbb{R}^d} \|\sigma(t, x)\|_F \leq M$ for some constant $M > 0$. Thus, for every $t \in \mathbb{N}_+$, $x \in \mathbb{R}^d$, and $s \in \cup_{r=0}^t \{s_r, \tilde{s}_r\}$ we have that

$$\|\sigma(t, x) + s\|_F \leq \|\sigma(t, x)\|_F + \|s\|_F \leq M + R.$$

Consequently, for each $t \in \mathbb{N}_+$, every $x_{[0:t]}, \tilde{x}_{[0:t]} \in \mathbb{R}^{(1+t)d}$, and $s_{[0:t], \tilde{s}_{[0:t]}} \in \overline{\text{Ball}}_{(\text{Sym}(d), \|\cdot\|_F)}(\mathbf{0}_d, R)^{1+t}$ we have by the triangle inequality that

$$\begin{aligned}
 & \left\| \sum_{r=0}^t \kappa(t,r) [\sigma(t,x_r) + s_r] \right\|_F \leq M + R, \\
 & \left\| \sum_{r=0}^t \kappa(t,r) [\sigma(t,\tilde{x}_r) + \tilde{s}_r] \right\|_F \leq M + R,
 \end{aligned}$$

because κ takes non-negative values whose sum is not bigger than 1. Since for any $A \in \text{Sym}(d)$ it holds $\|\text{vec}(A)\| \leq \|A\|_F$, we conclude that

$$\left\| \text{vec}\left(\sum_{r=0}^t \kappa(t,r) [\sigma(t,x_r) + s_r]\right) \right\|, \left\| \text{vec}\left(\sum_{r=0}^t \kappa(t,r) [\sigma(t,\tilde{x}_r) + \tilde{s}_r]\right) \right\| \leq M + R.$$

Therefore, upon recalling (E.3), Lemma E.2 applies; whence (Cov-Term) can be bounded as

$$\begin{aligned}
 & d_{\mathfrak{J}}(\mathcal{N}_d(\tilde{x}_t + \text{Drift}(t, \tilde{x}_{[0:t]}), \Sigma_{t,x_{[0:t]},s_{[0:t]})), \mathcal{N}_d(\tilde{x}_t + \text{Drift}(t, \tilde{x}_{[0:t]}), \Sigma_{t,\tilde{x}_{[0:t]},\tilde{s}_{[0:t]}})) \quad (\text{E.4}) \\
 &\leq \frac{2\sqrt{2}}{M+R} \sinh\left(\frac{M+R}{\sqrt{2}}\right) \left\| \text{vec}\left(\sum_{r=0}^t \kappa(t,r) [\sigma(t,x_r) + s_r]\right) - \text{vec}\left(\sum_{r=0}^t \kappa(t,r) [\sigma(t,\tilde{x}_r) + \tilde{s}_r]\right) \right\| \\
 &\leq \frac{2\sqrt{2}}{M+R} \sinh\left(\frac{M+R}{\sqrt{2}}\right) \left\| \left(\sum_{r=0}^t \kappa(t,r) [\sigma(t,x_r) + s_r]\right) - \left(\sum_{r=0}^t \kappa(t,r) [\sigma(t,\tilde{x}_r) + \tilde{s}_r]\right) \right\|_F \\
 &\leq \frac{2\sqrt{2}}{M+R} \sinh\left(\frac{M+R}{\sqrt{2}}\right) \sum_{r=0}^t \kappa(t,r) \left\| [\sigma(t,x_r) + s_r] - [\sigma(t,\tilde{x}_r) + \tilde{s}_r] \right\|_F \\
 &\leq \frac{2\sqrt{2}}{M+R} \sinh\left(\frac{M+R}{\sqrt{2}}\right) \sum_{r=0}^t \kappa(t,r) \max\{1, L_\sigma\} (\|x_r - \tilde{x}_r\| + \|s_r - \tilde{s}_r\|_F) \\
 &\leq \max\{1, L_\sigma\} \frac{2\sqrt{2}}{M+R} \sinh\left(\frac{M+R}{\sqrt{2}}\right) \sum_{r=0}^t \kappa(t,r) (\|x_r - \tilde{x}_r\| + \|s_r - \tilde{s}_r\|_F), \quad (\text{E.5})
 \end{aligned}$$

for every $t \in \mathbb{N}_+$, each $x_{[0:t]}, \tilde{x}_{[0:t]} \in \mathbb{R}^{(1+t)d}$, and each $s_{[0:t]}, \tilde{s}_{[0:t]} \in \overline{\text{Ball}_{(\text{Sym}(d), \|\cdot\|_F)}(\mathbf{0}_d, R)}^{1+t}$.

Concerning the (Mean-Term), in force of Proposition 7, we have

$$d_{\mathfrak{J}}\left(\mathcal{N}(x_t + \text{Drift}(t, x_{[0:t]}), \Sigma_{t,x_{[0:t]},s_{[0:t]}}), \mathcal{N}(\tilde{x}_t + \text{Drift}(t, \tilde{x}_{[0:t]}), \Sigma_{t,x_{[0:t]},s_{[0:t]}})\right) \quad (\text{E.6})$$

$$\begin{aligned} &= \| (x_t + \text{Drift}(t, x_{[0:t]})) - (\tilde{x}_t + \text{Drift}(t, \tilde{x}_{[0:t]})) \| \\ &= \left\| \left(x_t + \sum_{r=0}^t \kappa(t, r) \mu(t, x_r) \right) - \left(\tilde{x}_t + \sum_{r=0}^t \kappa(t, r) \mu(t, \tilde{x}_r) \right) \right\| \\ &\leq \|x_t - \tilde{x}_t\| + L_\mu \sum_{r=0}^t \kappa(t, r) \|x_r - \tilde{x}_r\| \\ &\leq \max\{1, L_\mu\} \left(\|x_t - \tilde{x}_t\| + \sum_{r=0}^t \kappa(t, r) \|x_r - \tilde{x}_r\| \right). \end{aligned} \quad (\text{E.7})$$

We put it all together: by Cauchy-Schwarz inequality and since

$$\left[\sum_{r=0}^t \kappa(t, r)^2 \right]^{1/2} \leq \left[\sum_{r=0}^t \kappa(t, r) \right]^{1/2} \leq 1.$$

We therefore, find that

$$\begin{aligned} &d_{\mathfrak{J}}\left(\Psi_t(x_{[0:t]}, \text{vec} \circ s_{[0:t]}), \Psi_t(\tilde{x}_{[0:t]}, \text{vec} \circ \tilde{s}_{[0:t]})\right) \\ &\leq 2 \left(\max\{1, L_\mu\} + \max\{1, L_\sigma\} \frac{\sqrt{2}}{M+R} \sinh\left(\frac{M+R}{\sqrt{2}}\right) \right) \|x_{[0:t]} - \tilde{x}_{[0:t]}\| \\ &\quad + 2 \max\{1, L_\sigma\} \frac{\sqrt{2}}{M+R} \sinh\left(\frac{M+R}{\sqrt{2}}\right) \|s_{[0:t]} - \tilde{s}_{[0:t]}\|_F, \end{aligned}$$

because trivially $\|x_t - \tilde{x}_t\| \leq \|x_{[0:t]} - \tilde{x}_{[0:t]}\|$. The Lemma has been proven. \blacksquare

We now have the following lemma.

Lemma E.4 (Dependence of $x_{[0:t]} \mapsto \mathbb{Q}_{x_{[0:t]}}$ on the realizations of $X_{[0:t]}$)

Suppose that Assumption 5 and the Volterra kernel κ satisfies either of the following decay conditions

(i) **Exponential decay:** For some $0 < \alpha < 1$ and $C > 0$, $\kappa(T, r) \leq C \alpha^{T-r}$ for all integers

$$0 \leq r \leq T, T > 0;$$

(ii) **Polynomial decay:** For some $C > 0 > \alpha$, $\kappa(T, r) \leq C(T-r)^\alpha$ for all integers $0 \leq r < T$;

Fix $T \in \mathbb{N}_+$ and a compact $\mathcal{K}_{[0:T]} \subseteq \mathbb{R}^{(1+T)d}$. For every pair of integers H, t , with $0 \leq H < t \leq T$, there is a Lipschitz function $f^{(t,H)} : (\mathbb{R}^{(1+H)d}, \|\cdot\|) \rightarrow (\mathcal{P}_1 \mathcal{N}_d, \mathcal{W}_1)$ satisfying

$$\mathcal{W}_1(\mathbb{Q}_{x_{[0:t]}}, f^{(t,H)}(x_{[t-H:t]})) \leq c \text{ diam}(\mathcal{K}_{[0:T]}) \begin{cases} \frac{C\alpha}{\alpha-1} (\alpha^t - \alpha^H) & \text{if (i) holds} \\ C(H+1)^\alpha (t-H) & \text{if (ii) holds} \end{cases}$$

for each $x_{[0:T]} \in \mathcal{K}_{[0:T]}$, where $c > 0$ only depends on $M, R > 0$ (in Assumption 5) and on L_μ .

Proof of Lemma E.4 Fix $0 \leq H < T$ and $H < t \leq T$. Define the map $\iota^{(t,H)} : \mathbb{R}^{(1+H)d} \rightarrow \mathbb{R}^{(1+t)d}$ sending any $x_{[t-H:t]} \in \mathbb{R}^{(1+H)d}$ to $(0, \dots, 0, x_{t-M}, \dots, x_t) \in \mathbb{R}^{(1+t)d}$ and define the map $f^{(t,H)}$ by

$$f^{(t,H)}(x_{[t-H:t]}) \stackrel{\text{def.}}{=} \mathbb{Q}_{\iota^{(t,H)}(x_{[t-H:t]})} \quad (\text{E.8})$$

for $x_{[t-H:t]} \in \mathbb{R}^{(1+H)d}$. Since $\mathbb{Q}_{x_{[0:t]}} \in \mathcal{P}_1(\mathcal{N}_d, \mathfrak{J})$ for each $x_{[0:t]}$ then $f^{(t,H)}$ takes values in $\mathcal{P}_1(\mathcal{N}_d, \mathfrak{J})$.

Fix an arbitrary $x_{[0:t]} \in \mathbb{R}^{(1+t)d}$. Since the 1-Wasserstein distance \mathcal{W}_1 between $\mathbb{Q}_{x_{[0:t]}}$ and $f^{(t,H)}(x_{[t-H:t]})$ is defined as the infimum over all transport plans/couplings having these two laws as marginals, we have

$$\mathcal{W}_1(\mathbb{Q}_{x_{[0:t]}}, f^{(t,H)}(x_{[t-H:t]})) \leq \mathbb{E} \left[d_{\mathfrak{J}} \left(\Psi_t(x_{[0:t]}, \text{vec} \circ \mathbf{S}_{[0:t]}), \Psi_t(\iota^{(t,H)}(x_{[t-H:t]}), \text{vec} \circ \mathbf{S}_{[0:t]}) \right) \right]. \quad (\text{E.9})$$

By Assumption (5), we may apply Lemma E.3 to upper-bound the quantity under expectation in (E.9) via the estimate (E.2). This yields

$$\mathbb{E} \left[d_{\mathfrak{J}} \left(\Psi_t(x_{[0:t]}, \text{vec} \circ \mathbf{S}_{[0:t]}), \Psi_t(\iota^{(t,H)}(x_{[t-H:t]}), \text{vec} \circ \mathbf{S}_{[0:t]}) \right) \right] \leq \mathbb{E} \left[c \sum_{r=0}^t \kappa(t, r) \|x_r - \iota^{(t,H)}(x_{[t-H:t]})_r\| \right] \quad (\text{E.10})$$

because $x_t = \iota^{(t,H)}(x_{[t-H:t]})_t$. Since $0 \leq M < t$, the right-hand side of (E.10) can be bounded above as follows

$$\begin{aligned} & \mathbb{E} \left[d_{\mathfrak{J}} \left(\Psi_t(x_{[0:t]}, \text{vec} \circ \mathbf{S}_{[0:t]}), \Psi_t(\iota^{(t,H)}(x_{[t-H:t]}), \text{vec} \circ \mathbf{S}_{[0:t]}) \right) \right] \leq \mathbb{E} \left[c \sum_{r=0}^t \kappa(t, r) \|x_r - \iota^{(t,H)}(x_{[t-H:t]})_r\| \right] \\ &= \mathbb{E} \left[c \sum_{r=0}^{t-H-1} \kappa(t, r) \|x_r\| \right] \\ &= c \sum_{r=0}^{t-H-1} \kappa(t, r) \|x_r\| \\ &\leq c \text{diam}(\mathcal{K}_{[0:T]}) \sum_{r=0}^{t-H-1} \kappa(t, r), \end{aligned} \quad (\text{E.11})$$

where the compactness of $\mathcal{K}_{[0:T]}$ implies that $\text{diam}(\mathcal{K}_{[0:T]})$ is finite. Set $C \stackrel{\text{def.}}{=} c \text{diam}(\mathcal{K}_{[0:T]})$. Combining (E.9) with (E.11) we have

$$\mathcal{W}_1(\mathbb{Q}_{x_{[0:t]}}, f^{(t,H)}(x_{[t-H:t]})) \leq C \sum_{r=0}^{t-H-1} \kappa(t, r),$$

for each $x_{[0:T]} \in \mathcal{K}_{[0:T]}$. Applying either Lemmata H.1 or H.2 yields the first conclusion.

It only remains to show that $f^{(t,H)}$ is Lipschitz. Let $x_{[t-H:t]}, \tilde{x}_{[t-H:t]} \in \mathbb{R}^{(1+H)d}$ and $t \in [[T]]$. Arguing similarly as above, using Lemma E.3, we find that

$$\begin{aligned} \mathcal{W}_1(f^{(t,H)}(x_{[t-H:t]}), f^{(t,H)}(\tilde{x}_{[t-H:t]})) &\leq \mathbb{E} \left[d_{\mathfrak{J}} \left(\Psi_t(\iota^{(t,H)}(x_{[t-H:t]}), \text{vec} \circ \mathbf{S}_{[0:t]}), \right. \right. \\ &\quad \left. \left. \Psi_t(\iota^{(t,H)}(\tilde{x}_{[t-H:t]}), \text{vec} \circ \mathbf{S}_{[0:t]}) \right) \right] \\ &\leq c \mathbb{E} \left[\left\| \iota^{(t,H)}(x_{[t-H:t]}) - \iota^{(t,H)}(\tilde{x}_{[t-H:t]}) \right\| \right. \\ &\quad \left. + \|x_t - \tilde{x}_t\| \right] \\ &= c \mathbb{E} \left[\|x_{[t-H:t]} - \tilde{x}_{[t-H:t]}\| + \|x_t - \tilde{x}_t\| \right] \end{aligned} \quad (\text{E.12})$$

$$\leq 2c \|x_{[t-H:t]} - \tilde{x}_{[t-H:t]}\|,$$

where (E.12) follows from the second part of Lemma E.3; relabelling $2c$ to c yields the statement. \blacksquare

Since Π is a Lipschitz function of the path $x_{[0:t]}$ then, perturbations to the realized path $x_{[0:t]}$ result in at-most linear changes of the value of $\Pi_{x_{[0:t]}}$. To quantify this stability, let $\tilde{\mathbf{S}}_{\cdot}$ be another $d \times d$ -dimensional matrix-valued processes, also defined on $(\Omega, \mathcal{F}, \mathbb{P})$ and satisfying Assumption 5.

Proposition E.5 (Lipschitz stability wrt. perturbations of the paths of X and of \mathbf{S} .) *Fix $t \in \mathbb{N}$ and a compact $\mathcal{K}_{[0:t]} \subseteq \mathbb{R}^{(1+t)d}$. If both \mathbf{S}_{\cdot} and $\tilde{\mathbf{S}}_{\cdot}$ satisfy Assumption 5 then, for each $x_{[0:t]} \in \mathcal{K}_{[0:t]}$, $\beta(\text{Law}(\Psi_t(x_{[0:t]}, \text{vec} \circ \mathbf{S}_{[0:t]})))$ is well-defined. Furthermore*

$$d_{\mathfrak{J}}\left(\beta(\text{Law}(\Psi_t(x_{[0:t]}, \text{vec} \circ \mathbf{S}_{[0:t]}))), \beta(\text{Law}(\Psi_t(\tilde{x}_{[0:t]}, \text{vec} \circ \tilde{\mathbf{S}}_{[0:t]})))\right) \lesssim \|x_{[0:t]} - \tilde{x}_{[0:t]}\| + \mathbb{E}[\|\mathbf{S}_{[0:t]} - \tilde{\mathbf{S}}_{[0:t]}\|_F],$$

holds for each $x_{[0:t]}, \tilde{x}_{[0:t]} \in \mathcal{K}_{[0:t]}$, where \lesssim suppresses a positive constant depending only on t and on R . In particular, the following holds for each $x_{[0:t]}, \tilde{x}_{[0:t]} \in \mathcal{K}_{[0:t]}$

$$d_{\mathfrak{J}}\left(\beta(\mathbb{Q}_{x_{[0:t]}}, \beta(\mathbb{Q}_{\tilde{x}_{[0:t]}}))\right) \lesssim \|x_{[0:t]} - \tilde{x}_{[0:t]}\|.$$

Proof of Lemma E.5 By Proposition 7 $(\mathcal{N}_d, d_{\mathfrak{J}})$ is a global NPC and by Assumption 5 (ii) we may apply Theorem 4 to deduce that for every $t \in \mathbb{N}_+$

$$\begin{aligned} d_{\mathfrak{J}}\left(\beta(\text{Law}(\Psi_t(x_{[0:t]}, \text{vec}(\mathbf{S}_{[0:t]}))), \beta(\text{Law}(\Psi_t(\tilde{x}_{[0:t]}, \text{vec}(\tilde{\mathbf{S}}_{[0:t]}))))\right) \\ \leq \mathcal{W}_1\left(\text{Law}(\Psi_t(x_{[0:t]}, \text{vec}(\mathbf{S}_{[0:t]})), \text{Law}(\Psi_t(\tilde{x}_{[0:t]}, \text{vec}(\tilde{\mathbf{S}}_{[0:t]})))\right) \end{aligned} \quad (\text{E.13})$$

$$\leq \mathbb{E}[d_{\mathfrak{J}}(\Psi_t(x_{[0:t]}, \text{vec}(\mathbf{S}_{[0:t]})), \Psi_t(\tilde{x}_{[0:t]}, \text{vec}(\tilde{\mathbf{S}}_{[0:t]})))] \quad (\text{E.14})$$

where (E.13) follows from the definition of the 1-Wasserstein distance on $(\mathcal{N}_d, \mathfrak{J})$. Applying Lemma E.3 to the right-hand side of (E.14), allows us to deduce the estimate

$$\begin{aligned} d_{\mathfrak{J}}\left(\beta(\text{Law}(\Psi_t(x_{[0:t]}, \text{vec}(\mathbf{S}_{[0:t]}))), \beta(\text{Law}(\Psi_t(\tilde{x}_{[0:t]}, \text{vec}(\tilde{\mathbf{S}}_{[0:t]}))))\right) \\ \lesssim \mathbb{E}\left[\|x_{[0:t]} - \tilde{x}_{[0:t]}\| + \|\mathbf{S}_{[0:t]} - \tilde{\mathbf{S}}_{[0:t]}\|_F\right] \\ = (\|x_{[0:t]} - \tilde{x}_{[0:t]}\| + \mathbb{E}[\|\mathbf{S}_{[0:t]} - \tilde{\mathbf{S}}_{[0:t]}\|_F]). \end{aligned}$$

This completes the proof of the first claim; the second claim directly follows by definition of $\mathbb{Q}_{x_{[0:t]}}$. \blacksquare

Proof of Theorem 11 Since the conditions of Lemma E.4 are met, for each pair of non-negative integers H, T with $H < T$ and every compact $\mathcal{K}_{[0:T]} \subseteq \mathbb{R}^{(1+T)d}$ there is a constant $C > 0$, depending only on $\mathcal{K}_{[0:T]}$, and functions $f^{(t,H)} : (\mathbb{R}^{(1+H)d}, \|\cdot\|) \rightarrow (\mathcal{P}_1(\mathcal{N}_d, \mathfrak{J}), \mathcal{W}_1)$, for $T - H \leq H$, satisfying

$$\mathcal{W}_1(\mathbb{Q}_{x_{[0:t]}}, f^{(t,H)}(x_{[t-H:t]})) \leq c \text{ diam}(\mathcal{K}_{[0:T]}) \begin{cases} \frac{C\alpha}{\alpha-1} (\alpha^t - \alpha^H) & \text{if (i) holds} \\ C(H+1)^\alpha (t-H) & \text{if (ii) holds} \end{cases} \quad (\text{E.15})$$

where $c > 0$ depends only on M and on R and where $C \geq 0$ depends only on K, T , and on which of (i) or (ii), holds in Lemma E.4.

In particular, \tilde{C} only depends on $\mathcal{K}_{[0:T]}$ and on T . By Proposition 2, $(\mathcal{N}_d, d_{\mathfrak{J}})$ is a non-positively curved metric space since it is complete, simply connected, and it has everywhere non-positive sectional curvatures. Thus, Theorem 4 implies that the barycenter map $\beta : (\mathcal{P}_1(\mathcal{N}_d, \mathfrak{J}), \mathcal{W}_1) \rightarrow$

$(\mathcal{N}_d, d_{\mathfrak{J}})$ is 1-Lipschitz. Therefore, the existence and 1-Lipschitz regularity of β , together with estimate in (E.15) imply

$$\begin{aligned} d_{\mathfrak{J}}(\beta(\mathbb{Q}_{x_{[0:t]}}, \mathbb{Q}_{x_{[t-H:t]}}), \beta \circ f^{(t,H)}(x_{[t-H:t]})) &\leq \mathcal{W}_1\left(\text{Law}(\mathbb{Q}_{x_{[0:t]}}, \mathbb{Q}_{x_{[t-H:t]}}, f^{(t,H)}(x_{[t-H:t]}))\right) \\ &\leq c \text{ diam}(\mathcal{K}_{[0:T]}) \begin{cases} \frac{C\alpha}{\alpha-1} (\alpha^t - \alpha^H) & \text{if (i) holds} \\ C(H+1)^\alpha (t-H) & \text{if (ii) holds} \end{cases}, \end{aligned}$$

for each $x_{[0:T]} \in \mathcal{K}_{[0:T]}$ and each $T-H \leq t \leq T$. Lastly, for each $T-H \leq t \leq T$, set $\tilde{f}^{(t,H)} \stackrel{\text{def.}}{=} \beta \circ f^{(t,H)}$ to obtain the conclusion. Relabelling $c \stackrel{\text{def.}}{=} C_{M,R,\mu}$ yields the conclusion. \blacksquare

Finally, we demonstrate the smoothness of the Gaussian random projection.

Proof of Proposition 10 Fix any $t \in \mathbb{N}_+$ and any $x_{[0:t]} \in \mathbb{R}^{(1+t)d}$. Observe that

$$\Pi_{x_{[0:t]}} = \beta(\text{Law}(\Psi_t(x_{[0:t]}, \mathbf{0}))) = \beta(\delta_{\Psi_t(x_{[0:t]}, \mathbf{0})}) = \delta_{\Psi_t(x_{[0:t]}, \mathbf{0})}, \quad (\text{E.16})$$

where $\mathbf{0} = (0, \dots, 0) \in \text{Sym}(d)^{1+t}$ and where the right-hand side of (E.16) follows from the fact that $\mathbf{S}_{[0:t]} = 0$ \mathbb{P} -a.s. and that β is a (contracting) barycenter map then $\beta(\delta_\mu) = \mu$ for every $\mu \in \mathcal{N}_d$. Since ψ is real-analytic (whence it is C^∞ ; i.e. smooth) and since the composition and sums of C^∞ (smooth) maps defined a C^∞ (smooth) map then each Ψ_t is C^∞ (smooth) map if μ and σ are. Therefore, the map $x_{[0:T]} \mapsto \Psi_t(x_{[0:t]}, \mathbf{0}) = \Pi_{x_{[0:t]}}$ is smooth. \blacksquare

Appendix F. Proof of universality in the static case - Theorem 13 and Corollary 14

Before proceeding with the proof of Theorem 13, we give some preparatory material. First, we state and prove a special case of the universal approximation theorem of Galimberti et al. (2022), Theorem 1; see Subsection F.1. Second, we provide a Universal Approximation result for a general f and finite \mathcal{K} ; see Subsection F.2.

F.1 A brief review of feedforward theory

Lemma F.1 is a multi-dimensional consequence of the main results of Shen et al. (2022) and Lu et al. (2021). We record the results here, since they can be obtained by modifying only one step of the proof of Theorem 1 in Galimberti et al. (2022), by decoupling the condition that the width and depth parameters are set to be equal. In particular, in this formulation, the ReLU feed-forward network's depth is kept as a hyperparameter. This is useful since it will allow us to synchronize the depths of our convolutional neural networks, and to avoid parity issues or the need to deploy a trainable PReLU activation function (Acciaio et al., 2023) capable of implementing the identity.

Lemma F.1 (Universal approximation for ReLU feedforward Neural Networks) *Fix positive integers d^*, D , let \mathcal{K} be a non-empty compact of \mathbb{R}^{d^*} . Consider $f : \mathcal{K} \rightarrow \mathbb{R}^D$ such that either:*

- (i) f extends to an λ -Lipschitz C^k function $F : \mathbb{R}^{d^*} \rightarrow \mathbb{R}^D$,
- (ii) f extends to a C^α -Hölder function $F : \mathbb{R}^{d^*} \rightarrow \mathbb{R}^D$ for some $0 < \alpha \leq 1$ with Hölder constant λ .

Then, for every “approximation error” ε and every “depth hyperparameter” $J \in \mathbb{N}_+$ there exists a ReLU feedforward neural network $\hat{f} : \mathbb{R}^{d^} \rightarrow \mathbb{R}^D$ satisfying the uniform estimate*

$$\max_{x \in \mathcal{K}} \|f(x) - \hat{f}(x)\| < \varepsilon.$$

Furthermore the depth and width of \hat{f} are recorded in Table 13.

Table 13: Approximation Rates - ReLU feedforward Neural Network with fixed depth

In case (i), the constants in Table 13 are $C_0 \stackrel{\text{def.}}{=} d^*(D-1)$, $C_1 \stackrel{\text{def.}}{=} 17k^{d^*+1}3^{d^*}$ and $C_{\bar{F}} \stackrel{\text{def.}}{=} \max_{i=1,\dots,D} \|F_i \circ W\|_{C^k([0,1]^d)}$; where W is any bijective affine self-map on \mathbb{R}^{d^*} map satisfying $W(K) \subseteq [0, 1]^{d^*}$.

In case (ii), the constants in Table 13 are $C_0 \stackrel{\text{def.}}{=} d^*(D-1)$, $C_1 \stackrel{\text{def.}}{=} 3^{d^*+3}$, $C_2 \stackrel{\text{def.}}{=} 19+2d^*$, $C_3 \stackrel{\text{def.}}{=} (131(d^*D)^{1/2})$, and $V : [0, \infty) \rightarrow [0, \infty)$ is the “special function” defined as the inverse of $t \mapsto t^2 \log_3(t+2)$.

In case (iii), the constant in Table 13 is $C = (1+H)d(D-1) + 9(\text{diam}(\mathcal{K}_{[0:H]})) \left(\frac{(1+H)d}{2(1+H)d+2}\right)^{1/2} DN$.

Hyperparam.	Exact Quantity - High Regularity (Case (i))
Depth	$D\left(1 + 18k^2(J+2) \log_2(4J) + 2d^*\right)$
Width	$C_0 + C_1\left(2 + \left\lceil J\left(\frac{C_{\bar{F}}D^{1/2}}{\varepsilon}\right)^{d^*/(2k)}\right\rceil\right) \log_2\left(8\left\lceil J\left(\frac{C_{\bar{F}}D^{1/2}}{\varepsilon}\right)^{d^*/(2k)}\right\rceil\right)$
Hyperparam.	Exact Quantity - Low Regularity - (Case (ii))
Depth	$D\left(11J + C_2\right)$
Width	$C_0 + C_1 \max\left\{d^*\left\lfloor\left(V(J^{-2}(C_1\varepsilon/\lambda)^{d^*/\alpha})\right)\right\rfloor^{1/d^*}\right\rfloor, 2 + \left\lceil V(J^{-2}(C_1\varepsilon/\lambda)^{d^*/\alpha})\right\rceil\right\}$
Hyperparam.	Exact Quantity - No Regularity - Finite $\#\mathcal{K} = N$ (Case (iii))
Depth	$D\left(28N^2J\right)$
Width	$\left\lceil(\varepsilon^{-1}C)^{1/(2NJ)}\right\rceil - 1 + 2N - 8$

F.2 Static universality: The case of general f and finite \mathcal{K}

Lemma F.2 (Universal approximation: General f and finite \mathcal{K}) *Let $M, d, D, N \in \mathbb{N}$. Fix any N -point subset $\mathcal{K}_{[0:H]} \subseteq \mathbb{R}^{(1+H)d}$ and any function $f : \mathbb{R}^{(1+H)d} \rightarrow \mathbb{R}^D$. For every “approximation error” $\varepsilon > 0$ and every “depth hyperparameter” $J \in \mathbb{N}_+$, there exists a ReLU neural network $\hat{f} : \mathbb{R}^{(1+H)d} \rightarrow \mathbb{R}^D$ satisfying the uniform estimate*

$$\max_{x \in \mathcal{K}_{[0:H]}} \|f(x) - \hat{f}(x)\| < \varepsilon.$$

Moreover, the depth and width of \hat{f} are:

1. **Depth:** $D(28N^2J)$,
2. **Width:** $D\left((1+H)d(D-1) + 9\left(\left\lceil(\varepsilon^{-1}C)^{1/(2NJ)}\right\rceil - 1\right) + 2N - 8\right)$,
3. **Number of trainable parameters:** $\left((11/4)(1+H)dD - 1\right) \times (28N^2J + 1)\left((1+H)d(D-1) + 9\left(\left\lceil(\varepsilon^{-1}C)^{1/(2NJ)}\right\rceil - 1\right) + 2N - 8\right)^2 + 2(1+H)d + 2D$

where $C > 0$ is a constant independent of J and of ε .

Proof of Lemma F.2 The proof consists of several *Steps*.

Step 1: Re-scaling to the unit cube

We begin by enumerating $\mathcal{K}_{[0:H]} = \{x_{[0:H]}^{(n)}\}_{n=0}^{N-1}$. Clearly, there exists some invertible affine maps

$A : \mathbb{R}^{(1+\mathrm{H})d} \rightarrow \mathbb{R}^{(1+\mathrm{H})d}$ and $\tilde{A} : \mathbb{R}^D \rightarrow \mathbb{R}^D$ “re-normalizing the linearized data to the unite cubes”; i.e. satisfying

$$A(\{x^{(n)}\}_{n=1}^N) \subseteq [0, 1]^{(1+\mathrm{H})d} \quad \text{and} \quad \tilde{A}(\{f(x^{(n)})\}_{n=1}^N) \subseteq [0, 1]^D. \quad (\mathrm{F}.1)$$

Accordingly, for each $n = 1, \dots, N$ we label these “re-normalized datasets” by

$$u^{(n)} \stackrel{\text{def.}}{=} A(x^{(n)}) \quad \text{and} \quad w^{(n)} \stackrel{\text{def.}}{=} \tilde{A}(f(x^{(n)})). \quad (\mathrm{F}.2)$$

Furthermore, Jung’s Theorem, see e.g. (Lang and Schroeder, 1997, Theorem A) (in the case where the Alexandrov curvature $\kappa = 0$), implies that there exists $y_0 \in \mathbb{R}^D$ such that

$$\tilde{A}(y) = \frac{1}{\text{diam}(f(\mathcal{K}_{[0:\mathrm{H}]}))} \left(\frac{2(1+\mathrm{H})d+2}{(1+\mathrm{H})d} \right)^{1/2} (y - y_0) \stackrel{\text{def.}}{=} D_{\tilde{A}}y + \tilde{a} \quad (\mathrm{F}.3)$$

for each $y \in \mathbb{R}^D$. A similar expression of A is also implied by Jung’s Theorem. In particular, the affine map $\tilde{A} = D_{\tilde{A}} \cdot + \tilde{a}$ (resp. $A = D_A \cdot + a$) is defined by multiplication against a square diagonal matrix $D_{\tilde{A}}$ (resp. D_A) and a shift by a vector $\tilde{a} \in \mathbb{R}^{(1+\mathrm{H})d}$ (resp. $a \in \mathbb{R}^D$) and therefore

$$\|\tilde{A}\|_0 + \|\tilde{a}\|_0 \leq 2(1+\mathrm{H})d \text{ and } \|A\|_0 + \|a\|_0 \leq 2D. \quad (\mathrm{F}.4)$$

We will come back the the parameter count in (F.4) towards the end of the proof.

Step 2: A polynomial extension of the target function on the transformed dataset

Note that the squared Euclidean norm $\|\cdot\|$ is a polynomial function. Define the polynomial function $F : \mathbb{R}^{(1+\mathrm{H})d} \rightarrow \mathbb{R}^D$ of degree $2N$ by

$$\begin{aligned} F(u) &\stackrel{\text{def.}}{=} \sum_{\tilde{n}=1}^N \left(\prod_{\substack{n=1, \dots, N \\ n \neq \tilde{n}}} \left(\frac{\|u^{(n)} - u\|^2}{\|u^{(n)} - u^{(\tilde{n})}\|^2} \right) \right) \cdot w^{(n)} \\ &= \sum_{\tilde{n}=1}^N \left(c_{\tilde{n}} \prod_{\substack{n=1, \dots, N \\ n \neq \tilde{n}}} \left(\sum_{k=1}^{d^*} (u_k^{(n)} - u_k)^2 \right) \right) \cdot w^{(n)}; \end{aligned}$$

where $c_{\tilde{n}} \stackrel{\text{def.}}{=} \prod_{n=1, \dots, N; n \neq \tilde{n}} (\|u^{(n)} - u^{(\tilde{n})}\|^2)^{-1}$. By construction, the polynomial function F interpolates the re-normalized datasets in (F.2); that is: for each $n = 1, \dots, N$ we have

$$F(u^{(n)}) = w^{(n)}. \quad (\mathrm{F}.5)$$

Depending now on a few parameters, we approximate the function F by a “small” ReLU feed-forward neural network.

Step 3: Efficient approximation of the target functions polynomial extension

Fix a “width hyperparameter” w and a “depth hyperparameter” J , both of which are positive integers and such that the value of w will be determined at the end of the proof. By construction, each of the components $F(x)_i, i = 1, \dots, D$ of the function F are polynomial. Thus, (Lu et al., 2021, Proposition 4.1) implies that for each $i = 1, \dots, D$ there are deep ReLU networks $f^{(i)} : \mathbb{R}^{(1+\mathrm{H})d} \rightarrow \mathbb{R}$ each having width $9w + (2N) - 8$ and depth $7(2N)^2J$, and each satisfying the uniform estimate

$$\max_{i=1, \dots, D} \max_{x \in [0, 1]^{(1+\mathrm{H})d}} \left| f^{(i)}(x) - [F(x)]_i \right| \leq C_N \frac{1}{(w+1)^{(2N)J}}; \quad (\mathrm{F}.6)$$

where $C_N \stackrel{\text{def.}}{=} 9(2N) \geq 0$; in particular, C_N is independent of w and J . We would like to efficiently “parallelize” these deep feedforward networks; that is, we seek a deep ReLU feedforward neural

network $\tilde{f} : \mathbb{R}^{(1+H)d} \rightarrow \mathbb{R}^D$ satisfying

$$\tilde{f}(u) = \sum_{i=1}^D f^{(i)}(u) \cdot e_i, \quad (\text{F.7})$$

for all $u \in \mathbb{R}^{(1+H)d}$, where e_1, \dots, e_D denotes the standard orthonormal basis of \mathbb{R}^D . Since the (activation) function ReLU has the 2-identity property (see (Cheridito et al., 2021, Definition 4)) then (Cheridito et al., 2021, Proposition 5) implies that there exists a deep ReLU feedforward neural network $f : \mathbb{R}^{(1+H)d} \rightarrow \mathbb{R}^D$ satisfying (F.7) and whose

$$\begin{aligned} \text{Depth} &\text{ is at-most } D(28N^2J) \\ \text{Width} &\text{ is at-most } D((1+H)d(D-1) + 9w + 2N - 8) \end{aligned}$$

$$\begin{aligned} \text{N. Trainable parameters} &\leq ((11/4)(1+H)dD - 1) \\ &\times (28N^2J + 1)((1+H)d(D-1) + 9w + 2N - 8)^2. \end{aligned}$$

Therefore, together (F.6) and (F.7) imply that

$$\begin{aligned} \max_{u \in [0,1]^{(1+H)d}} \|\tilde{f}(u) - F(u)\| &= \max_{u \in [0,1]^{(1+H)d}} \left\| \sum_{i=1}^D (f^{(i)}(u) - [F(u)]_i) e_i \right\| \\ &\leq \max_{u \in [0,1]^{(1+H)d}} \sum_{i=1}^D |f^{(i)}(u) - [F(u)]_i| \\ &\leq D \max_{u \in [0,1]^{(1+H)d}} \|f(u) - F(u)\| \\ &\leq DNC_N \frac{1}{(w+1)^{2N\bar{J}}}. \end{aligned} \quad (\text{F.8})$$

Restricting the estimate in (F.8) from all of $[0,1]^{(1+H)d}$ down to the subset $\{u^{(n)}\}_{n=1}^N \subseteq [0,1]^{(1+H)d}$ and recalling the interpolation property of F on the pairs $\{(u^{(n)}, w^{(n)})\}_{n=1}^N$ in (F.5), we deduce that

$$\max_{n=1, \dots, N} \|\tilde{f}(u^{(n)}) - w^{(n)}\| \leq C_{N,D} \frac{1}{(w+1)^{2N\bar{J}}}, \quad (\text{F.9})$$

where $C_{N,D} \stackrel{\text{def.}}{=} DNC_N$ and we note that the constant $C_{N,D} > 0$ is independent of w and of \bar{J} .

Next, we observe that the pre-composition and post-composition of any deep ReLU neural network by invertible affine self-maps is again a deep ReLU neural network of the same depth and width. Therefore,

$$\hat{f} \stackrel{\text{def.}}{=} \tilde{A}^{-1} \circ \tilde{f} \circ A$$

is a ReLU neural network with the same depth and width as \tilde{f} . Furthermore, is defined by at-most

$$P + 2(1+H)d + 2D \quad (\text{F.10})$$

trainable parameters, due to the sparse representation of \tilde{A}^{-1} and A and the parameter count in (F.4); here P denotes the number of trainable parameters of \tilde{f} .

Putting it all together, we find that

$$\begin{aligned} \max_{n=1, \dots, N} \|\hat{f}(x_n) - f(x_n)\| &= \max_{n=1, \dots, N} \|\tilde{A}^{-1} \circ \tilde{f} \circ A(x_n) - f(x_n)\| \\ &= \max_{n=1, \dots, N} \|\tilde{A}^{-1} \circ \tilde{f} \circ A(x_n) - \tilde{A}^{-1} \circ \tilde{A} \circ f(x_n)\| \end{aligned}$$

$$\begin{aligned}
 &= \max_{n=1,\dots,N} \|\tilde{A}^{-1} \circ \tilde{f}(u_n) - \tilde{A}^{-1}(w^{(n)})\| \\
 &\leq \text{Lip}(\tilde{A}^{-1}) \max_{n=1,\dots,N} \|\tilde{f}(u_n) - w^{(n)}\| \\
 &\leq \text{Lip}(\tilde{A}^{-1}) C_{N,D} \frac{1}{(w+1)^{2NJ}} \\
 &= \text{diam}(f(\mathcal{K}_{[0:H]})) \left(\frac{(1+H)d}{2(1+H)d+2} \right)^{1/2} C_{N,D} \frac{1}{(w+1)^{2NJ}} \quad (\text{F.11})
 \end{aligned}$$

$$= C \frac{1}{(w+1)^{2NJ}} \quad (\text{F.12})$$

where (F.11) follows from the expression for \tilde{A} in (F.3) which implies the expression and Lipschitz constant of its inverse $\tilde{A}^{-1}(w) \mapsto \text{diam}(f(\mathcal{K}_{[0:H]})) \left(\frac{(1+H)d}{2(1+H)d+2} \right)^{1/2} y + y_0$ and where (F.12) follows by definition of the constant $C \stackrel{\text{def.}}{=} \text{diam}(f(\mathcal{K}_{[0:H]})) \left(\frac{(1+H)d}{2(1+H)d+2} \right)^{1/2} C_{N,D}$. We note that $C > 0$ and that it does not depend on J nor does it depend on w . Upon setting $w \stackrel{\text{def.}}{=} \lceil (\varepsilon^{-1} C)^{1/(2NJ)} \rceil - 1$, the right-hand side of (F.12) is bounded-above by ε and we obtain the conclusion and \hat{f} is as in Table 13 case (iii). \blacksquare

The diagram in Figure 5 is used to illustrate the workflow used in the proof of Theorem 13.

$$\begin{array}{ccccc}
 \mathcal{K}_{[0:H]} & \xhookrightarrow{\quad} & \mathcal{N}^{1+H} & \xrightarrow{f} & \mathcal{M} \\
 \downarrow \varphi & & \downarrow \varphi & & \uparrow \rho \\
 \prod_{m=0}^M \text{Log}_{\bar{x}_m}(\tilde{\mathcal{K}}_m) & \xhookrightarrow{\quad} & \mathbb{R}^{(1+H)d} & \xrightarrow{\hat{f}} & \mathbb{R}^D
 \end{array}$$

Figure 5: Diagram chase in the proof of Theorem 13.

Proof of Theorem 13 The proof is divided into three steps, highlighted in the following. We first begin by introducing some convenient notation. Fix $x^* \in \mathcal{N}$, $y^* \in \mathcal{Y}$, and define

$$\begin{aligned}
 \varphi : \mathcal{N}^{1+H} &\ni x_{[0:H]} \mapsto \left(\text{Log}_{\bar{x}_m}^h \circ \iota_{\mathcal{N}, \bar{x}_m}(x_m) \right)_{m=0}^M \in \mathbb{R}^{(1+H)D} \\
 \rho : \mathbb{R}^d &\ni y \mapsto \text{Exp}_{\bar{y}}^g \circ \iota_{\mathcal{M}, y}^{-1}(y) \in \mathcal{M}.
 \end{aligned}$$

where $\bar{x}_{[0:H]}$ and \bar{y} are defined as in (5.2).

Step 0: Preliminary definitions

Fix a non-empty compact subset $\mathcal{K}_{[0:H]} \subseteq \mathcal{N}^{1+H}$, a map $f : \mathcal{N}^{1+H} \rightarrow \mathcal{M}$, and some pre-specified “approximation error” $0 < \varepsilon \leq 1$. Chasing the diagram in Figure 5, we define the following subset of \mathcal{M} :

$$\tilde{\mathcal{K}} \stackrel{\text{def.}}{=} \rho \left(\left\{ u \in \mathbb{R}^D : \inf_{v \in \rho^{-1} \circ f(\mathcal{K}_{[0:H]})} \|u - v\| \leq 1 \right\} \right),$$

which is the closure of the 1-fattening/thickening of the set $\rho^{-1} \circ f(\mathcal{K}_{[0:H]})$ with respect to the Euclidean distance on \mathbb{R}^D . By construction, $\tilde{\mathcal{K}}$ is a compact subset of \mathcal{M} , since $\{u \in \mathbb{R}^D : \inf_{v \in \rho^{-1} \circ f(\mathcal{K}_{[0:H]})} \|u - v\| \leq 1\}$ is compact in \mathbb{R}^D and ρ is a homeomorphism, $\tilde{\mathcal{K}}$ contains $\rho^{-1} \circ f(\mathcal{K}_{[0:H]})$, and it does not depend on the approximation error ε .

Comment: The role of the set $\tilde{\mathcal{K}}$ is to define a compact region in \mathcal{M} , containing what will be the image of our approximation of $\rho^{-1} \circ f$ on $\mathcal{K}_{[0:H]}$, in which the local Lipschitz constant of the map ρ may be controlled independently of ε . Note, we need to do so, since ρ is not globally Lipschitz.

Step 1: Reduction to a function approximation problem between Euclidean spaces

For any map $F : \mathbb{R}^{(M+1)D} \rightarrow \mathbb{R}^d$, the following preliminary estimates holds true. Since ρ and φ are global diffeomorphisms, then, in particular, they admit smooth inverses, and these smooth inverses are respectively defined on all of \mathcal{M} and over all of \mathcal{N} .

Chasing the diagram in Figure 5, again, we define the induced maps $\tilde{f} : \mathbb{R}^{(1+H)D} \rightarrow \mathbb{R}^d$ and $\tilde{F} : \mathcal{N}^{1+H} \rightarrow \mathcal{M}$ by

$$\tilde{f} \stackrel{\text{def.}}{=} \rho^{-1} \circ f \circ \varphi^{-1} \text{ and } \tilde{F} \stackrel{\text{def.}}{=} \rho \circ F \circ \varphi.$$

We deduce that:

$$\begin{aligned} \sup_{x_{[0:H]} \in \mathcal{K}_{[0:H]}} d_g(f(x), \tilde{F}(x)) &= \sup_{x_{[0:H]} \in \mathcal{K}_{[0:H]}} d_g((\rho \circ \rho^{-1}) \circ f \circ (\varphi^{-1} \circ \varphi)(x), (\rho \circ \rho^{-1}) \circ \tilde{F} \circ (\varphi^{-1} \circ \varphi)(x)) \\ &= \sup_{x_{[0:H]} \in \mathcal{K}_{[0:H]}} d_g(\rho \circ \tilde{f} \circ \varphi(x), (\rho \circ \rho^{-1}) \circ \tilde{F} \circ (\varphi^{-1} \circ \varphi)(x)) \\ &= \sup_{x_{[0:H]} \in \mathcal{K}_{[0:H]}} d_g(\rho \circ \tilde{f} \circ \varphi(x), \rho \circ (\rho^{-1} \circ \rho) \circ F \circ (\varphi \circ \varphi^{-1}) \circ \varphi(x)) \\ &= \sup_{x_{[0:H]} \in \mathcal{K}_{[0:H]}} d_g(\rho \circ \tilde{f} \circ \varphi(x), \rho \circ F \circ \varphi(x)) \\ &= \sup_{u_{[0:H]} \in \varphi(\mathcal{K}_{[0:H]})} d_g(\rho \circ \tilde{f}(u), \rho \circ F(u)). \end{aligned} \quad (\text{F.13})$$

Notice that if g is any function satisfying the following uniform estimate on $\varphi(\mathcal{K}_{[0:H]})$

$$\sup_{u \in \varphi(\mathcal{K}_{[0:H]})} \|\tilde{f}(u) - g(u)\| \leq 1, \quad (\text{F.14})$$

then, $F \circ \varphi(\mathcal{K}_{[0:H]}) \subseteq \rho^{-1}[\tilde{\mathcal{K}}]$, and since ρ is bijective, this implies that $\rho \circ F \circ \varphi(\mathcal{K}_{[0:H]}) \subseteq \tilde{\mathcal{K}}$. Moreover, by construction, $\rho \circ \tilde{f} \circ \varphi(\mathcal{K}_{[0:H]}) \subseteq \tilde{\mathcal{K}}$. Therefore the compact set $\tilde{\mathcal{K}}$ contains $\rho \circ F(\varphi(\mathcal{K}_{[0:H]})) \cup \rho \circ \tilde{f}(\varphi(\mathcal{K}_{[0:H]}))$. Since smooth functions are locally-Lipschitz and since ρ is smooth, then the restriction $\rho|_{\tilde{\mathcal{K}}}$ of ρ to the compact set $\tilde{\mathcal{K}}$ is Lipschitz. Denote its local-Lipschitz constant of ρ thereon by $\text{Lip}(\rho|_{\tilde{\mathcal{K}}})$. Thus, under the Assumption that F satisfies (F.14), the right-hand side of (F.13) can be bounded-above as

$$\sup_{u_{[0:H]} \in \varphi(\mathcal{K}_{[0:H]})} d_g(\rho \circ \tilde{f}(u), \rho \circ F(u)) \leq \text{Lip}(\rho|_{\tilde{\mathcal{K}}}) \sup_{u_{[0:H]} \in \varphi(\mathcal{K}_{[0:H]})} \|\tilde{f}(u) - F(u)\|. \quad (\text{F.15})$$

Note that $\text{Lip}(\rho|_{\tilde{\mathcal{K}}})$ cannot be 0 since it is a diffeomorphism and \mathcal{M} was assumed to be of dimension at-least 1; thus, set $\tilde{\varepsilon} \stackrel{\text{def.}}{=} \varepsilon \min\{1, \text{Lip}(\rho|_{\tilde{\mathcal{K}}})^{-1}\}$.

Step 2: Universal approximation by ReLU feedforward Neural Networks:

By Lemma F.1, there exists a ReLU feedforward neural network $F : \mathbb{R}^{(M+1)D} \rightarrow \mathbb{R}^d$ satisfying the following uniform estimate:

$$\sup_{u_{[0:H]} \in \varphi(\mathcal{K}_{[0:H]})} \|\tilde{f}(u) - F(u)\| \leq \tilde{\varepsilon}. \quad (\text{F.16})$$

In particular, (F.16) implies that F satisfies (F.14) since $\varepsilon \leq 1$. Inputting the estimate in (F.16) into the right-hand side of (F.15), and thus (F.13), yields

$$\begin{aligned} \sup_{x_{[0:H]} \in \mathcal{K}_{[0:H]}} d_g(f(x), \tilde{F}(x)) &\leq \text{Lip}(\rho|_{\tilde{\mathcal{K}}}) \varepsilon \min\left\{1, \frac{1}{\text{Lip}(\rho|_{\tilde{\mathcal{K}}})}\right\} \\ &= \varepsilon \min\{\text{Lip}(\rho|_{\tilde{\mathcal{K}}}), 1\} \\ &\leq \varepsilon. \end{aligned}$$

Furthermore, the depth and width of g are given in Table 13 with their specifications $d^* = (1+H)D$, ε in their notation is set to $\varepsilon \min\{1, \text{Lip}(\rho|\tilde{K})\}$, and $\lambda \stackrel{\text{def.}}{=} \text{Lip}_\alpha(\rho^{-1} \circ f \circ \varphi^{-1} | \varphi(\overline{B(\mathcal{K}_{[0:H]}, 1)}))$, is the α -Hölder constant of $\rho^{-1} \circ f \circ \varphi^{-1}$ on the 1-thickening of $\mathcal{K}_{[0:H]}$.

In the case where f is smooth, then since the composition of smooth functions is again smooth and all smooth functions are locally-Lipschitz then \tilde{f} is smooth on $\mathbb{R}^{(1+H)D}$ and it is Lipschitz on the compact set $\varphi(\mathcal{K}_{[0:H]})$. The depth and width of F is recorded in Table 13 with $d^* = (1+H)D$, ε in their notation is set to $\varepsilon \min\{1, \text{Lip}(\rho|\tilde{K})\}$, $F = \rho^{-1} \circ f \circ \varphi^{-1}$, and W is any bijective affine self-map on $\mathbb{R}^{(1+H)D}$ sending the compact set $\varphi(\overline{B(\mathcal{K}_{[0:H]}, 1)})$ to $[0, 1]^{(1+H)D}$. \blacksquare

Proof of Corollary 14 Since \mathcal{N}^{1+H} endowed with the product metric is Polish, we have that $\mathbb{P} \stackrel{\text{def.}}{=} (X_1)_{\#}\mu$ is a Radon measure on \mathcal{N}^{1+H} . We consider the Borel function $\rho^{-1} \circ f : \mathcal{N}^{1+H} \rightarrow \mathbb{R}^D$. By Lusin theorem, we may find $\ell_\varepsilon : \mathcal{N}^{1+H} \rightarrow \mathbb{R}^D$ continuous such that

$$\mathbb{P}[z \in \mathcal{N}^{1+H}; \rho^{-1} \circ f(z) = \ell_\varepsilon(z)] > 1 - \varepsilon.$$

Therefore, the function $\rho \circ \ell_\varepsilon : \mathcal{N}^{1+H} \rightarrow \mathcal{M}$ is continuous and $\mathbb{P}[z \in \mathcal{N}^{1+H}; f(z) = \rho \circ \ell_\varepsilon(z)] > 1 - \varepsilon$. Since \mathbb{P} is Radon, we may find $\mathcal{K}_\varepsilon \subset \{z \in \mathcal{N}^{1+H}; f(z) = \rho \circ \ell_\varepsilon(z)\}$ compact and such that $\mathbb{P}[\mathcal{K}_\varepsilon] > 1 - \varepsilon$. Applying Theorem 14, we obtain a GDN $\hat{f} : \mathcal{N}^{1+H} \rightarrow \mathcal{M}$ such that

$$d_h(\hat{f}(z), \rho \circ \ell_\varepsilon(z)) < \varepsilon, \quad z \in \mathcal{K}_\varepsilon.$$

That is, we have

$$d_h(\hat{f}(z), f(z)) < \varepsilon, \quad z \in \mathcal{K}_\varepsilon.$$

Since trivially, $\mathcal{K}_\varepsilon \subset [z \in \mathcal{N}^{1+H}; d_h(\hat{f}(z), f(z)) < \varepsilon]$, the thus result follows. \blacksquare

Appendix G. Proof of universality in the dynamic case - Theorem 17

Proof [Theorem 17] Fix $Q, J \in \mathbb{N}_+$, define the time horizon $T \stackrel{\text{def.}}{=} T_{\delta, Q} \stackrel{\text{def.}}{=} \lfloor \delta^{-Q} \rfloor$, and let $\varepsilon > 0$.

Step 1: Obtaining proxy target functions via the finite virtual memory of f

In each case (1), (2), and (3), f was assumed to have finite virtual memory with virtual memory $r \geq 0$ (see Definition 16). Therefore, there is an $\tilde{H} \stackrel{\text{def.}}{=} H(\varepsilon, T, \mathcal{K}) \in \mathbb{N}$ with $\tilde{H} \lesssim (\varepsilon/2)^{-r}$ and functions $f_1, \dots, f_T \in C(\mathcal{N}^H, \mathcal{M})$ satisfying

$$\max_{t \in [T]} \sup_{x \in \mathcal{K}} d_g(f(x)_t, f_t(x_{(t-\tilde{H}:t)})) < \frac{\varepsilon}{2}. \quad (\text{G.1})$$

Define $H \stackrel{\text{def.}}{=} \max\{T, \tilde{H}\}$.

Comment: Next, we approximate each f_t with an “expert” GDN specialized at that time t .

We consider three cases, depending on which of the assumptions on f held.

- (1) If f is (r, k, λ) -smooth then, each $\{f_t\}_{t=0}^T \in C^{k, \lambda}(\mathcal{N}^H, \mathcal{M})$,
- (2) If f is (r, α, λ) -Hölder then, each $\{f_t\}_{t=0}^T \in C^{\alpha, \lambda}(\mathcal{N}^H, \mathcal{M})$,
- (3) If each \mathcal{K}_t is finite, then no additional condition on the f_t is required.

Step 2: Parallelized “expert” approximation on separate time-windows

Fix $\tilde{x}^* \in \mathcal{N}$, define $r \stackrel{\text{def.}}{=} \max_{x \in \mathcal{K}_{[0:T]}} \max_{t=0, \dots, T} d_h(x_t, \tilde{x}^*)$ and construct the compact subset $\mathcal{K}^{*,T}$ of \mathcal{N}^{1+T} , containing $\mathcal{K}_{[0:T]}$ as follows:

$$\mathcal{K}^{*,T} \stackrel{\text{def.}}{=} \begin{cases} \{x_{[0:T]} \in \mathcal{N}^{1+T} : \max_{t=0, \dots, T} d_h(x_t, x^*) \leq r\} & \text{if } \#\bigcup_{t=0}^T \mathcal{K}_t = \infty \\ \{x_{[0:T]} \in \mathcal{N}^{1+T} : (\forall s = 0, \dots, T) x_s \in \bigcup_{t=0}^T \mathcal{K}_t\} & \text{if } \#\bigcup_{t=0}^T \mathcal{K}_t < \infty. \end{cases}$$

Observe, that $\mathcal{K}^{\star:T}$ is finite, if $\mathcal{K}_{[0:T]}$ is finite. Furthermore, by the stars-and-bars problem from elementary combinatorics, we know that each $t \in \{H, \dots, T\}$

$$\#K_{(t-H:t]}^{\star:T} \leq N_M^{\star} \stackrel{\text{def.}}{=} \binom{N_M^{\star} + M - 1}{M} \text{ and } N_H^{\star:T} \stackrel{\text{def.}}{=} \max_{t=0, \dots, T} \mathcal{K}_t \quad (\text{G.2})$$

where $K_{(t-H:t]}^{\star:T} = \{(x_{(t-H, \dots, t]} : \exists z_{[0:T]} \in \mathcal{K}^{\star:T} \forall t-H \leq s \leq t (x_{(t-H:t]})_s = (x_{[0:T]})_s\}$.

Once for each $t \in [[T]]$, we apply Theorem 13, to deduce that for each $t \in [[T]]$ there is are GDNs \hat{f}_{θ_t} , satisfying

$$\max_{x \in \mathcal{K}^{\star:T}} \max_{t=H, \dots, T} d_g(f_t(x_{(t-H:t]}), \hat{f}_{\theta_t}(x_{(t-H:t]})) < \varepsilon/2, \quad (\text{G.3})$$

where, for $t = H, \dots, T$, we have set the distinguished base-point in (5.2) to be $x_m^* = \tilde{x}^*$, for each $m = 0, \dots, H$. Furthermore, the depth and width of each GDN $\hat{f}_{\theta_{T-M}}, \dots, \hat{f}_{\theta_T}$ depends only on:

- (1) **If f is (r, k, λ) -Smooth:** the quantity (r, k, λ) and on the diameter of $\mathcal{K}^{\star:T}$,
- (2) **If f is (r, α, λ) -Hölder:** the quantity (r, α, λ) and on the diameter of $\mathcal{K}^{\star:T}$,
- (3) **If $\mathcal{K}_{[0:T]}$ has finite Cardinality:** on $N_H^{\star:T}$ which bounds the cardinality of $\mathcal{K}^{\star:T}$ above.

as detailed in Table 10, in each respective case. Note that each GDN \hat{f}_{θ_t} has the same domain and each f_t has the same regularity (i.e. as in cases 1-3 above); therefore Theorem 13 implies that the depth, width, multi-index $[\mathbf{d}]$, and parameter space $\mathbb{R}^{P([\mathbf{d}])}$ of each $\hat{f}_{\theta_H}, \dots, \hat{f}_{\theta_T}$ are all the same. The quantities ℓ and w are recorded in Table 10 with the following relevant constants

- (i) **Smooth case:** Since f is (r, k, λ) -smooth, then each f_t belongs to $C^{k,\lambda}(\mathcal{N}^{1+H}, \mathcal{M})$ define

$$C_{\bar{f}} \stackrel{\text{def.}}{=} \max_{\substack{t=T-H, \dots, T \\ i=1, \dots, D}} \frac{\|(\rho^{-1} \circ f_t \circ \varphi^{-1} \circ W_t)_i\|_{C^k([0,1]^d)}}{\max\{1, \text{Lip}(\rho|f_t \circ \varphi(\mathcal{K}^{\star:T}))\}},$$

where for each $t = H, \dots, T$, $W_M, \dots, W_T : \mathbb{R}^{(1+H)d} \rightarrow \mathbb{R}^{(1+H)d}$ are affine bijections satisfying $W_t(\varphi(\mathcal{K}^{\star:T})) \subseteq [0, 1]^{(1+H)d}$. In particular, the definition of $\mathcal{K}^{\star:T}$, Lemma C.2 (ii), and Jung's Thereom (see Jung (1901)), there are $\tilde{x}_t \in \mathbb{R}^{(1+H)d}$ such that: for each $x \in \mathbb{R}^{d(1+H)}$

$$W_t(x) \stackrel{\text{def.}}{=} \frac{1}{C_{\bar{x}} \sqrt{M} 2r} \sqrt{\frac{2d(1+H) + 2}{d(1+H)}} (x - \tilde{x}_t). \quad (\text{G.4})$$

- (ii) **Hölder case:** Since f is (r, α, λ) -Hölder, then each f_t belongs to $C_{\alpha}^{\lambda}(\mathcal{N}^{1+H}, \mathcal{M})$, set

$$C_f \stackrel{\text{def.}}{=} \min_{t=T-H, \dots, H} \text{Lip}_{\alpha}(\rho^{-1} \circ f_t \circ \varphi^{-1} | \varphi(\mathcal{K}^{\star:T})),$$

(note this is because we are maximizing $1/\text{Lip}_{\alpha}(\rho^{-1} \circ f_t \circ \varphi^{-1} | \varphi(\mathcal{K}^{\star:T}))$ across $t = T-H, \dots, T$.

Combining the estimates in (5.3) and the family of estimates in (G.3) (indexed by $[[T]]$) we deduce that: for each $x \in \mathcal{K}$ and every $t = T-H, \dots, T$ the following holds

$$\begin{aligned} d_g(f(x)_t, \hat{f}_{\theta_t}(x_{(t-H:t]}^{(n)})) &\leq d_g(f(x)_t, f_t(x_{(t-H:t]})) \\ &\quad + d_g(f_t(x_{(t-H:t]}), \hat{f}_{\theta_t}(x_{(t-H:t]})) \\ &< \varepsilon/2 + \varepsilon/2. \end{aligned} \quad (\text{G.5})$$

Step 3: Weaving the approximators together

Fix a $Q \in \mathbb{N}_+$, with $Q + P([\bar{J}]) \geq \max\{12, P([\bar{J}]) + 1\}$. Upon applying the “dynamic weaving lemma” (Galimberti et al., 2022, Lemma 5), we deduce that there exists a $z \in \mathbb{R}^{P([\bar{J}])+Q}$, a linear map $L : \mathbb{R}^{P([\bar{J}])+Q} \rightarrow \mathbb{R}^{P([\bar{J}])}$, and a deep ReLU FFNN $\hat{f} : \mathbb{R}^{P([\bar{J}])+Q} \rightarrow \mathbb{R}^{P([\bar{J}])+Q}$ with

1. **Width:** $(P([\bar{J}]) + Q)T + 12$,

2. **Depth:** $\mathcal{O}\left(T\left(1 + \sqrt{T \log(T)}\left(1 + \frac{\log(2)}{\log(T)}\left[C + \frac{\left(\log(T^2 2^{1/2}) - \log(\delta)\right)}{\log(2)}\right]_+\right)\right)\right)$,

3. **N. Parameters:**

$$\mathcal{O}\left(T^3(P([\mathbf{d}]) + Q)^2 \left(1 + (P([\mathbf{d}]) + Q)\sqrt{T \log(T)} \left(1 + \frac{\log(2)}{\log(T)} \left[C_d + \frac{\left(\log(T^2 2^{1/2}) - \log(\delta)\right)}{\log(2)}\right]_+\right)\right)\right),$$

satisfying the interpolation

$$\theta_t = L(h^{\circ t}(z)) \quad \text{for } t = T - H, \dots, T; \quad (\text{G.6})$$

where $h^{\circ t}$ denotes the t -hold composition of h with itself. Upon setting $d^* \stackrel{\text{def.}}{=} P([\bar{J}]) + Q$ we obtain the conclusion. \blacksquare

Appendix H. Memory persistence estimates for Volterra kernels

In this appendix, we derive estimates of the error incurred by truncating the realized path in a Volterra series when predicting its evolution. We consider three types of Volterra kernels, those which decay fast (exponentially) and slowly (logarithmically).

Lemma H.1 (Rapidly (exponential) vanishing memory) *Suppose there are $C > 0$, $0 < \alpha < 1$ such that for every pair of integers $0 \leq r \leq t$ with $t \neq 0$*

$$\kappa(t, r) \leq C \alpha^{t-r}.$$

For every $t \in \mathbb{N}_+$ and each integer $0 \leq H < t$ one has

$$\sum_{r=0}^{t-H-1} \kappa(t, r) \leq \frac{C \alpha}{\alpha - 1} (\alpha^t - \alpha^H)$$

Proof We have

$$\sum_{r=0}^{t-H-1} \kappa(t, r) \leq \sum_{r=0}^{t-H-1} C \alpha^{t-r} = \frac{C \alpha}{\alpha - 1} (\alpha^t - \alpha^H). \quad (\text{H.1})$$

\blacksquare

Lemma H.2 (Moderately (Polynomially) vanishing memory) *Suppose there is $\alpha \in \mathbb{R}$, $C > 0$ such that for each pair of integers $0 \leq r < t$*

$$\kappa(t, r) \leq C(t - r)^\alpha.$$

Then, for each $t \in \mathbb{N}_+$ and each integer $0 \leq H \leq t$ one has

$$\sum_{r=0}^{t-H-1} \kappa(t, r) \leq C (H+1)^\alpha (t - H)$$

Proof Employing the growth assumption $\kappa(t, r) \leq C(t - r)^\alpha$ and the fact that $t - H - 1 < t$ we find that

$$\sum_{r=0}^{t-H-1} \kappa(t, r) \leq \sum_{r=0}^{t-H-1} C(t - r)^\alpha \quad (\text{H.2})$$

$$= C \sum_{u=H+1}^t u^\alpha. \quad (\text{H.3})$$

Since $\alpha < 0$ then, $\sum_{u=M+1}^t u^\alpha \leq (H+1)^\alpha (t - H)$. ■

Appendix I. Experiment Details

We include the details of the experiments in Section 6. We first explicitly describe the algorithms we used to implement generate the sample paths from the Volterra process in (6.1), to compute its Gaussian random projections, and to train the HGN from this data. We then provide details on the hardware used to train these models.

I.1 Experiment and Compute Details

The architecture used to tackle those problems (identical for all the models) had six layers with a maximum size of 512 in the GDN part and eight layers with a maximum size of 1024 in the hypernetwork (ignoring the input-output layers). Since the base parameter's T value was 200, we had to train 200 GDNs and 1 hypernetwork. Considering the architecture mentioned, we had around 500 thousand parameters in each GDN and 750 million in the hypernetwork to train. Despite their outrageous look, these calculations are highly parallelizable. We trained our models within a reasonable time by exploiting the most basic optimizations and employing the graphic processing unit (GPU) to run the computations within each model in parallel. We know that there are some obvious ideas to improve the performance of these networks, like training GDNs in parallel using multiple GPUs simultaneously. However, there was no need to do that since our training time was short enough, and more GPUs would be needed to achieve that.

We ran experiments on the Vector Institute for Artificial Intelligence's computing cluster. Since each problem (process created with a specific set of parameters) is entirely independent, we used 30 machines, one for each problem in parallel. All the machines had the same config with 6 CPU cores, 1 Nvidia T4 GPU, 20GB of RAM, and 40GB of SSD memory. The run-time limit for the instances was 12 hours, although all machines finished their jobs in less than 8.5 hours. The problem with the base parameter set took about 4 hours and 44 minutes, and the overall average was around 6 hours. Note that these differences might be seen because not all machines were on the same host computing node. Thus, the CPU and RAM models and clock frequencies were not the same for all the machines.

I.2 Algorithm Descriptions

The following algorithm is used to generate sample paths of the Volterra process defined in (6.1).

Algorithm 1: Construct \mathbf{X}

Require: Number of training samples $N \in \mathbb{N}_+$, time-horizon $T \in \mathbb{N}_+$, dynamics μ , σ , and ς , “noise” parameter $0 \leq \lambda$, memory $1 \leq w \leq 0$.

For $n : 0, \dots, N - 1$ **in parallel**

for $t : 0, \dots, T$ **do**

if $t = 0$ **then**

$x_{-1}^n \leftarrow 0$

$x_0^n \leftarrow 0$ *// Get Initial States*

end if

else

Sample: $Z \sim N_d(0, I_d)$ *// Generate Gaussian Noise*

Sample: $B \sim \text{Binom}(\{0, 1\}; 1/2)$ *// Generate Hidden Process*

$x \leftarrow w\mu(x_{t-1}^n) + (1 - w)\mu(x_t^n)$ *// Get Drift*

$y \leftarrow (\varsigma(x_t^n) \cdot \sigma + B\lambda I_d)Z$ *// Get Diffusion*

$x_{t+1}^n \leftarrow x_t^n + x + y$ *// Update Diffusion*

end if

$x^n \leftarrow (x_t^n)_{t=0}^T$ *// Save Sample Path*

end for

end

$\mathbf{X} \leftarrow \{x^n\}_{n=0}^{N-1}$ *// Compile Dataset*

return \mathbf{X}

The next algorithm (Algorithm 2) implements the Gaussian projection of the Volterra process in (6.1). This is given by the closed-form expression derived in (6.3).

Algorithm 2: Given a set of paths \mathbf{X} in $\mathbb{R}^{(2+T)d}$, this algorithm returns an array of input-output pairs, whose elements are pairs of paths $x_{[-1:T]}$ in \mathbf{X} paired with the parameters determining the path of Gaussian distributions $y^x \stackrel{\text{def.}}{=} (\mathbb{Q}_{x_{[-1:t]}})_{t=0}^T$ traced out by sequentially applying the barycenter map to the process $(\mathbb{Q}_{x_{[-1:t]}})_{t=0}^T$.

Require: Time-Horizon, finite set of paths $\mathbf{X} \subseteq \mathbb{R}^{(2+T)d}$, drift μ , diffusion parameters σ and ς , and a “randomness” $\lambda \geq 0$.

For $x \stackrel{\text{def.}}{=} x_{[-1:T]} \in \mathbf{X}$ **in parallel**

for $t : 0, \dots, T$ **do**

$\mu_t^x \leftarrow x_t + \text{Drift}(x_{[t-1:x_t]})$ *// Get Mean of Projection*

$\sigma_t^x \leftarrow \varsigma(x_t) \cdot \sigma^2 (\sigma^{-2} (\lambda I_d + \varsigma(x_t) \cdot \sigma)^2)^{1/2}$ *// Get Covariance of Projection*

end for

$y^x \leftarrow (\mu_t^x, \text{vec}(\sigma_t^x))_{t=0}^T$ *// Get Outputs*

end for

return $\mathbf{Z} \leftarrow \{(x, y^x)\}_{x \in \mathbf{X}}$ *// Return Array of Input-Output Pairs $\{(x, y^x)\}_{x \in \mathbf{X}}$*

Once the input data has been generated using Algorithm 1 and the corresponding Gaussian random projections have been computed using Algorithm 2, then we have input-output with which the HGN model can be trained. Observe that the training scheme which we used and which encodes the proof strategy of the dynamic universal approximation theorem 17, avoids backpropagating in time (as with RNNs). Thus, even if the HGN has a recursion, it can be trained without recursion similarly and thus enjoys some of the training stability properties of transformers which RNNs do not share; namely, no backpropagation in time.

Algorithm 3: Construct HG-CNN

Require: A dataset $Z \leftarrow \{(x, y^x)\}_{x \in \mathcal{X}}$, GDN depth and widths, (ReLU) hypernetwork dimensions $[\mathbf{d}]$.

For $t : 0, \dots, T$ **in parallel**

$\hat{f}_{\theta_t} \leftarrow \underset{\hat{f}_{\theta} \in \mathcal{G} - \mathcal{C}\mathcal{N}\mathcal{N}_{[S], [L]}}{\operatorname{argmin}} \sum_{x \in \mathcal{X}} \|\hat{f}_{\theta}(x_{[t-1:t]}) - y_t^x\|^2$

// Optimize G-CNN Nodes

$z_t \leftarrow (\theta_t, t)$

// Separate Parameters

end

/* Create Recurrence/ Encode Causality */

$\hat{h} \leftarrow \underset{h \in \mathcal{N}\mathcal{N}_{[\mathbf{d}]}^{\text{ReLU}}}{\operatorname{argmin}} \sum_{t=0}^T \|h(z_t) - z_{t+1}\|_2^2$

*/

/* Server receives parameters of optimized neural filters for each time window */

$L : \mathbb{R}^{P([\mathbf{d}])} \times \mathbb{R}^Q \rightarrow \mathbb{R}^{P([\mathbf{d}])}$ projection onto first component

return Trained HG-CNN: (\hat{f}, z_0, L) .

I.3 Additional Loss Curves

We plot the loss curves, in the test set, of a representative subset of the experiments reported in Tables 4, (7), (5), (8), and (8). Figure 6 shows that the behaviour illustrated in Figures 3 and (4) persists across our experiments.

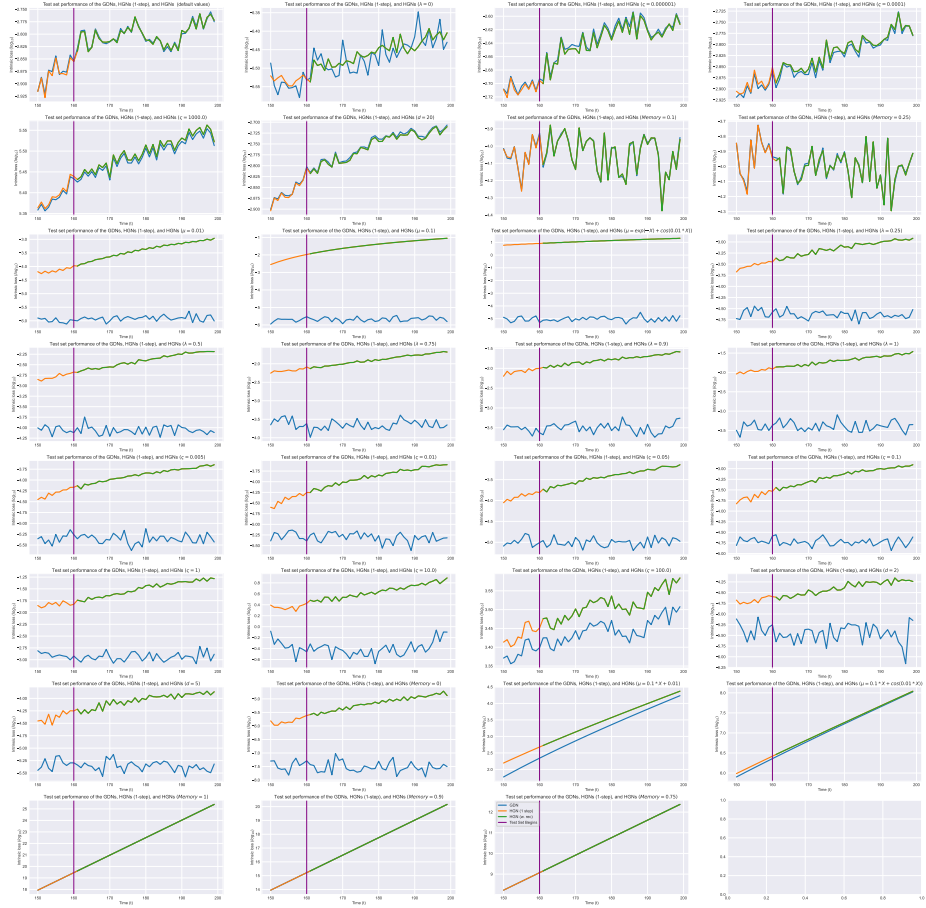


Figure 6: Typical Learning Curves - Including Cases With Exploding Gradients

I.4 Exploding Gradients due to Small Eigenvalues

There is one additional case, illustrated in Figure 6, where the HNN or HGN suffers from exploding gradients during training. We included some examples of learning curves illustrating the exploding gradients phenomenon that occurs.

A prior, there is nothing particular about the target function being learned when this occurs. For instance, the experiments in Table 4 where $x \mapsto \frac{1}{2}(\frac{1}{100} - x)$ is essentially the same as when $x \mapsto \frac{1}{10}x + \frac{1}{100}$; thus both should be equally easy to learn. However, in the latter experiment, recorded in Table 14, the gradients exploded during training, resulting in a loss (both in and out of the sample). Similarly, the drift $x \mapsto e^{-x} + \cos(\frac{x}{100})$ and $x \mapsto \frac{x}{10} + \cos(\frac{x}{100})$ are essentially the same; but again the latter is not being learned due to exploding gradients during training (see Table 14 again) while the former is not due since gradients did not explode (see Table 4 again). Similarly, the

value of w is similar to those considered in Table 7; however, the loss in situations where gradients exploded during training is several magnitudes larger.

Table 14: Examples of Exploding Gradients:

μ	GDN Loss Mean	GDN Loss 95% C.I.	HGN Loss Mean	HGN Loss 95% C.I.
$\frac{1}{10}x + \frac{1}{100}$	$4.19 \times 10^{+3}$	$[2.75, 5.64] \times 10^{+3}$	$6.22 \times 10^{+3}$	$[4.24, 8.21] \times 10^{+3}$
$\frac{x}{10} + \cos(\frac{x}{100})$	$2.82 \times 10^{+7}$	$[1.92, 3.71] \times 10^{+7}$	$2.98 \times 10^{+7}$	$[2.05, 3.91] \times 10^{+7}$
w	GDN Loss Mean	GDN Loss 95% C.I.	HGN Loss Mean	HGN Loss 95% C.I.
0.75	$3.32 \times 10^{+11}$	$[1.55, 5.09] \times 10^{+11}$	$3.32 \times 10^{+11}$	$[1.55, 5.09] \times 10^{+11}$
0.9	$1.42 \times 10^{+19}$	$[0.45, 2.40] \times 10^{+19}$	$1.42 \times 10^{+19}$	$[0.45, 2.40] \times 10^{+19}$

A closer look at the error logs shows that the exploding gradient occurs due to rounding errors in the Riemannian distance function (D.3) when the logarithm is applied to small eigenvalues of the relevant positive-definite matrix. Though gradient clipping typically solves this issue, it occasionally resurfaces, and we thus report it here.

References

Eduardo Abi Jaber, Martin Larsson, and Sergio Pulido. Affine Volterra processes. *Ann. Appl. Probab.*, 29(5):3155–3200, 2019. ISSN 1050-5164. doi: 10.1214/19-AAP1477. URL <https://doi.org/10.1214/19-AAP1477>.

Beatrice Acciaio, Anastasis Kratsios, and Gudmund Pammer. Designing universal causal deep learning models: The geometric (hyper)transformer. *Mathematical Finance*, pages 1–65, 2023. URL <https://onlinelibrary.wiley.com/doi/10.1111/mafi.12389>. (to appear) Special Issue: Machine Learning in Finance.

Bijan Afsari. Riemannian lp center of mass: existence, uniqueness, and convexity. *Proceedings of the American Mathematical Society*, 139(2):655–673, 2011.

Samuel Ainsworth, Jonathan Hayase, and Siddhartha Srinivasa. Git re-basin: Merging models modulo permutation symmetries. In *The Eleventh International Conference on Learning Representations*, 2023. URL <https://openreview.net/forum?id=CQsmMYmlP5T>.

A. D. Aleksandrov. A theorem on triangles in a metric space and some of its applications. *Trudy Mat. Inst. Steklov.*, 38:5–23, 1951.

Jason M. Altschuler and Enric Boix-Adserà. Wasserstein barycenters can be computed in polynomial time in fixed dimension. *J. Mach. Learn. Res.*, 22:Paper No. 44, 19, 2021. ISSN 1532-4435,1533-7928.

Martin Arjovsky, Soumith Chintala, and Léon Bottou. Wasserstein generative adversarial networks. In *International conference on machine learning*, pages 214–223. PMLR, 2017.

M. Atçeken and S. Keleş. On the product Riemannian manifolds. *Differ. Geom. Dyn. Syst.*, 5(1):1–8, 2003.

Colin Atkinson and Ann F. S. Mitchell. Rao’s distance measure. *Sankhyā Ser. A*, 43(3):345–365, 1981. ISSN 0581-572X.

Nihat Ay, Jürgen Jost, Hông Vân Lê, and Lorenz Schwachhöfer. *Information geometry*, volume 64 of *Ergebnisse der Mathematik und ihrer Grenzgebiete. 3. Folge. A Series of Modern Surveys in*

Mathematics [Results in Mathematics and Related Areas. 3rd Series. A Series of Modern Surveys in Mathematics]. Springer, Cham, 2017. ISBN 978-3-319-56477-7; 978-3-319-56478-4. doi: 10.1007/978-3-319-56478-4. URL <https://doi.org/10.1007/978-3-319-56478-4>.

Kerry Back, Tomasz R Bielecki, Christian Hipp, Shige Peng, Walter Schachermayer, and Kerry Back. Incomplete and asymmetric information in asset pricing theory. *Stochastic Methods in Finance: Lectures given at the CIME-EMS Summer School held in Bressanone/Brixen, Italy, July 6-12, 2003*, pages 1–25, 2004.

Fred Espen Benth, Nils Detering, and Luca Galimberti. Neural networks in fréchet spaces. *Annals of Mathematics and Artificial Intelligence*, 91(1):75–103, 2023.

Jose-M. Bernardo and Adrian F. M. Smith. *Bayesian theory*. Wiley Series in Probability and Mathematical Statistics: Probability and Mathematical Statistics. John Wiley & Sons, Ltd., Chichester, 1994. ISBN 0-471-92416-4. doi: 10.1002/9780470316870. URL <https://doi.org/10.1002/9780470316870>.

Rabi Bhattacharya and Vic Patrangenaru. Large sample theory of intrinsic and extrinsic sample means on manifolds. I. *Ann. Statist.*, 31(1):1–29, 2003. ISSN 0090-5364,2168-8966. doi: 10.1214/aos/1046294456. URL <https://doi.org/10.1214/aos/1046294456>.

Rabi Bhattacharya and Vic Patrangenaru. Large sample theory of intrinsic and extrinsic sample means on manifolds. II. *Ann. Statist.*, 33(3):1225–1259, 2005. ISSN 0090-5364,2168-8966. doi: 10.1214/009053605000000093. URL <https://doi.org/10.1214/009053605000000093>.

Dario A. Bini and Bruno Iannazzo. Computing the Karcher mean of symmetric positive definite matrices. *Linear Algebra Appl.*, 438(4):1700–1710, 2013. ISSN 0024-3795,1873-1856. doi: 10.1016/j.laa.2011.08.052. URL <https://doi.org/10.1016/j.laa.2011.08.052>.

Christopher M Bishop. Mixture density networks. *Aston University*, 1994.

V. I. Bogachev. *Measure theory. Vol. I, II*. Springer-Verlag, Berlin, 2007. ISBN 978-3-540-34513-8; 3-540-34513-2. doi: 10.1007/978-3-540-34514-5. URL <https://doi.org/10.1007/978-3-540-34514-5>.

Alessandro Bondi, Giulia Livieri, and Sergio Pulido. Affine Volterra processes with jumps. *Stochastic Process. Appl.*, 168:Paper No. 104264, 25, 2024. ISSN 0304-4149,1879-209X. doi: 10.1016/j.spa.2023.104264. URL <https://doi.org/10.1016/j.spa.2023.104264>.

Anastasia Borovykh, Sander Bohte, and Cornelis W Oosterlee. Conditional time series forecasting with convolutional neural networks. *arXiv preprint arXiv:1703.04691*, 2017.

Martin R. Bridson and André Haefliger. *Metric spaces of non-positive curvature*, volume 319 of *Grundlehren der mathematischen Wissenschaften [Fundamental Principles of Mathematical Sciences]*. Springer-Verlag, Berlin, 1999. ISBN 3-540-64324-9. doi: 10.1007/978-3-662-12494-9. URL <https://doi.org/10.1007/978-3-662-12494-9>.

Daniel Brooks, Olivier Schwander, Frederic Barbaresco, Jean-Yves Schneider, and Matthieu Cord. Riemannian batch normalization for spd neural networks. *Advances in Neural Information Processing Systems*, 32, 2019.

Evelyn Buckwar. Introduction to the numerical analysis of stochastic delay differential equations. *Journal of computational and applied mathematics*, 125(1-2):297–307, 2000.

Élie Cartan. *Leçons sur la géométrie des espaces de Riemann*. Les Grands Classiques Gauthier-Villars. [Gauthier-Villars Great Classics]. Éditions Jacques Gabay, Sceaux, 1988. ISBN 2-87647-008-X. Reprint of the second (1946) edition.

Ines Chami, Albert Gu, Vaggos Chatziafratis, and Christopher Ré. From trees to continuous embeddings and back: Hyperbolic hierarchical clustering. *Advances in Neural Information Processing Systems*, 33:15065–15076, 2020.

Mou-Hsiung Chang and Roger K Youree. Infinite-dimensional black-scholes equation with hereditary structure. *Applied Mathematics and Optimization*, 56:395–424, 2007.

Tianping Chen and Hong Chen. Universal approximation to nonlinear operators by neural networks with arbitrary activation functions and its application to dynamical systems. *IEEE transactions on neural networks*, 6(4):911–917, 1995.

Patrick Cheridito, Arnulf Jentzen, and Florian Rossmann. Efficient approximation of high-dimensional functions with neural networks. *IEEE Transactions on Neural Networks and Learning Systems*, 2021.

Ilya Chevyrev and Harald Oberhauser. Signature moments to characterize laws of stochastic processes. *Journal of Machine Learning Research*, 23(176):1–42, 2022.

Mohammed Nowaz Rabbani Chowdhury, Shuai Zhang, Meng Wang, Sijia Liu, and Pin-Yu Chen. Patch-level routing in mixture-of-experts is provably sample-efficient for convolutional neural networks. In *International Conference on Machine Learning*, pages 6074–6114. PMLR, 2023.

Sueli I. R. Costa, Sandra A. Santos, and João E. Strapasson. Fisher information distance: a geometrical reading. *Discrete Appl. Math.*, 197:59–69, 2015. ISSN 0166-218X. doi: 10.1016/j.dam.2014.10.004. URL <https://doi.org/10.1016/j.dam.2014.10.004>.

Christopher Criscitiello and Nicolas Boumal. An accelerated first-order method for non-convex optimization on manifolds. *Foundations of Computational Mathematics*, 2022. doi: 10.1007/s10208-022-09573-9. URL <https://doi.org/10.1007/s10208-022-09573-9>.

I. Csiszár. I -divergence geometry of probability distributions and minimization problems. *Ann. Probability*, 3:146–158, 1975. ISSN 0091-1798. doi: 10.1214/aop/1176996454. URL <https://doi.org/10.1214/aop/1176996454>.

Imre Csiszár. Sanov property, generalized I -projection and a conditional limit theorem. *Ann. Probab.*, 12(3):768–793, 1984. ISSN 0091-1798. URL [http://links.jstor.org/sici?si=0091-1798\(198408\)12:3<768:SPGAAC>2.0.CO;2-Y&origin=MSN](http://links.jstor.org/sici?si=0091-1798(198408)12:3<768:SPGAAC>2.0.CO;2-Y&origin=MSN).

Imre Csiszár and Frantisek Matus. Information projections revisited. *IEEE Transactions on Information Theory*, 49(6):1474–1490, 2003.

Christa Cuchiero and Josef Teichmann. Generalized Feller processes and Markovian lifts of stochastic Volterra processes: the affine case. *J. Evol. Equ.*, 20(4):1301–1348, 2020. ISSN 1424-3199. doi: 10.1007/s00028-020-00557-2. URL <https://doi.org/10.1007/s00028-020-00557-2>.

Christa Cuchiero, Philipp Schmocke, and Josef Teichmann. Global universal approximation of functional input maps on weighted spaces. *arXiv preprint arXiv:2306.03303*, 2023.

Marco Cuturi and Arnaud Doucet. Fast computation of wasserstein barycenters. In *International conference on machine learning*, pages 685–693. PMLR, 2014.

Haitz Sáez de Ocáriz Borde, Anees Kazi, Federico Barbero, and Pietro Lio. Latent graph inference using product manifolds. In *The Eleventh International Conference on Learning Representations*, 2022.

James G. Dowty. Chentsov's theorem for exponential families. *Inf. Geom.*, 1(1):117–135, 2018. ISSN 2511-2481. doi: 10.1007/s41884-018-0006-4. URL <https://doi.org/10.1007/s41884-018-0006-4>.

Salvatore Federico. A stochastic control problem with delay arising in a pension fund model. *Finance and Stochastics*, 15(3):421–459, 2011.

William Fedus, Barret Zoph, and Noam Shazeer. Switch transformers: Scaling to trillion parameter models with simple and efficient sparsity. *Journal of Machine Learning Research*, 23(120):1–39, 2022.

P Thomas Fletcher, Conglin Lu, Stephen M Pizer, and Sarang Joshi. Principal geodesic analysis for the study of nonlinear statistics of shape. *IEEE transactions on medical imaging*, 23(8):995–1005, 2004.

Marco Fuhrman, Federica Masiero, and Gianmario Tessitore. Stochastic equations with delay: Optimal control via bsdes and regular solutions of hamilton–jacobi–bellman equations. *SIAM Journal on Control and Optimization*, 48(7):4624–4651, 2010.

Takashi Furuya, Anastasis Kratsios, Matti Lassas, Maarten de Hoop, et al. Mixture of experts soften the curse of dimensionality in operator learning. *arXiv preprint arXiv:2404.09101*, 2024.

Luca Galimberti, Giulia Livieri, and Anastasis Kratsios. Designing universal causal deep learning models: The case of infinite-dimensional dynamical systems from stochastic analysis. *arXiv preprint arXiv:2210.13300*, 2022.

Jon Gauthier. Conditional generative adversarial nets for convolutional face generation. *Class project for Stanford CS231N: convolutional neural networks for visual recognition, Winter semester*, 2014 (5):2, 2014.

Lukas Gonon and Juan-Pablo Ortega. Reservoir computing universality with stochastic inputs. *IEEE transactions on neural networks and learning systems*, 31(1):100–112, 2019.

Lukas Gonon and Juan-Pablo Ortega. Fading memory echo state networks are universal. *Neural Networks*, 138:10–13, 2021.

Lukas Gonon, Lyudmila Grigoryeva, and Juan-Pablo Ortega. Reservoir kernels and volterra series. *arXiv preprint arXiv:2212.14641*, 2022.

Google. Gemini. Google, 2024. URL <https://gemini.google.com/>.

Fausto Gozzi, Sociali di Roma, and Carlo Marinelli. 13 stochastic optimal control of delay equations arising in advertising models. *Stochastic Partial Differential Equations and Applications-VII*, page 133, 2005.

Siegfried Graf and Harald Luschgy. *Foundations of quantization for probability distributions*, volume 1730 of *Lecture Notes in Mathematics*. Springer-Verlag, Berlin, 2000. ISBN 3-540-67394-6. doi: 10.1007/BFb0103945. URL <https://doi.org/10.1007/BFb0103945>.

Lyudmila Grigoryeva and Juan-Pablo Ortega. Universal discrete-time reservoir computers with stochastic inputs and linear readouts using non-homogeneous state-affine systems. *J. Mach. Learn. Res.*, 19:Paper No. 24, 40, 2018. ISSN 1532-4435.

Lyudmila Grigoryeva and Juan-Pablo Ortega. Differentiable reservoir computing. *J. Mach. Learn. Res.*, 20:Paper No. 179, 62, 2019. ISSN 1532-4435.

Karsten Grove and Hermann Karcher. How to conjugate c 1-close group actions. *Mathematische Zeitschrift*, 132(1):11–20, 1973.

David Ha, Andrew M. Dai, and Quoc V. Le. Hypernetworks. In *International Conference on Learning Representations*, 2017. URL <https://openreview.net/forum?id=rkpACe1lx>.

Joachim Hilgert and Karl-Hermann Neeb. *Structure and geometry of Lie groups*. Springer Monographs in Mathematics. Springer, New York, 2012. ISBN 978-0-387-84793-1; 978-0-387-84794-8. doi: 10.1007/978-0-387-84794-8. URL <https://doi.org/10.1007/978-0-387-84794-8>.

Kurt Hornik, Maxwell Stinchcombe, and Halbert White. Multilayer feedforward networks are universal approximators. *Neural networks*, 2(5):359–366, 1989.

Clemens Hutter, Recep Güçlü, and Helmut Bölcskei. Metric entropy limits on recurrent neural network learning of linear dynamical systems. *Appl. Comput. Harmon. Anal.*, 59:198–223, 2022. ISSN 1063-5203. doi: 10.1016/j.acha.2021.12.004. URL <https://doi.org/10.1016/j.acha.2021.12.004>.

Eduardo Abi Jaber, Christa Cuchiero, Luca Pelizzari, Sergio Pulido, and Sara Svaluto-Ferro. Polynomial volterra processes. *arXiv preprint arXiv:2403.14251*, 2024.

Antoine Jacquier, Claude Martini, and Aitor Muguruza. On VIX futures in the rough Bergomi model. *Quant. Finance*, 18(1):45–61, 2018. ISSN 1469-7688. doi: 10.1080/14697688.2017.1353127. URL <https://doi.org/10.1080/14697688.2017.1353127>.

Albert Q Jiang, Alexandre Sablayrolles, Antoine Roux, Arthur Mensch, Blanche Savary, Chris Bamford, Devendra Singh Chaplot, Diego de las Casas, Emma Bou Hanna, Florian Bressand, et al. Mixtral of experts. *arXiv preprint arXiv:2401.04088*, 2024.

Jürgen Jost. *Riemannian geometry and geometric analysis*. Universitext. Springer, Cham, seventh edition, 2017. ISBN 978-3-319-61859-3; 978-3-319-61860-9. doi: 10.1007/978-3-319-61860-9. URL <https://doi.org/10.1007/978-3-319-61860-9>.

Heinrich Jung. Ueber die kleinste kugel, die eine räumliche figur einschliesst. *Journal für die reine und angewandte Mathematik*, 123:241–257, 1901. URL <http://eudml.org/doc/149122>.

H. Karcher. Riemannian center of mass and mollifier smoothing. *Comm. Pure Appl. Math.*, 30(5):509–541, 1977a. ISSN 0010-3640. doi: 10.1002/cpa.3160300502. URL <https://doi.org/10.1002/cpa.3160300502>.

Hermann Karcher. Riemannian center of mass and mollifier smoothing. *Communications on pure and applied mathematics*, 30(5):509–541, 1977b.

Young-Heon Kim and Brendan Pass. Nonpositive curvature, the variance functional, and the wasserstein barycenter. *Proceedings of the American Mathematical Society*, 148(4):1745–1756, 2020.

Shoshichi Kobayashi and Katsumi Nomizu. *Foundations of differential geometry. Vol. II*. Wiley Classics Library. John Wiley & Sons, Inc., New York, 1996. ISBN 0-471-15732-5. Reprint of the 1969 original, A Wiley-Interscience Publication.

Alexander Kolesov, Petr Mokrov, Igor Udovichenko, Milena Gazdieva, Gudmund Pammer, Evgeny Burnaev, and Alexander Korotin. Estimating barycenters of distributions with neural optimal transport. *arXiv preprint arXiv:2402.03828*, 2024a.

Alexander Kolesov, Petr Mokrov, Igor Udovichenko, Milena Gazdieva, Gudmund Pammer, Anastasis Kratsios, Evgeny Burnaev, and Alexander Korotin. Energy-guided continuous entropic barycenter estimation for general costs, 2024b.

Michael J Korenberg and Ian W Hunter. The identification of nonlinear biological systems: Volterra kernel approaches. *Annals of biomedical engineering*, 24:250–268, 1996.

Yury Korolev. Two-layer neural networks with values in a banach space. *SIAM Journal on Mathematical Analysis*, 54(6):6358–6389, 2022.

Anastasis Kratsios. Universal regular conditional distributions. *Constr. Approx.*, 2023.

Anastasis Kratsios and Leonie Papon. Universal approximation theorems for differentiable geometric deep learning. *Journal of Machine Learning Research*, 23(196):1–73, 2022.

Anastasis Kratsios, Haitz Sáez de Ocáriz Borde, Takashi Furuya, and Marc T Law. Approximation rates and vc-dimension bounds for (p)relu mlp mixture of experts. *arXiv preprint arXiv:2402.03460*, 2024.

Urs Lang and Viktor Schroeder. Jung’s theorem for Alexandrov spaces of curvature bounded above. *Ann. Global Anal. Geom.*, 15(3):263–275, 1997. ISSN 0232-704X,1572-9060. doi: 10.1023/A:1006574402955. URL <https://doi.org/10.1023/A:1006574402955>.

Samuel Lanthaler and Andrew M. Stuart. The parametric complexity of operator learning, 2023.

Huiling Le. Locating fréchet means with application to shape spaces. *Advances in Applied Probability*, 33(2):324–338, 2001.

Alice Le Brigant, Stephen C Preston, and Stéphane Puechmorel. Fisher-rao geometry of dirichlet distributions. *Differential Geometry and its Applications*, 74:101702, 2021.

Pingzhi Li, Zhenyu Zhang, Prateek Yadav, Yi-Lin Sung, Yu Cheng, Mohit Bansal, and Tianlong Chen. Merge, then compress: Demystify efficient SMoe with hints from its routing policy. In *The Twelfth International Conference on Learning Representations*, 2024. URL <https://openreview.net/forum?id=eFWG9Cy3WK>.

Zhong Li, Jiequn Han, E Weinan, and Qianxiao Li. Approximation and optimization theory for linear continuous-time recurrent neural networks. *J. Mach. Learn. Res.*, 23:42–1, 2022a.

Zhong Li, Jiequn Han, E Weinan, and Qianxiao Li. Approximation and optimization theory for linear continuous-time recurrent neural networks. *J. Mach. Learn. Res.*, 23:42–1, 2022b.

Yongdo Lim and Miklós Pálfa. Strong law of large numbers for the L^1 -Karcher mean. *J. Funct. Anal.*, 279(7):108672, 37, 2020. ISSN 0022-1236,1096-0783. doi: 10.1016/j.jfa.2020.108672. URL <https://doi.org/10.1016/j.jfa.2020.108672>.

Miroslav Lovrić, Maung Min-Oo, and Ernst A. Ruh. Multivariate normal distributions parametrized as a Riemannian symmetric space. *J. Multivariate Anal.*, 74(1):36–48, 2000. ISSN 0047-259X. doi: 10.1006/jmva.1999.1853. URL <https://doi.org/10.1006/jmva.1999.1853>.

Jianfeng Lu, Zuowei Shen, Haizhao Yang, and Shijun Zhang. Deep network approximation for smooth functions. *SIAM J. Math. Anal.*, 53(5):5465–5506, 2021. ISSN 0036-1410. doi: 10.1137/20M134695X. URL <https://doi.org/10.1137/20M134695X>.

Mantas Lukoševičius and Herbert Jaeger. Reservoir computing approaches to recurrent neural network training. *Computer science review*, 3(3):127–149, 2009.

Jonathan Masci, Davide Boscaini, Michael Bronstein, and Pierre Vandergheynst. Geodesic convolutional neural networks on riemannian manifolds. In *Proceedings of the IEEE international conference on computer vision workshops*, pages 37–45, 2015.

Jiří Matoušek. *Lectures on discrete geometry*, volume 212 of *Graduate Texts in Mathematics*. Springer-Verlag, New York, 2002. ISBN 0-387-95373-6. doi: 10.1007/978-1-4613-0039-7. URL <https://doi.org/10.1007/978-1-4613-0039-7>.

Manor Mendel and Assaf Naor. Spectral calculus and Lipschitz extension for barycentric metric spaces. *Anal. Geom. Metr. Spaces*, 1:163–199, 2013. ISSN 2299-3274. doi: 10.2478/agms-2013-0003. URL <https://doi.org/10.2478/agms-2013-0003>.

Mehdi Mirza and Simon Osindero. Conditional generative adversarial nets. *arXiv preprint arXiv:1411.1784*, 2014.

MosaicAI. Introducing dbrx: A new state-of-the-art open llm. <https://www.databricks.com/blog/introducing-dbrx-new-state-art-open-llm>, 2024. Accessed: 2024-05-21.

Shin-ichi Ohta. Extending Lipschitz and Hölder maps between metric spaces. *Positivity*, 13(2):407–425, 2009. ISSN 1385-1292. doi: 10.1007/s11117-008-2202-2. URL <https://doi.org/10.1007/s11117-008-2202-2>.

Shin-ichi Ohta. Barycenters in alexandrov spaces of curvature bounded below. *Advances in geometry*, 12(4):571–587, 2012.

Barrett O’Neill. Semi-Riemannian geometry: With applications to relativity. *Bull. Amer. Math. Soc. (N.S.)*, 16(2):310–312, 1987. ISSN 0273-0979. doi: 10.1090/S0273-0979-1987-15529-7.

Xavier Pennec, Pierre Fillard, and Nicholas Ayache. A riemannian framework for tensor computing. *International Journal of computer vision*, 66(1):41–66, 2006.

Kaare Brandt Petersen, Michael Syskind Pedersen, et al. The matrix cookbook. *Technical University of Denmark*, 7(15):510, 2008.

Julianna Pinele, João E. Strapasson, and Sueli I. R. Costa. The Fisher-Rao distance between multivariate normal distributions: special cases, bounds and applications. *Entropy*, 22(4):Paper No. 404, 24, 2020. doi: 10.3390/e22040404. URL <https://doi.org/10.3390/e22040404>.

Giovanni Puccetti, Ludger Rüschenhoff, and Steven Vanduffel. On the computation of wasserstein barycenters. *Journal of Multivariate Analysis*, 176:104581, 2020.

Joan Puigcerver, Carlos Riquelme Ruiz, Basil Mustafa, and Neil Houlsby. From sparse to soft mixtures of experts. In *The Twelfth International Conference on Learning Representations*, 2024. URL <https://openreview.net/forum?id=jxpsAj7ltE>.

H. E. Rauch. A contribution to differential geometry in the large. *Ann. of Math. (2)*, 54:38–55, 1951. ISSN 0003-486X. doi: 10.2307/1969309. URL <https://doi.org/10.2307/1969309>.

Yu. G. Rešetnyak. On the theory of spaces with curvature no greater than K . *Mat. Sb. (N.S.)*, 52(94):789–798, 1960.

El Mehdi Saad, Nicolas Verzelen, and Alexandra Carpentier. Active ranking of experts based on their performances in many tasks. In *International Conference on Machine Learning*, pages 29490–29513. PMLR, 2023.

Raeid Saqr, Anastasis Kratsios, Florian Krach, Yannick Limmer1, Jacob-Junqi Tian, John Willes, Blanka Horvath, and Frank Rudzicz. Filtered not mixed: Stochastic filtering-based online gating for mixture of large language models. *ArXiV*, TBD, 2024.

Jean-Baptiste Schiratti, Stéphanie Allassonnière, Olivier Colliot, and Stanley Durrleman. A Bayesian mixed-effects model to learn trajectories of changes from repeated manifold-valued observations. *J. Mach. Learn. Res.*, 18:Paper No. 133, 33, 2017. ISSN 1532-4435,1533-7928.

Ekansh Sharma, Devin Kwok, Tom Denton, Daniel M Roy, David Rolnick, and Gintare Karolina Dzigaite. Simultaneous linear connectivity of neural networks modulo permutation. *arXiv preprint arXiv:2404.06498*, 2024.

Zuowei Shen, Haizhao Yang, and Shijun Zhang. Optimal approximation rate of ReLU networks in terms of width and depth. *J. Math. Pures Appl. (9)*, 157:101–135, 2022. ISSN 0021-7824. doi: 10.1016/j.matpur.2021.07.009. URL <https://doi.org/10.1016/j.matpur.2021.07.009>.

Sidney B Shiki, Samuel Da Silva, and Michael D Todd. On the application of discrete-time volterra series for the damage detection problem in initially nonlinear systems. *Structural Health Monitoring*, 16(1):62–78, 2017.

Lene Theil Skovgaard. A Riemannian geometry of the multivariate normal model. *Scand. J. Statist.*, 11(4):211–223, 1984. ISSN 0303-6898.

Steven Thomas Smith. Covariance, subspace, and intrinsic Cramér-Rao bounds. *IEEE Trans. Signal Process.*, 53(5):1610–1630, 2005. ISSN 1053-587X,1941-0476. doi: 10.1109/TSP.2005.845428. URL <https://doi.org/10.1109/TSP.2005.845428>.

Jascha Sohl-Dickstein, Eric Weiss, Niru Maheswaranathan, and Surya Ganguli. Deep unsupervised learning using nonequilibrium thermodynamics. In *International conference on machine learning*, pages 2256–2265. PMLR, 2015.

Edwin H Spanier. *Algebraic topology*. Springer Science & Business Media, 1989.

Sanvesh Srivastava, Cheng Li, and David B Dunson. Scalable bayes via barycenter in wasserstein space. *The Journal of Machine Learning Research*, 19(1):312–346, 2018.

Karl-Theodor Sturm. Nonlinear martingale theory for processes with values in metric spaces of nonpositive curvature. *Ann. Probab.*, 30(3):1195–1222, 2002. ISSN 0091-1798. doi: 10.1214/aop/1029867125. URL <https://doi.org/10.1214/aop/1029867125>.

Karl-Theodor Sturm. Probability measures on metric spaces of nonpositive curvature. In *Heat kernels and analysis on manifolds, graphs, and metric spaces (Paris, 2002)*, volume 338 of *Contemp. Math.*, pages 357–390. Amer. Math. Soc., Providence, RI, 2003. doi: 10.1090/conm/338/06080. URL <https://doi.org/10.1090/conm/338/06080>.

Asuka Takatsu. Wasserstein geometry of gaussian measures. *Osaka Journal of Mathematics*, 48(4): 1005–1026, 2011.

Saiteja Utpala, Praneeth Vepakomma, and Nina Miolane. Differentially private fréchet mean on the manifold of symmetric positive definite (SPD) matrices with log-euclidean metric. *Transactions on Machine Learning Research*, 2023. ISSN 2835-8856. URL <https://openreview.net/forum?id=mAx8QqZ14f>.

Johannes Von Oswald, Christian Henning, Benjamin F Grewe, and João Sacramento. Continual learning with hypernetworks. *arXiv preprint arXiv:1906.00695*, 2019.

Dmitry Yarotsky. Error bounds for approximations with deep relu networks. *Neural Networks*, 94: 103–114, 2017.

Dmitry Yarotsky. Optimal approximation of continuous functions by very deep relu networks. In Sébastien Bubeck, Vianney Perchet, and Philippe Rigollet, editors, *Proceedings of the 31st Conference On Learning Theory*, volume 75 of *Proceedings of Machine Learning Research*, pages 639–649. PMLR, 06–09 Jul 2018. URL <https://proceedings.mlr.press/v75/yarotsky18a.html>.

Dmitry Yarotsky and Anton Zhevnerchuk. The phase diagram of approximation rates for deep neural networks. *Advances in neural information processing systems*, 33:13005–13015, 2020.

Takumi Yokota. Convex functions and p -barycenter on CAT(1)-spaces of small radii. *Tsukuba J. Math.*, 41(1):43–80, 2017. ISSN 0387-4982. doi: 10.21099/tkbjm/1506353559. URL <https://doi.org/10.21099/tkbjm/1506353559>.

Chulhee Yun, Srinadh Bhojanapalli, Ankit Singh Rawat, Sashank Reddi, and Sanjiv Kumar. Are transformers universal approximators of sequence-to-sequence functions? In *International Conference on Learning Representations*, 2020. URL <https://openreview.net/forum?id=ByxRM0NtvR>.